CAPACITIVE RADIOFREQUENCY DISCHARGES AND DUSTY OR COMPLEX PLASMAS FROM FUNDAMENTAL TO APPLICATIONS

Laïfa BOUFENDI

École Polytechnique de l'Université d'Orléans.

GREMI Laboratory

laifa.boufendi@univ-orleans.fr

http://www.univ-orleans.fr/gremi/

OUT LINES

- Introduction: History and motivations
- Capacitively coupled capacitive discharge (CCCD)
- Particle charging and trapping in the plasma
- Nucleation and growth of dust particles in the gas phase
- Particle detection
- Temperature effects
- Applications
- Conclusions

From dust in plasmas
to
dusty plasma science

The first observations of dust in a laboratory plasma were made by Langmuir. He reported these observations on September 18, 1924 at the Centenary of the Franklin Institute in Philadelphia.

Langmuir, Found and Dittmer, Science, vol. 60, No. 1557, p 392 (1924)

"... we have observed some phenomena of remarkable beauty which may prove to be of theoretical interest."

Langmuir’s Streamer Discharge

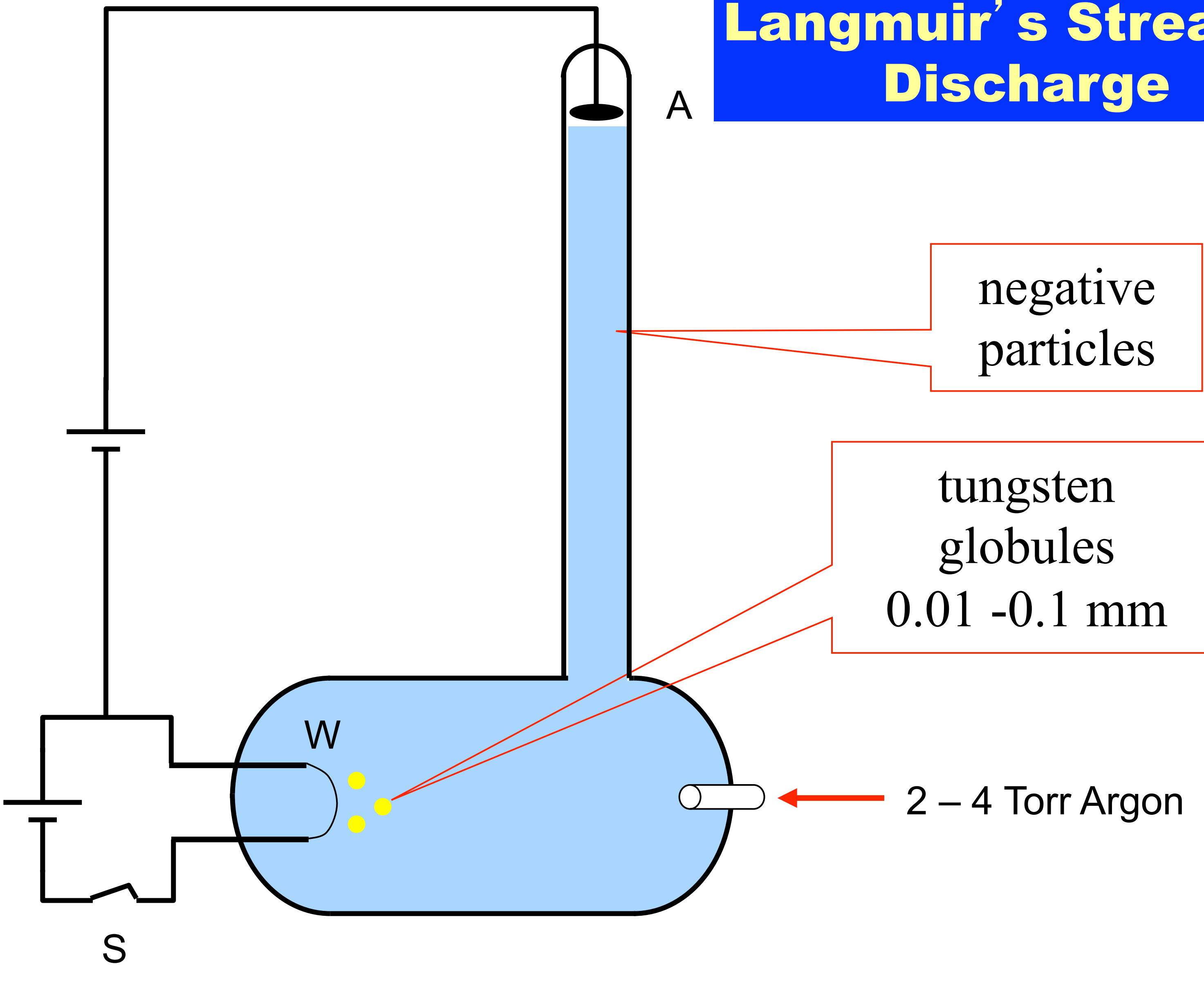

MORE RECENT WORKS 1924 → 1980

- 1945 : *Kenty and Cooper*: effect of impurities on fluorescent lamps.
- 1966 : *Garscadden and Lee*: constricted discharges.
- 1970 : *Emeleus and Breslin*: effect of dust on positive columns.

Take off

Dusty plasmas in astrophysics

In nature

- Comet tails
- Planetary atmospheres (Titan's atm. cont. N_2-CH_4)
- Planetary rings (Saturn's rings)
- Interstellar clouds

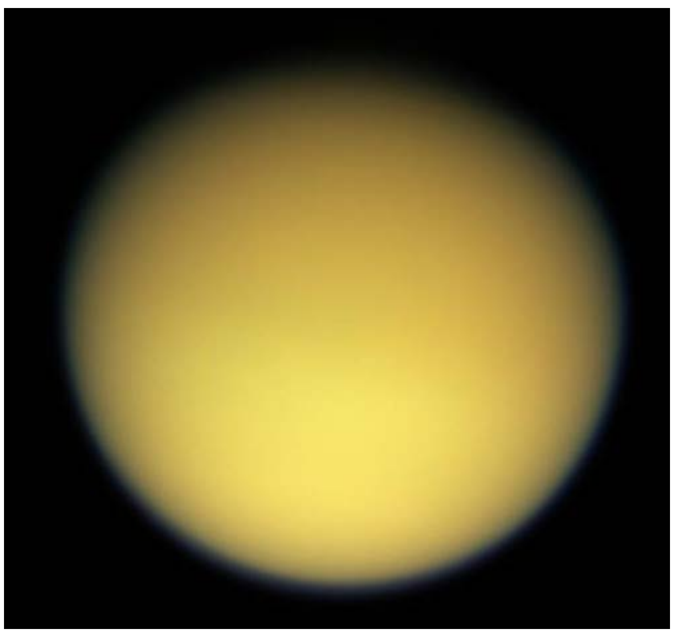

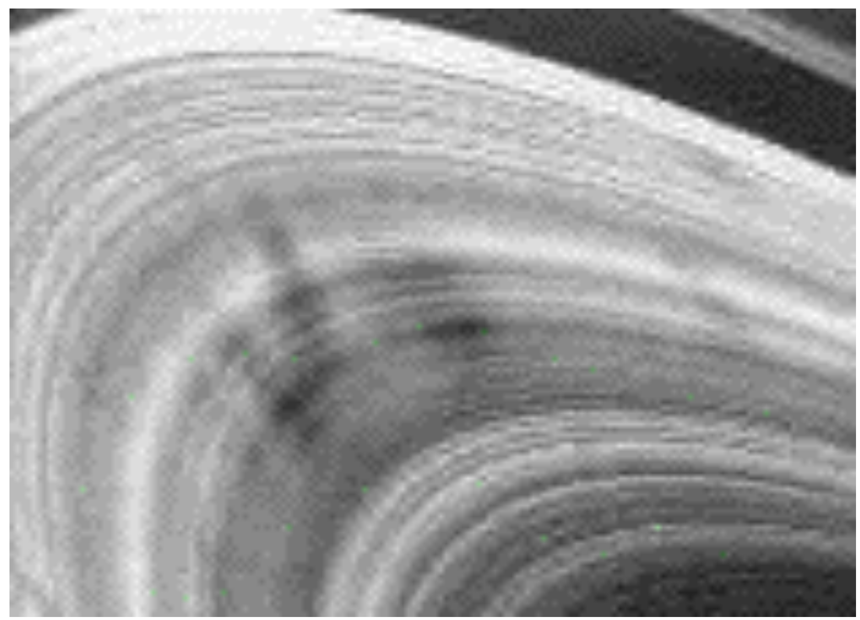

Take off

Unexpected dust problems in plasma-surface processing : pioneering works

-e.g. PECVD (a-Si:H): **Spears & al , IEEE trans. Plasma Sc. 14, 179, 1986.**

-e.g. etching (SiO_2): **G. Selwyn & al , J. Vac. Sci. Techn. A 7, 2758,1989.**

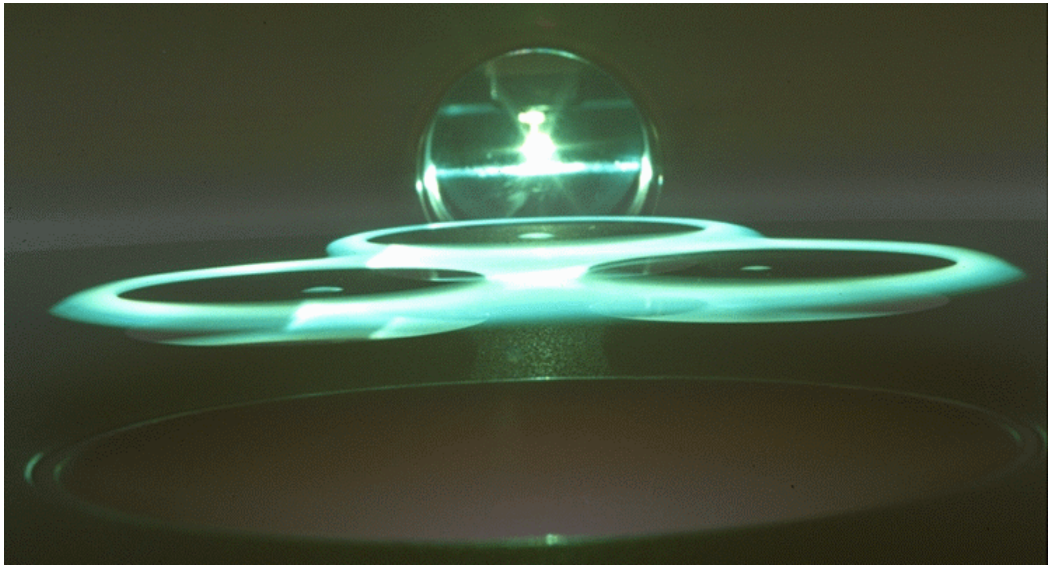

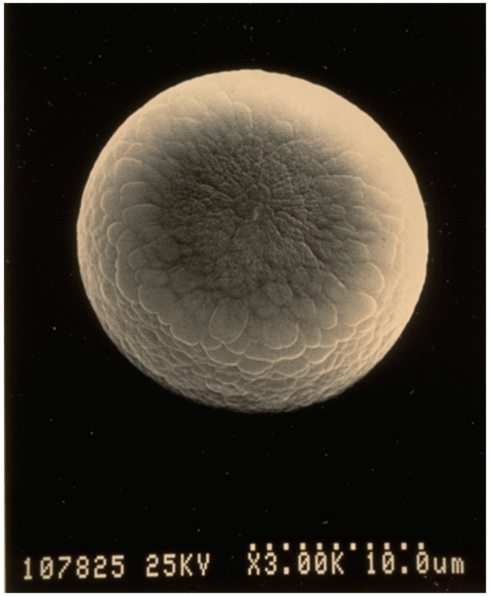

G.S. Selwyn, Plasma Sources Sci. Tehcnol. 3, 340 (1994).

Images from Gary Selwyn: The original discovery that RF plasmas (etching/deposition) can be appropriat medium for particle growth in the gas phase and particle levitation.

CAPACITEVELY COUPLED CAPACITIVE RADIOFREQUENCY DISCHARGES

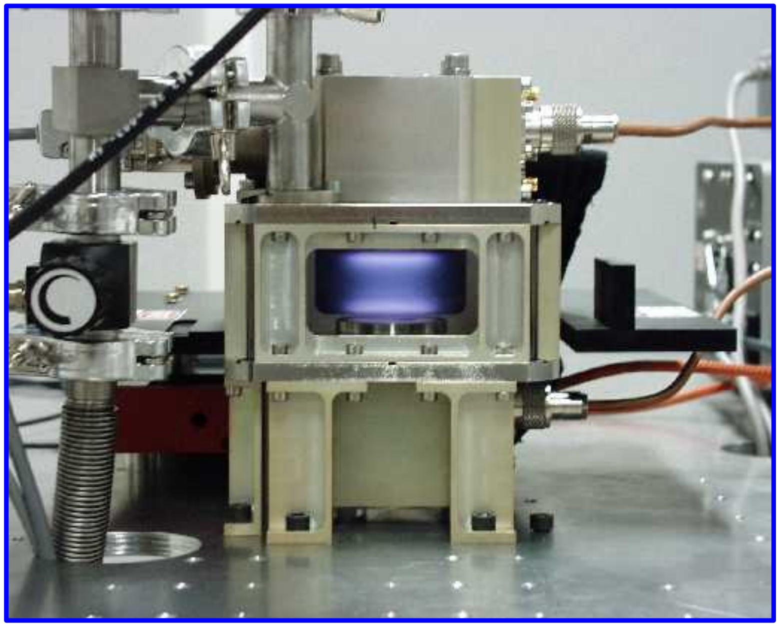

Frequency range [Hz]	Center frequency [Hz]	Availability
6.765–6.795 MHz	6.780 MHz	Subject to local acceptance
13.553–13.567 MHz	13.560 MHz	
26.957–27.283 MHz	27.120 MHz	
40.66–40.70 MHz	40.68 MHz	
433.05–434.79 MHz	433.92 MHz	only
902–928 MHz	915 MHz	only
2.400–2.500	2.450 GHz	
5.725–5.875 GHz	5.800 GHz	
24–24.25 GHz	24.125 GHz	
61–61.5 GHz	61.25 GHz	Subject to local acceptance
122–123 GHz	122.5 GHz	Subject to local acceptance
244–246 GHz	245 GHz	Subject to local acceptance

« Industrial, Scientific and Medical Frequencies » (ISM)

CAPACITEVELY COUPLED CAPACITIVE DISCHARGE

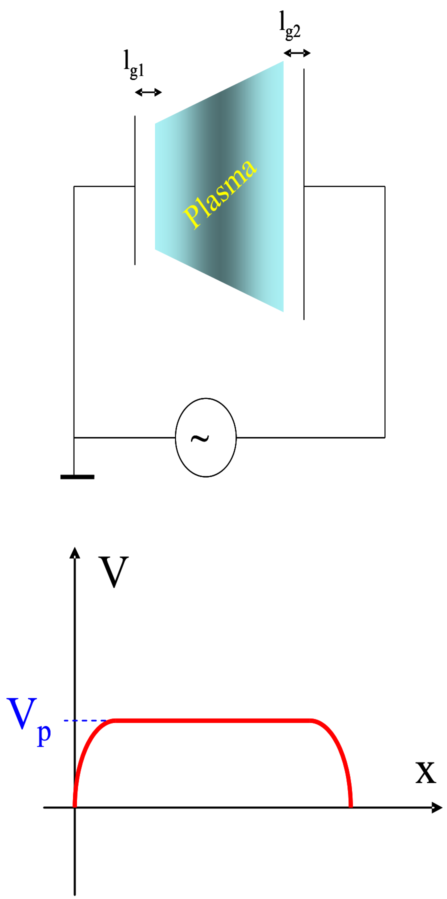

Direct coupling

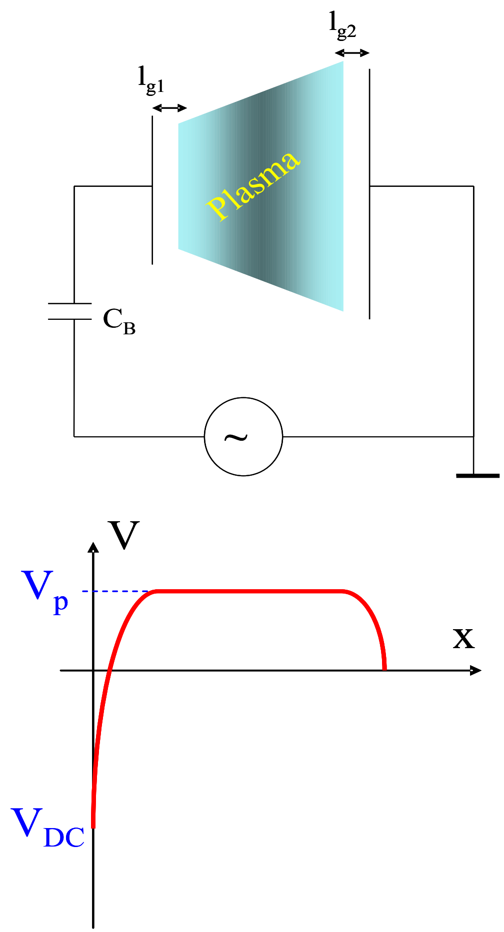

Capacitive coupling

CAPACITEVELY COUPLED CAPACITIVE DISCHARGE

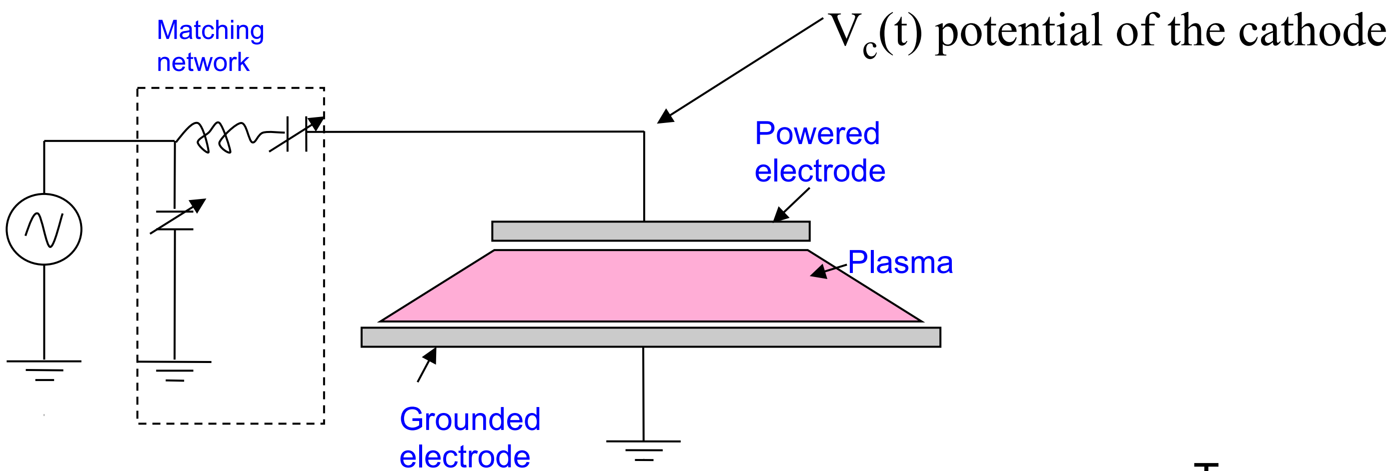

With such discharge structure a self bias (V_{DC}) occurs on the powered electrode.

$$V_C(t) = V_{RF}(t) + V_{DC}$$

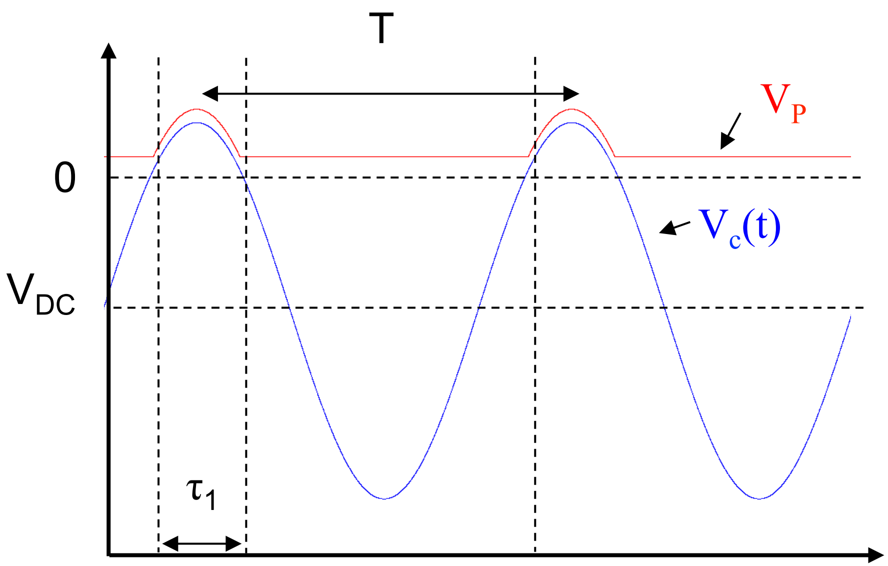

CAPACITEVELY COUPLED CAPACITIVE DISCHARGE

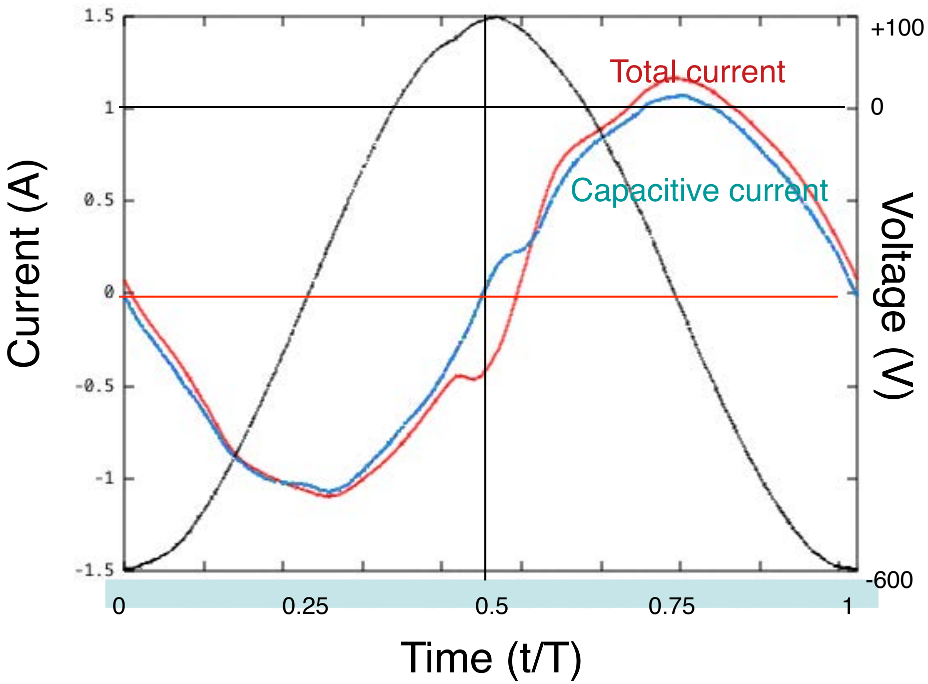

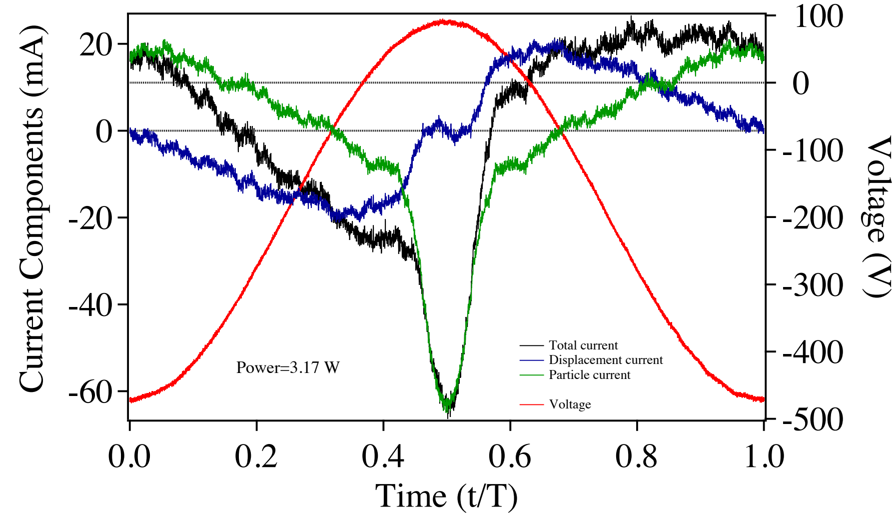

P. Belenguer et al, Surf Interface Anal., 35, (2003), 604.

The nonlinear relationship between the current and the voltage drop in the sheaths induces harmonics in the current waveform.

CAPACITEVELY COUPLED CAPACITIVE DISCHARGE

Ar plasma, analysis of the discharge current

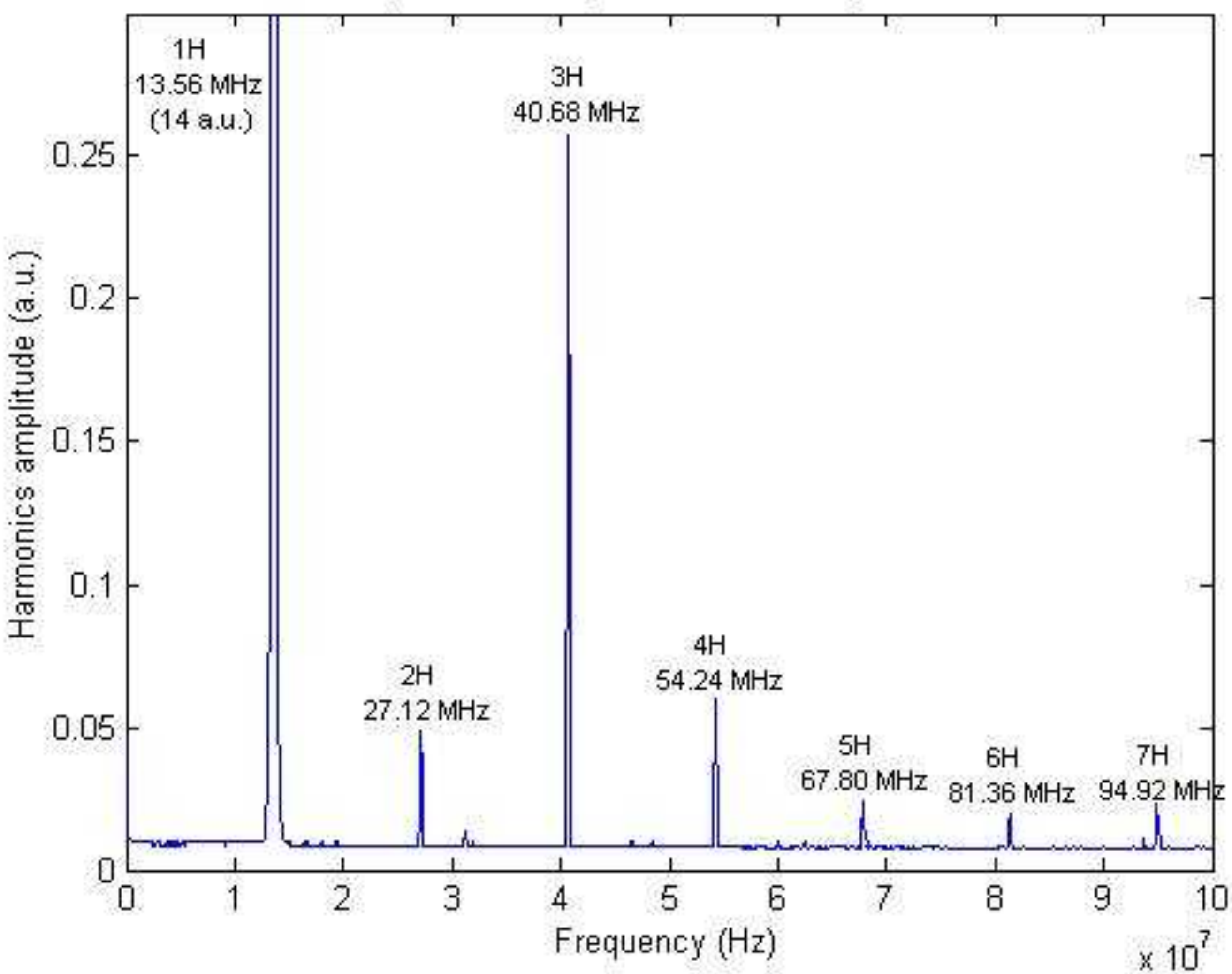

CAPACITEVELY COUPLED CAPACITIVE DISCHARGE

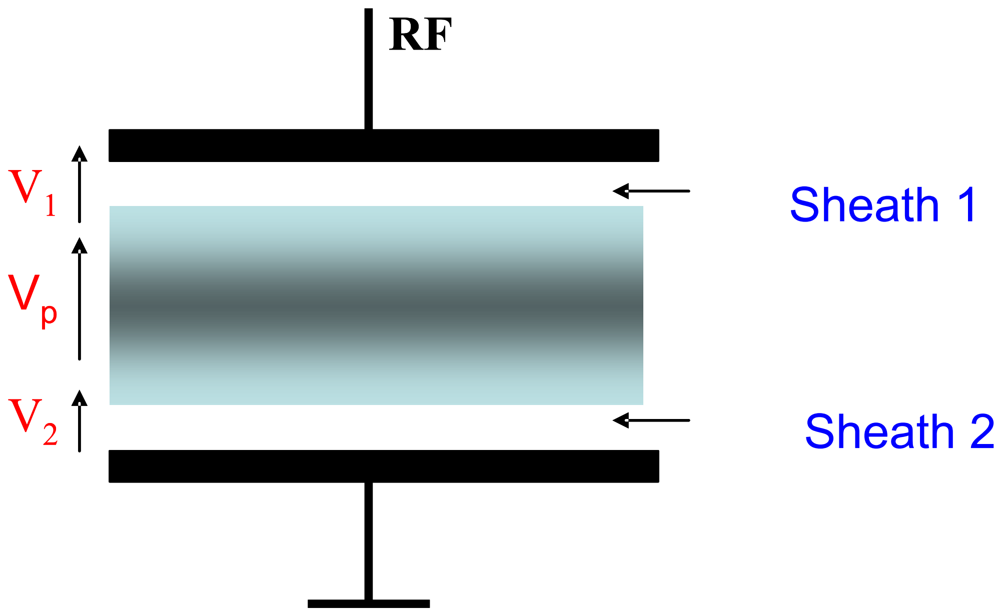

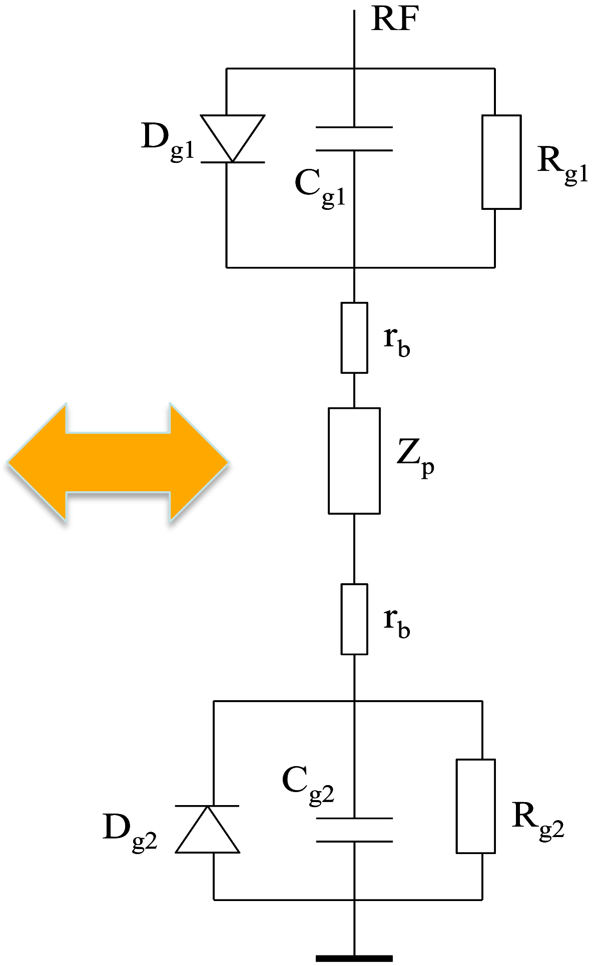

Equivalent Electrical circuit

CAPACITEVELY COUPLED CAPACITIVE DISCHARGE

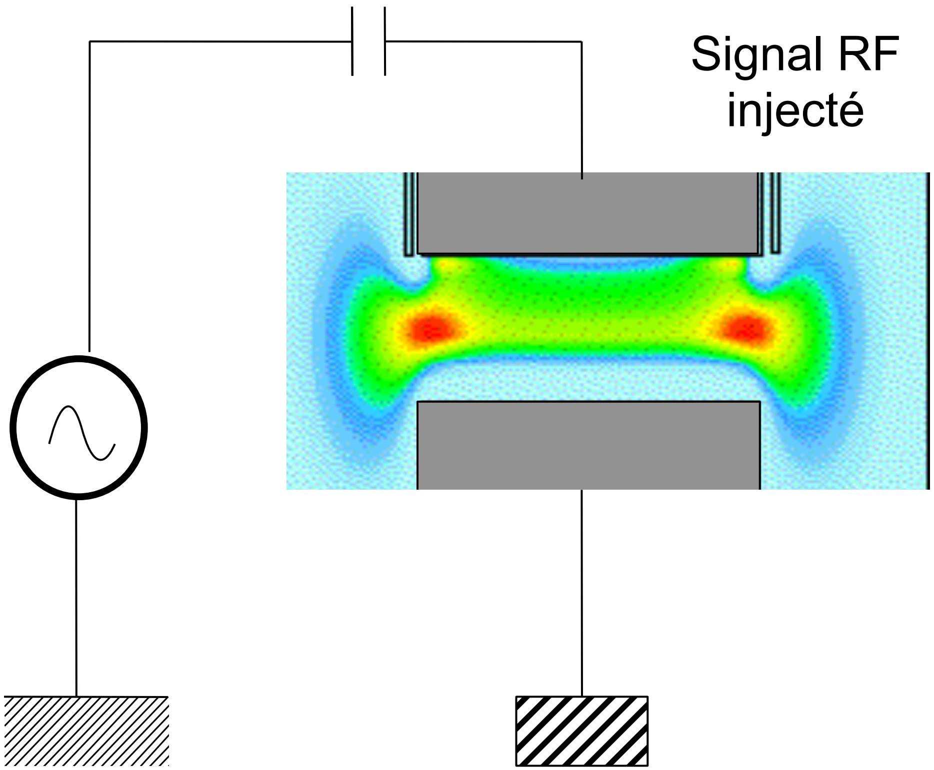

TYPICAL EXPERIMENTAL CONDITIONS

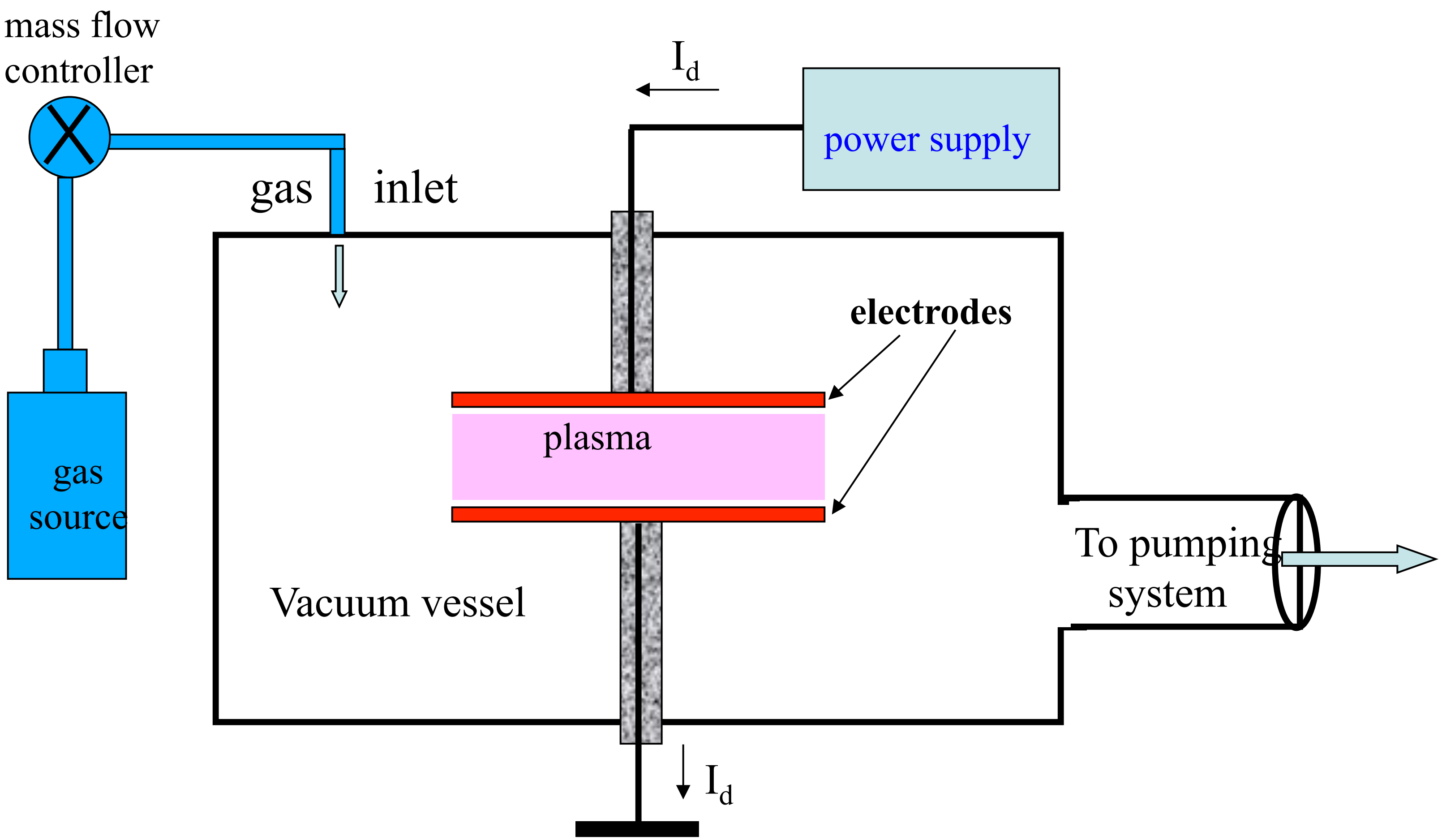

Typical parameters for low pressure discharge plasmas

Pressure: 10-1000 µbars, gas flow : 1-100 sccm, power : 0.01-1 W/cm^3

Electrical source: RF , DC , microwaves, ionization degree : 10^{-5}-10^{-3}

Low pressure discharge plasmas : typical microscopic characteristics

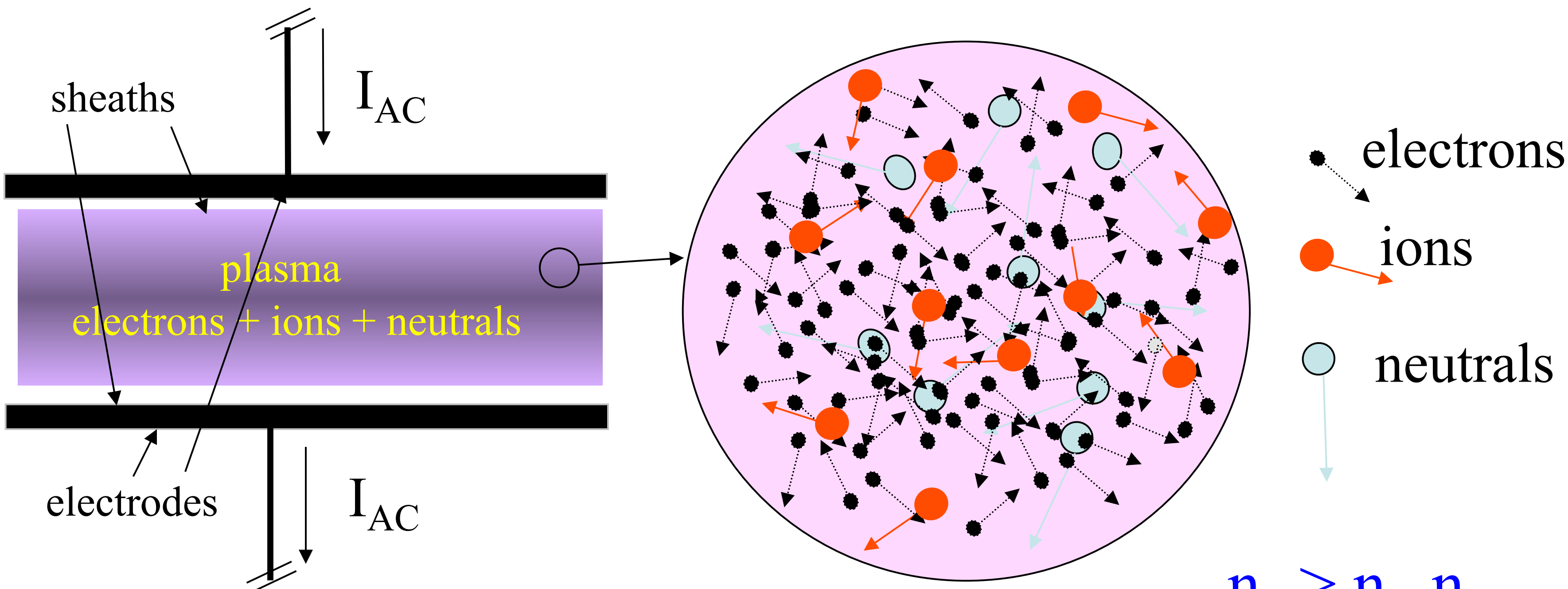

$n_n > n_i, n_e$

$n_i \sim n_e \sim 10^9 – 10^{10}$ cm^{-3}

1 eV $\leq T_e \leq$ 10 eV, $T_i \approx$ 0.03 eV

Low pressure discharge plasmas : typical microscopic characteristics

Electrons: achieve gas ionization, dissociation and excitation ⇒ thermal energy of few eV; thermal speed : few 10^6 m.s^{-1}

Ions : collisional equilibrium with gas ⇒ room temperature, thermal speed = few 100 m.s^{-1}

plasma core ~ equipotential limited by space charge sheaths that control charge losses

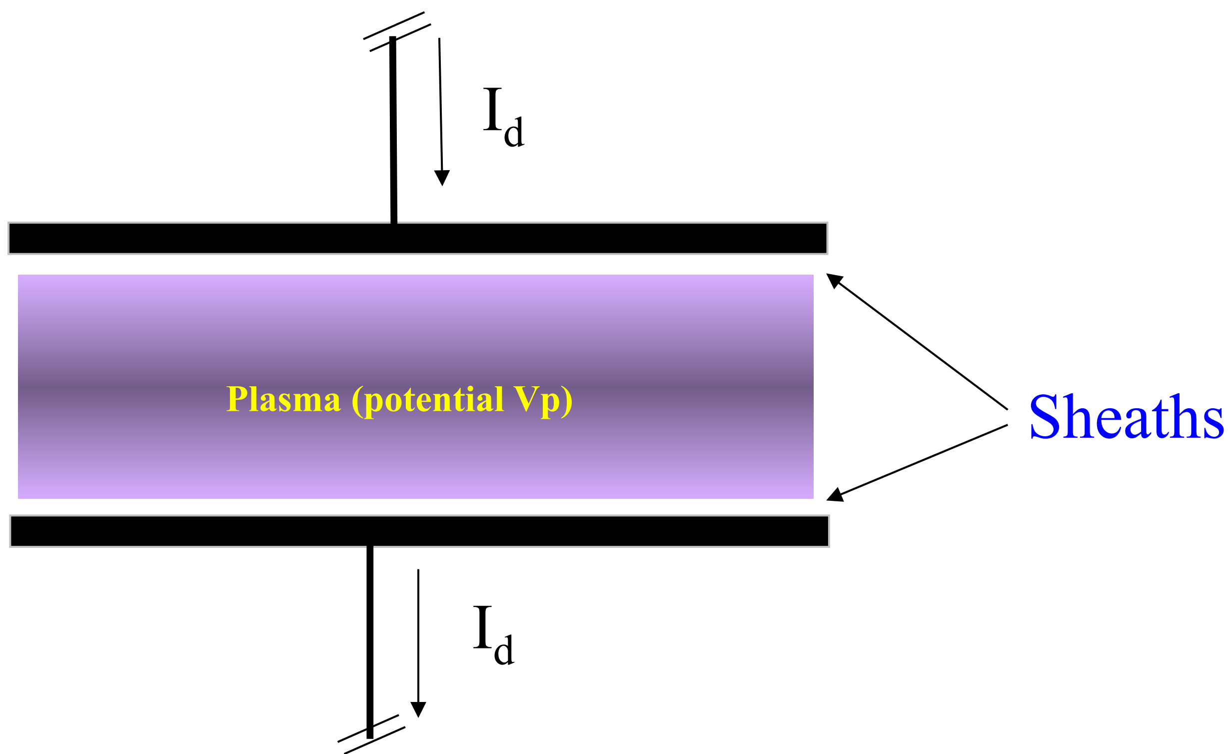

Low pressure discharge plasmas : typical microscopic characteristics

- **high mobility of electrons**: very low potential variation in the plasma core (B =0)

- **requirement of potential barriers** (sheaths) reducing the electron drift flow to the ion flow level (ambipolar diffusion)

- **height of barrier** : **few kTe/q** (repelling most of the electrons and all negative ions) . All the negatively charged species are trapped in the core of the plasma.

- **ions accelerated towards the walls** and ion flow velocity at the sheath edge = $[kT_e / M_i]^{0.5}$ (Bohm velocity).

DUST PARTICLE CHARGING AND TRAPPING IN LOW PRESSURE PLASMAS

PARTICLE CHARGING AND TRAPPING

Single particle immersed in the plasma is negatively charged

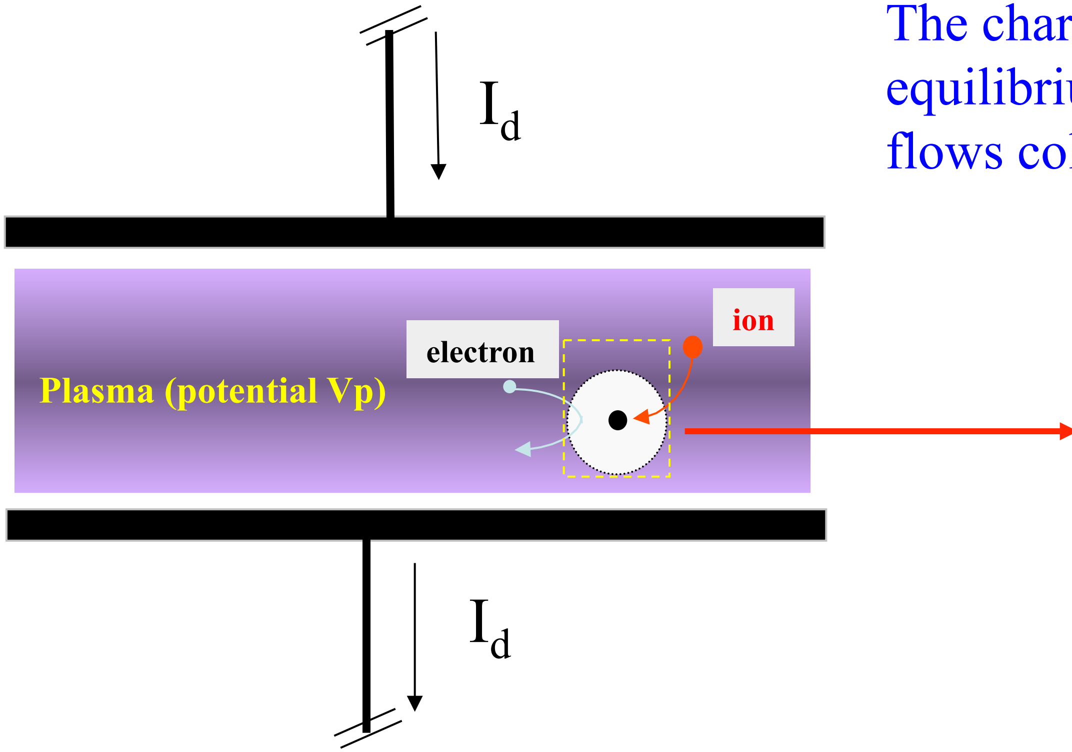

The charge corresponds to the electrostatic equilibrium between the ion and electron flows collected on the dust surface.

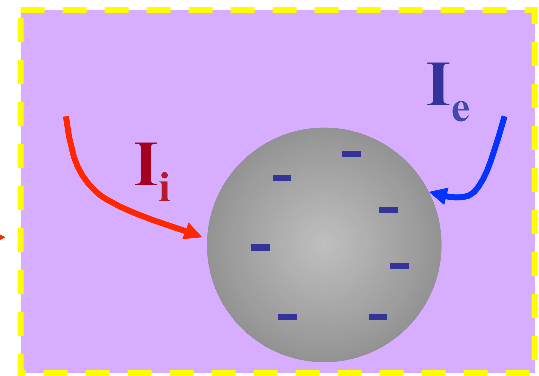

$$\boxed{I_e + I_i = 0}$$

Where

$$\begin{cases} I_i = 4\pi \times r_D^{\ 2} \times q \times n_i \sqrt{\dfrac{Ei}{2\pi \times m_i}} \left(1 - q \dfrac{V_f - V_p}{Ei} \right) \\[2ex] I_e = -4\pi \times r_D^{\ 2} \times q \times n_e \sqrt{\dfrac{k_B Te}{2\pi \times m_e}} \exp\left(q \dfrac{V_f - V_p}{k_B T_e} \right) \end{cases}$$

And

$$\boxed{\frac{dQ_d}{dt} = I_i + I_e}$$

PARTICLE CHARGING AND TRAPPING

Here we considered Maxwellian ion energy distribution

V_f and V_p are respectively the dust particle floating and plasma potentials.

The potential drop in the sheath is given by

$$\frac{n_i}{n_e}\sqrt{\frac{T_i m_e}{T_e m_i}}\left(1 - q\frac{V_f - V_p}{k_B T_i}\right) = \exp\left(q\frac{V_f - V_p}{k_B T_e}\right)$$

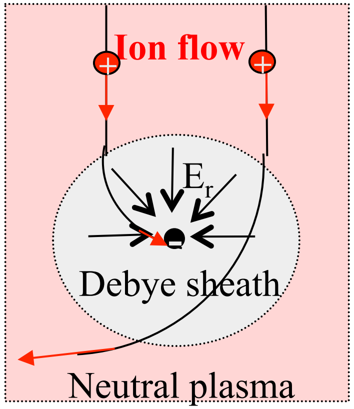

For an isolated spherical dust particle the acquired maximum charge is given by the following expression

$$\boxed{Q_d = \frac{4\pi\epsilon_0 k_B T_e}{e}\ln\left(\frac{ni}{n_e}\left(\frac{m_e T_e}{m_i T_i}\right)^{1/2}\right)}$$

PARTICLE CHARGING MECANISMS

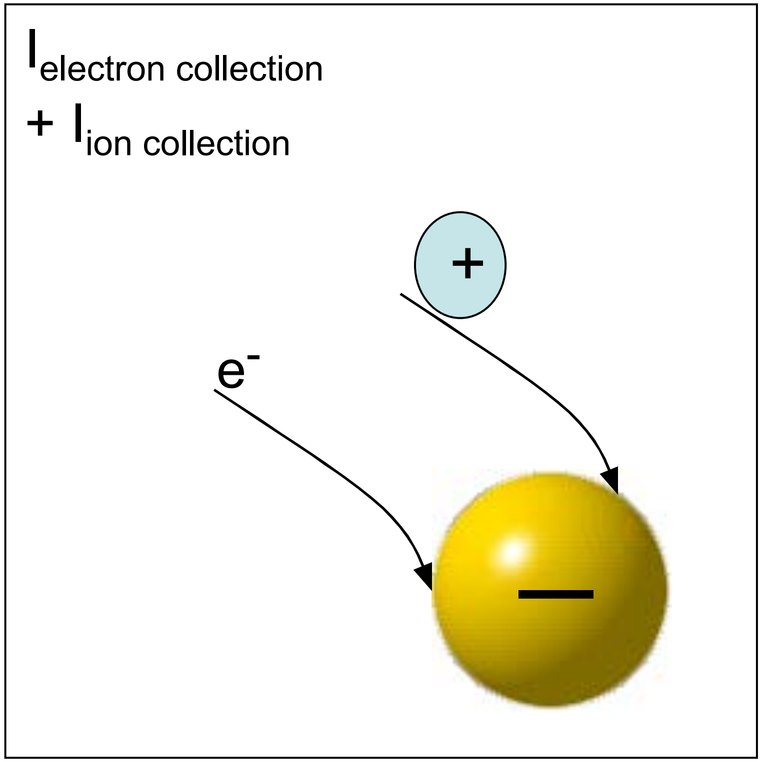

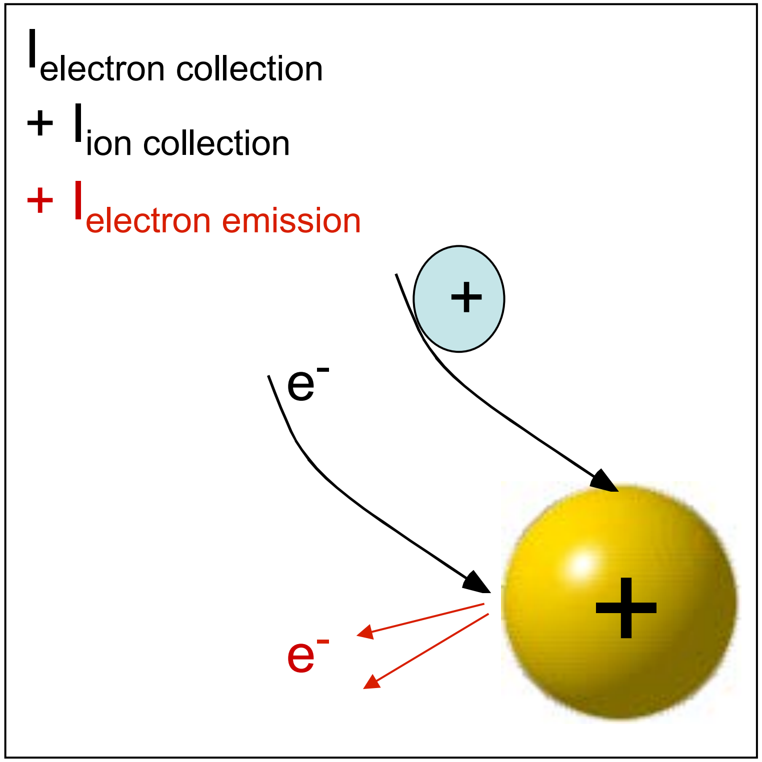

Charging by collecting electrons and ions only

$\Rightarrow Q < 0$

Electron emission

- secondary emission due to e^- impact
- photoemission
- thermionic

$\Rightarrow Q > 0$

Goree, Plasma Sources Sci. Technol. 1994

*Meyer-Vernet, Astron. Astrophys. 105,98 (1982)

Secondary emission from small dust grains at high electron energies
Chow, V.W. Mendis, D.A. Rosenberg, M.
IEEE Transactions on Plasma Science, 179-186, 1994

PARTICLE CHARGING AND TRAPPING

When immersed in a plasma, the dust particle acquire a negative charge and thus is confined in the plasma. It is submitted to a set of forces which are :

- Gravity
- Electrical force
- Ion drag force
- Neural drag force
- Thermophoretic force
- Photophoresis
- Particle-particle interaction.

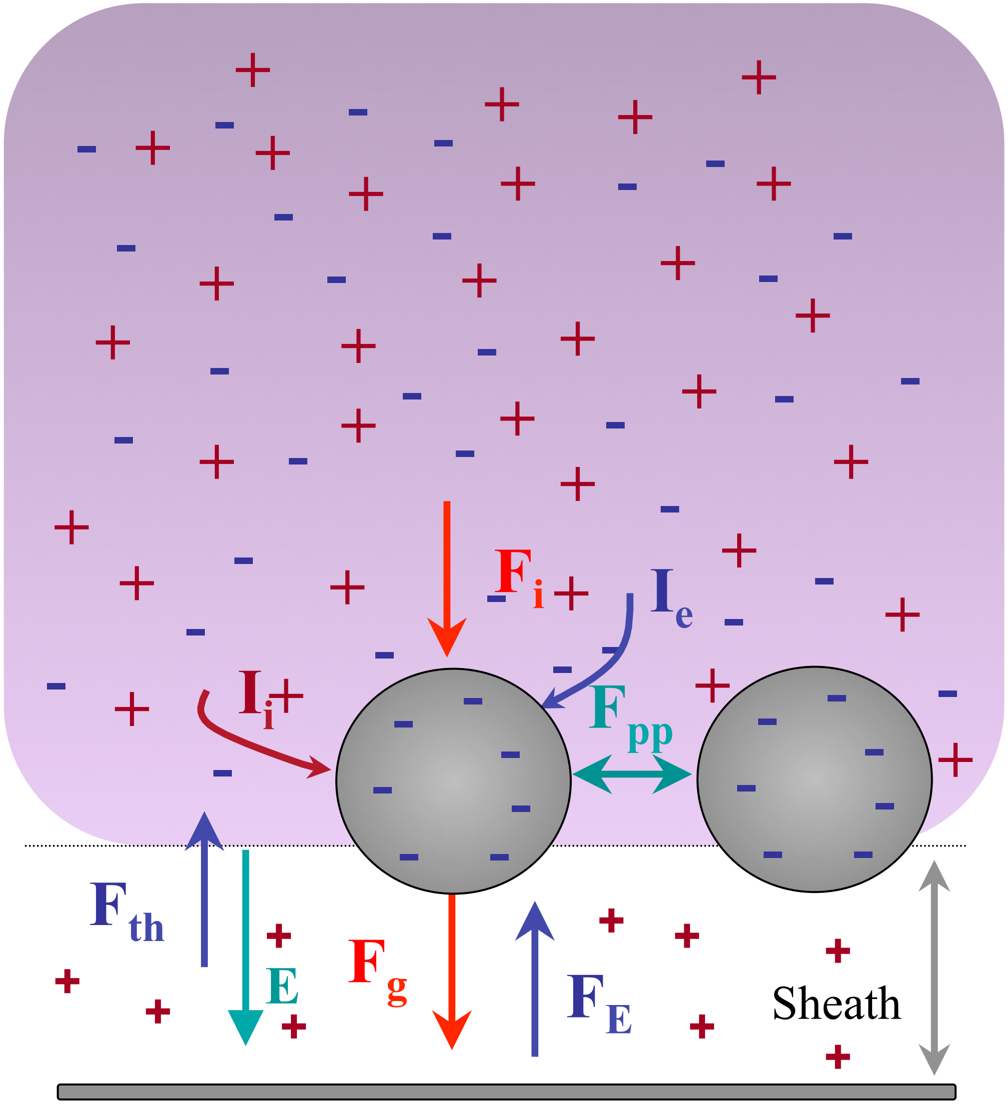

PARTICLE CHARGING AND TRAPPING

- Gravity $$F_g = \frac{4}{3}\pi r_d^3 \rho g$$

- Electrical Force : $$F_e = Q_d E_0 \left[1 + \frac{(r_d/\lambda_L)^2}{3(1 + r_d/\lambda_L)}\right]$$

- Ion Drag force $$\vec{F}_i = \vec{F}_i^o + \vec{F}_i^c = \pi b_c^2 n_i v_s m_i \vec{u}_i + 4\pi b_{\pi/2}^2 \mathrm{H} n_i v_s m_i \vec{u}_i$$

- with $b_c^2 = r_d^2 \left(1 - 2q \dfrac{V_f - V_p}{m_i v_i^2}\right)$ and $\mathrm{H} = \dfrac{1}{2} \ln\left(\dfrac{\lambda_e^2 + b_{\pi/2}^2}{b_c^2 + b_{\pi/2}^2}\right)$

- Thermophoretic force $$\vec{F}_{th} = -\frac{32}{15} \frac{r_d^2}{v_{th,n}} \left[1 + \frac{5\pi}{32}(1 - \alpha_T)\right] \kappa_T \vec{\nabla} T_{gas}$$

PARTICLE CHARGING AND TRAPPING

Momentum is imparted to the dust particle

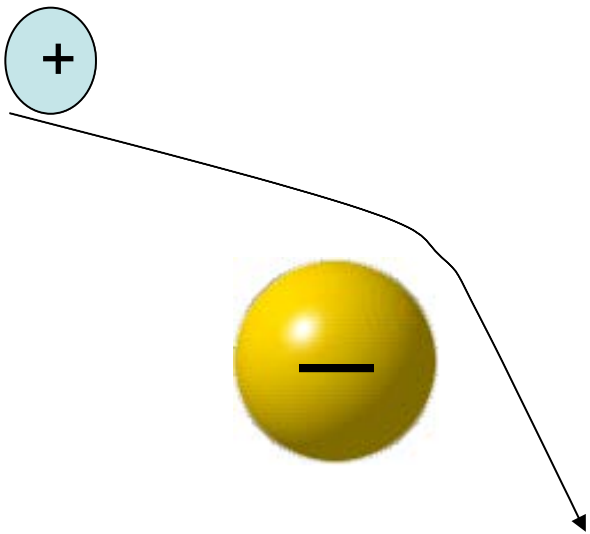

Orbit force:
Ion orbit is deflected

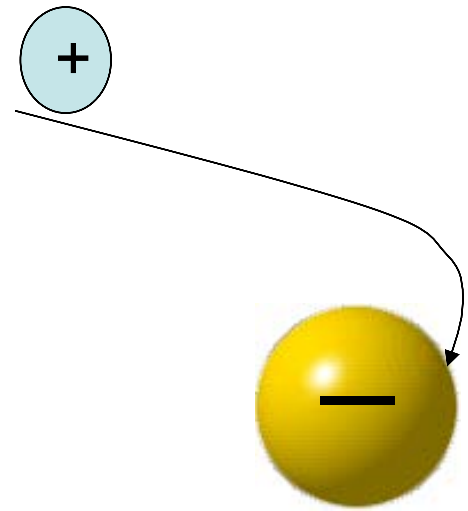

Collection force:
Ion strikes particle

PARTICLE CHARGING AND TRAPPING

Comparison of the different forces

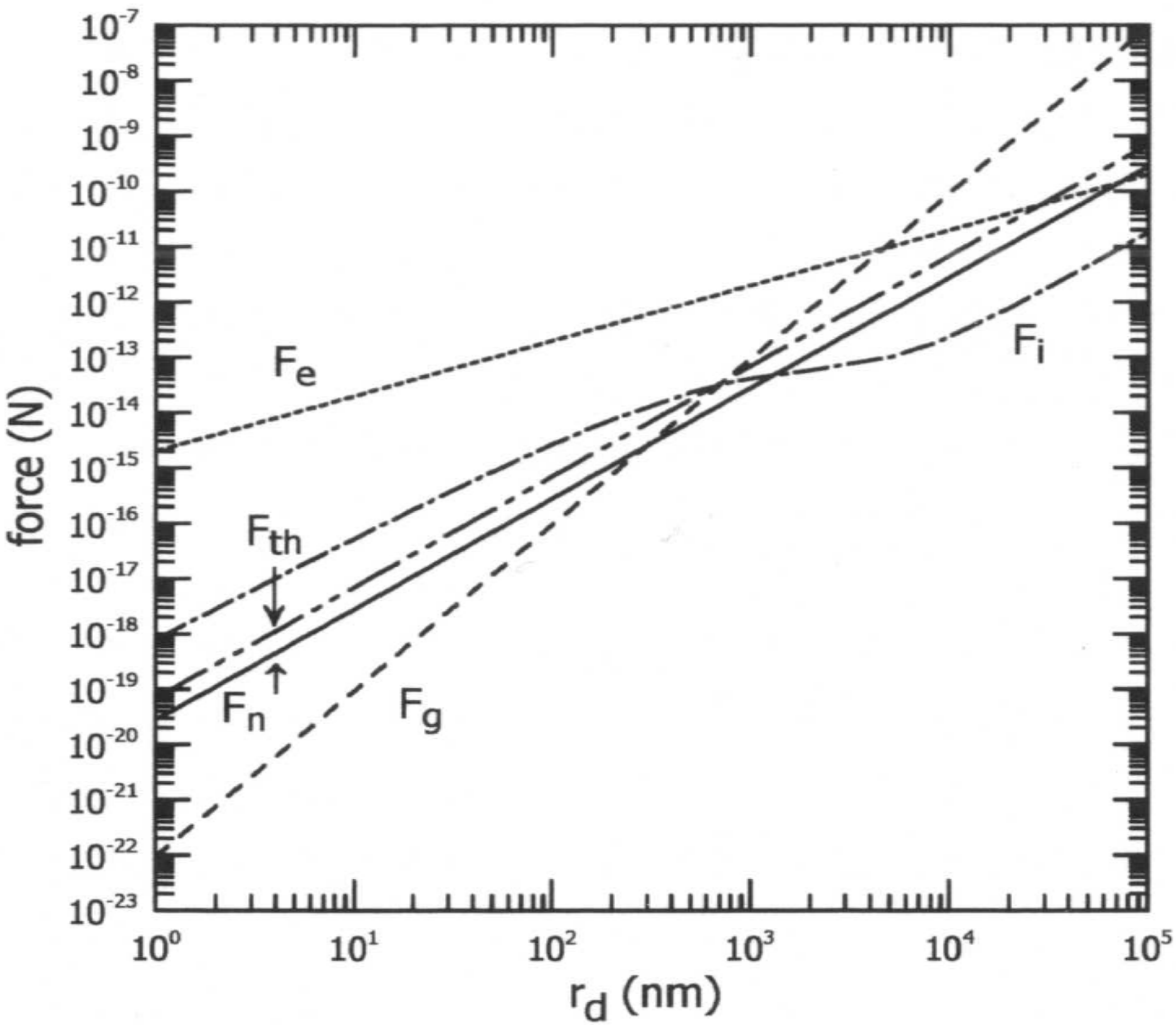

$T_e = 3$eV, $T_e/T_i \approx 100$, $T_g = 400$K, $\rho = 2.3\ 10^3$ kg/m^3, $v_{th,n} = 500$ m/s.

Dense particle cloud dynamics

Well localized traps

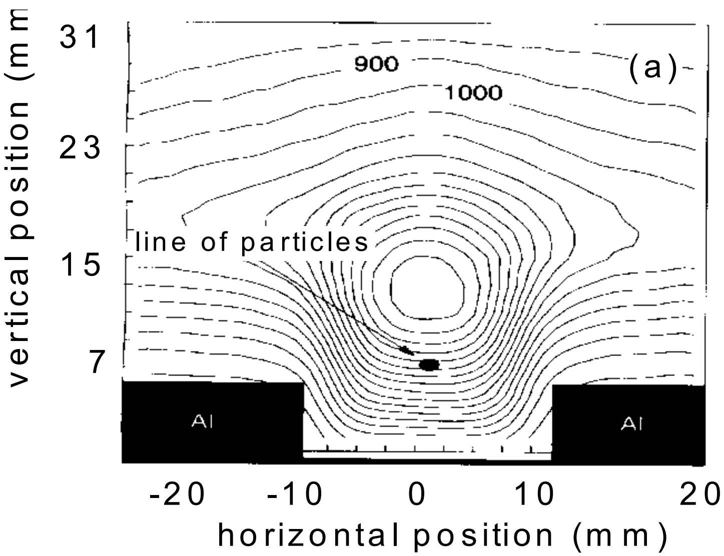

Simulation

J.P. Boeuf et al, PSST, 3, (1994)
Dalvie et al, PSST, 3, 442-447, (1994)

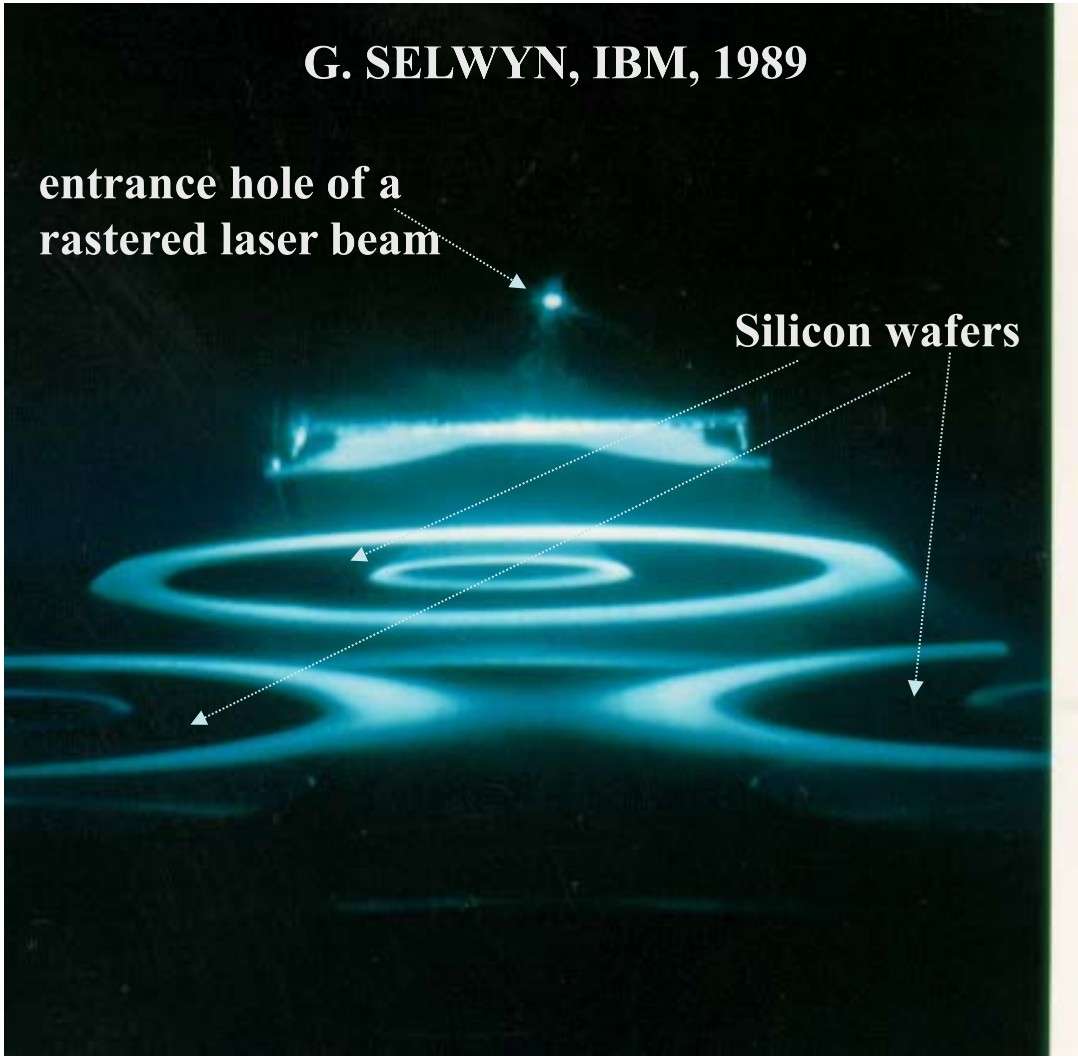

Experiment

Dense particle cloud trapped in plasma : from independent particles to coulomb crystals

Strongly coupled systems

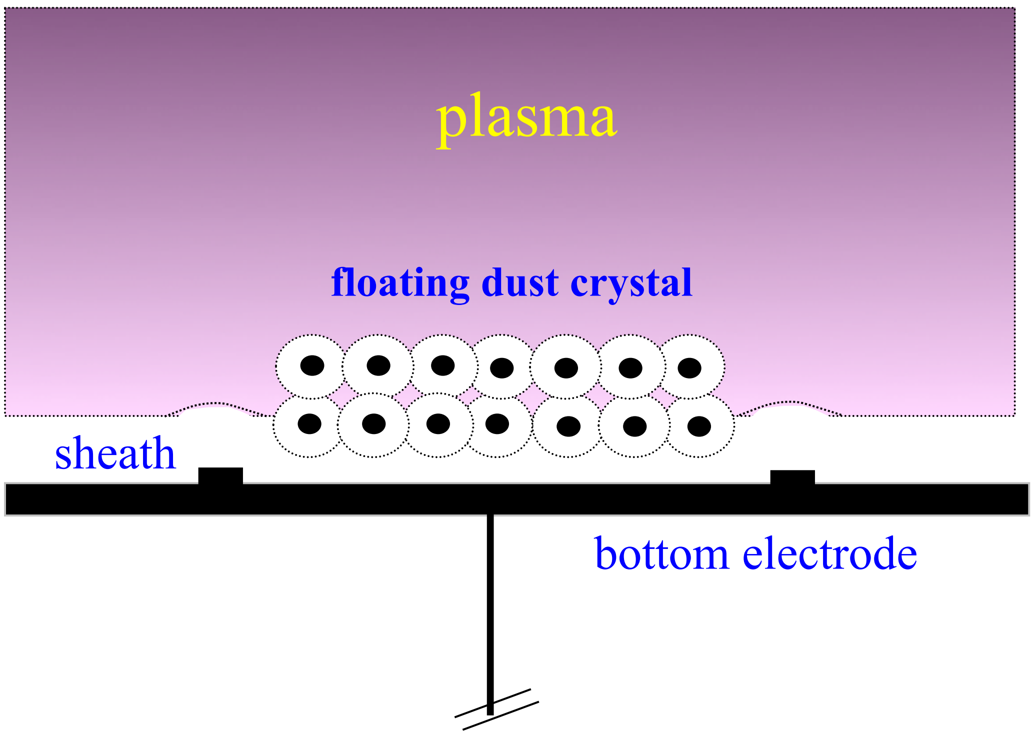

$$\Gamma = \frac{Q_d^2}{dk_B T_d}\exp\left(-\frac{d}{\lambda_D}\right)$$

Coupling parameter

1 : When the inter-particle distance is such that their « Debye spheres » overlapp : repelling forces appear

2 : If the kinetic energy is significantly lower than the interaction energy the particles cannot move freely

3 : Phase transition (liquid to crystal) predicted theoretically before experimental evidence

4 : Crystals defects and wave propagation observed

Dense particle cloud trapped in plasma : from independent particles to coulomb crystals

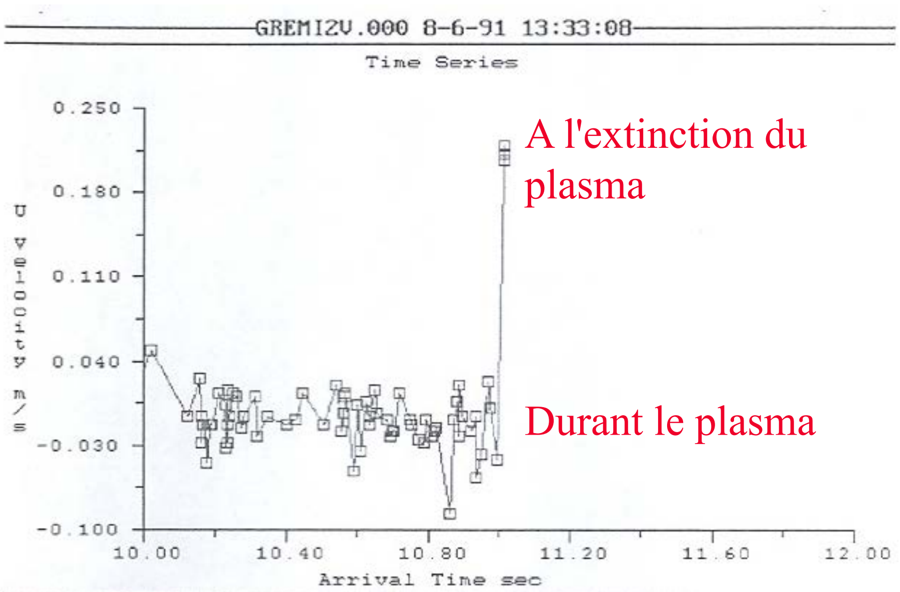

Plasma ON :
particle velocity RMS value = 0.0220 m/s
kinetic energy : kT_d = 0.035 eV (T_d = 410 K)

Plasma OFF :
instantaneous gas velocity = 0.215 m/s
particle-particle interaction energy : 0. 3 eV

from $$W_{dE} = \frac{1}{4\pi\varepsilon_0}\frac{Z^2 q^2}{D_{p-p}}$$

- dust cloud grown in Ar-SiH_4 plasma filling the whole plasma box - particle diameter : 0.4 µm , particle density 10^8 cm^{-3}
- particle charge : ~40 electrons
- Γ = 10, transition to crystal for > 170 (Ikezi)
-measurement of particle vertical velocity using LDA evidenced a rather incompressible liquid-like behavior
Ikezi H. Phys. Fluids 29, 1764 (1986).

Dense particle cloud trapped in plasma : from independent particles to coulomb crystals

Evidence of coulombian crystals

First publications as early as 1994

Chu & al, J Phys D , 27, 296
Melzer & al, Phys Lett. A 320, 301
Hayashi & al, Jpn J. Apl. Phys. 33, L 804,
Thomas & al , Phys Rev Lett, 73, 652

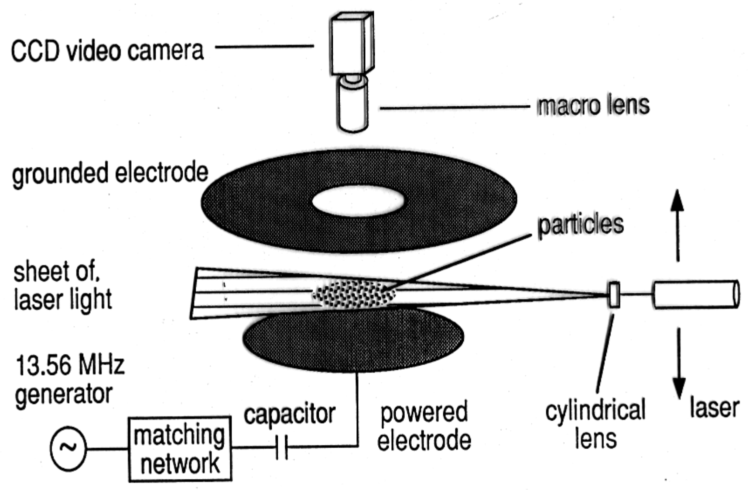

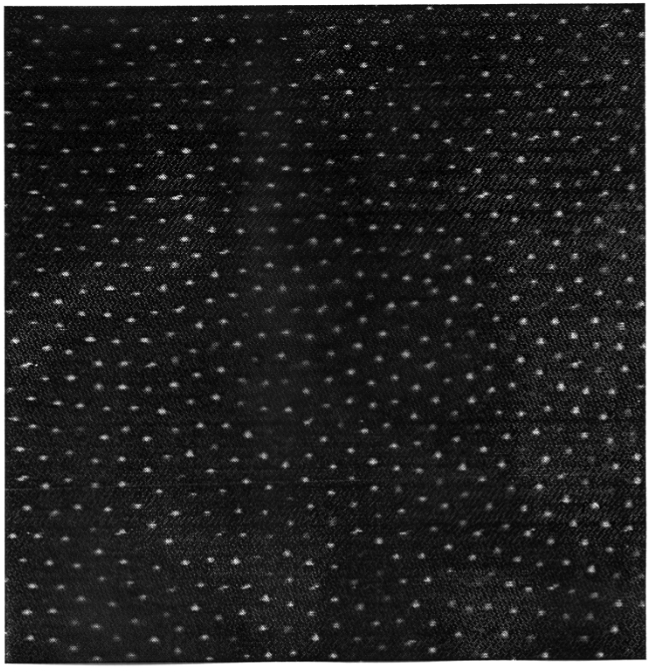

In these experiments $\Gamma > 1000$, well above the critical value (170)

Dense particle cloud trapped in plasma : from independent particles to coulomb crystals

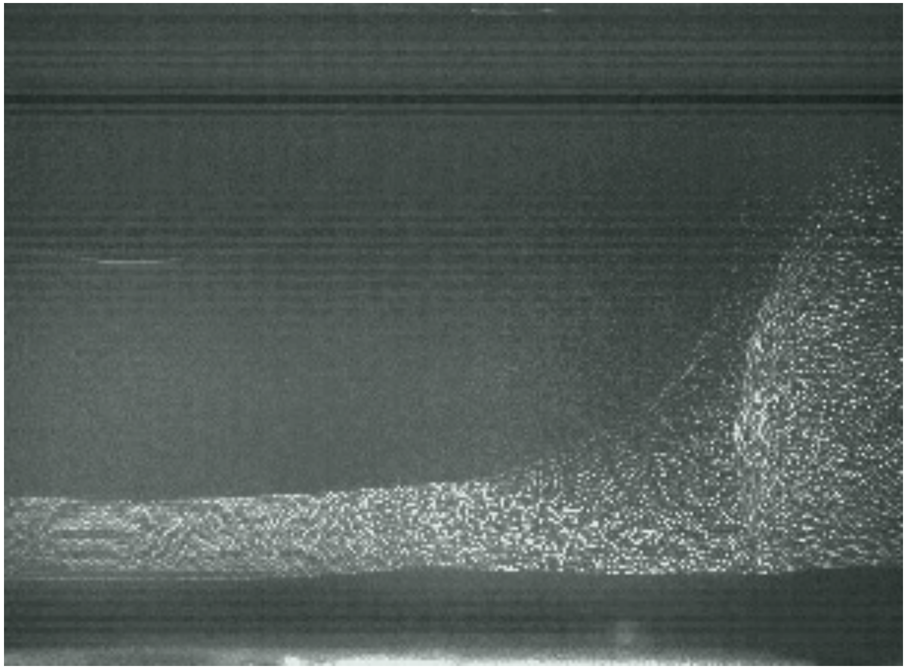

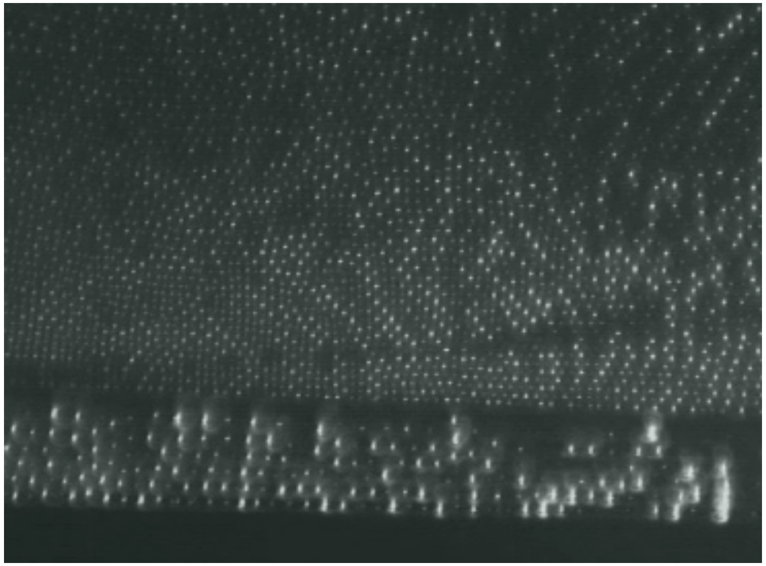

INSTABILITIES OF THE GROWN DUST CLOUD (*HEARTBEAT*)

Once the dust cloud is completely formed, a dust-free region can appear in the plasma center

This region can oscillate spontaneously: Successive contractions and expansions

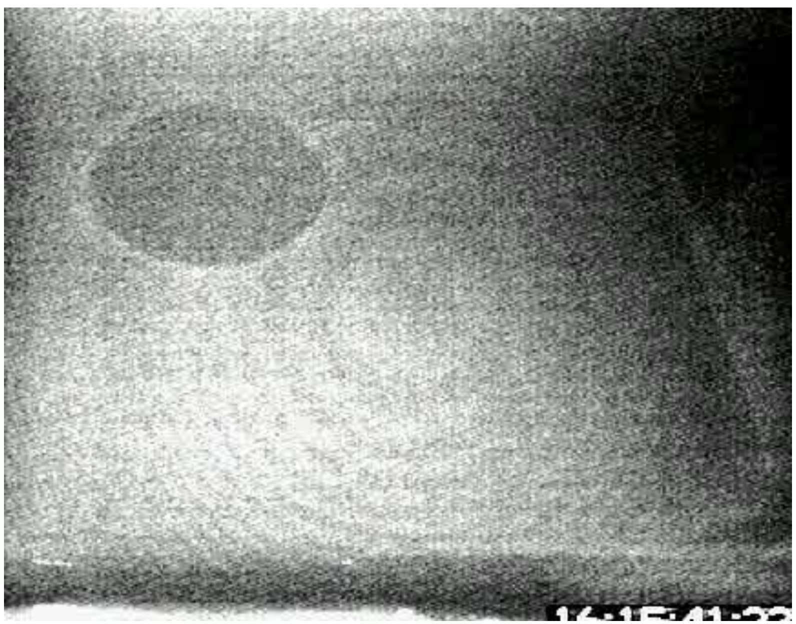

Electrical measurements for different pressures

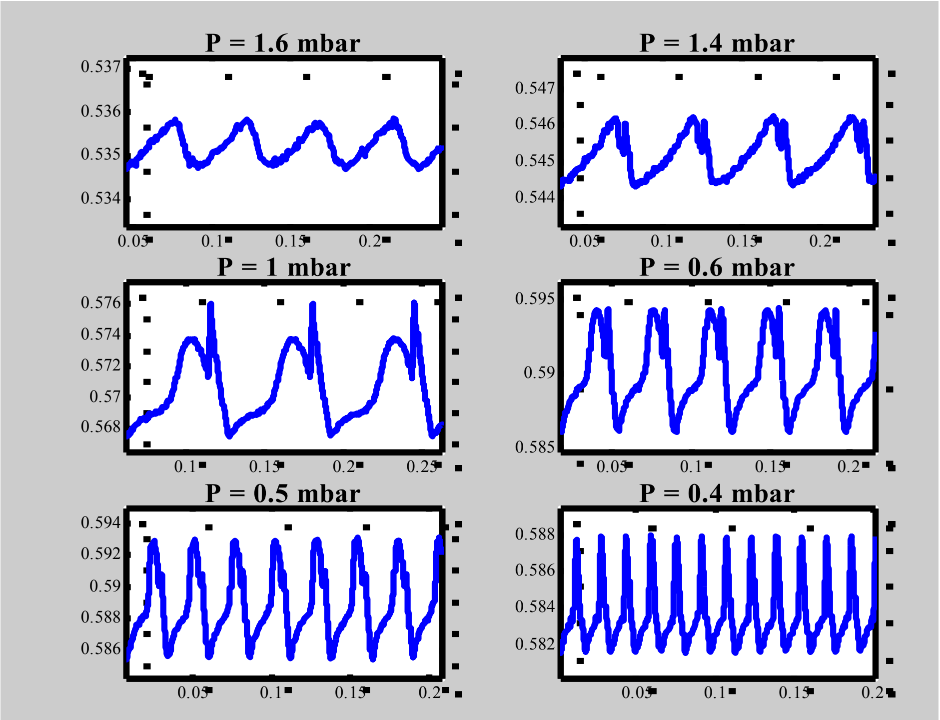

M. Mikikian, L. Boufendi, Phys. Plasmas **11**, 3733 (2004)

HEARTBEAT INSTABILITY
HIGH SPEED IMAGING

High speed imaging ~1800 fps

Direct observation of plasma glow

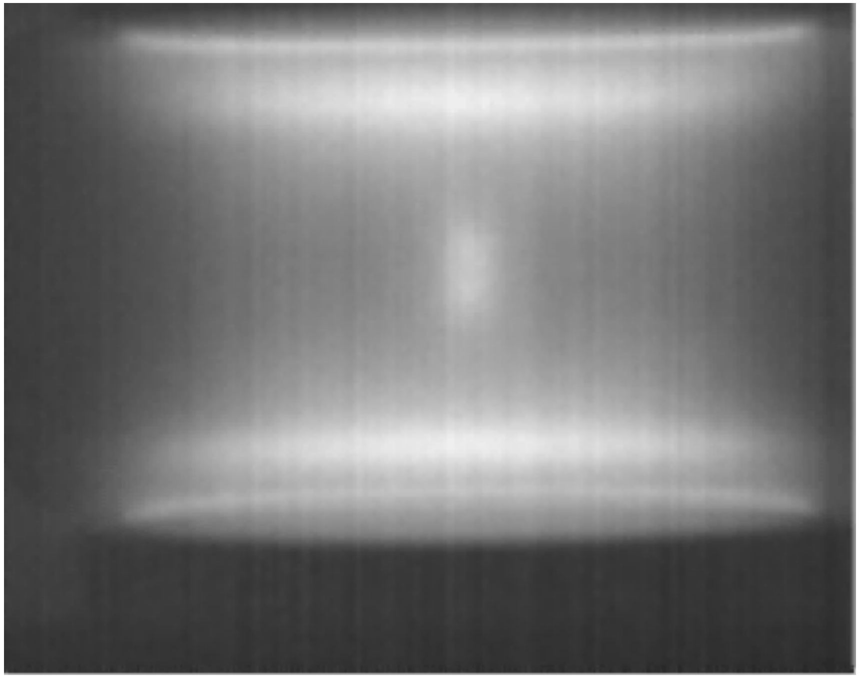

Dust cloud observed with Laser Light Scattering

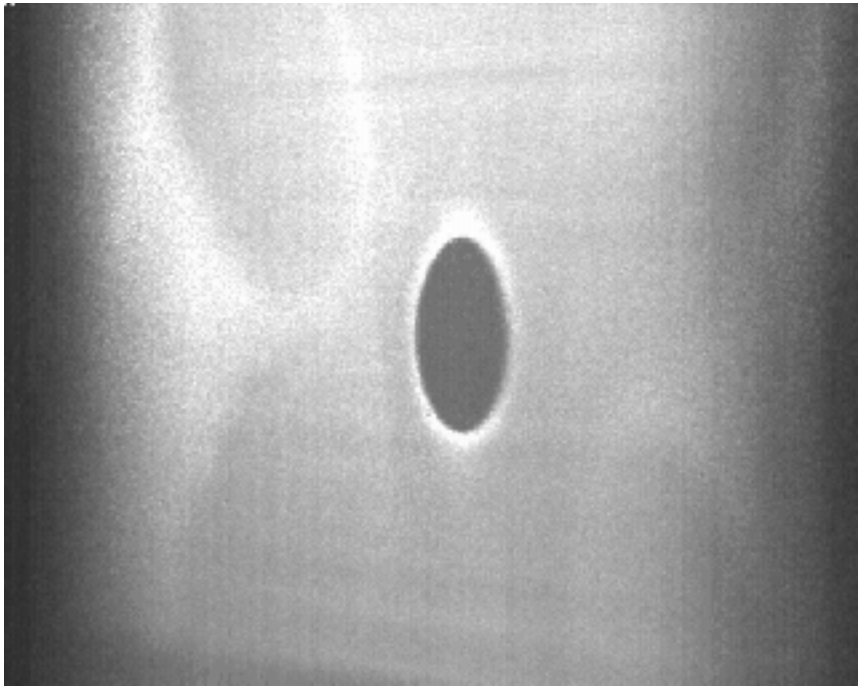

M. Mikikian, L. Couëdel, M. Cavarroc, Y. Tessier, L. Boufendi, New J. Phys. 9, 268 (2007)

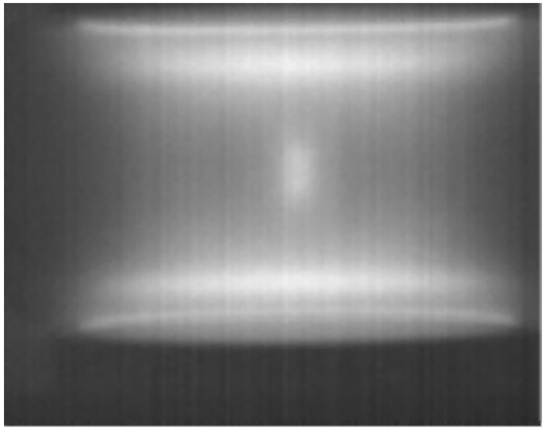

HEARTBEAT INSTABILITY
HIGH SPEED IMAGING

Direct observation of plasma glow

Evolution of dust cloud during one contraction-expansion sequence

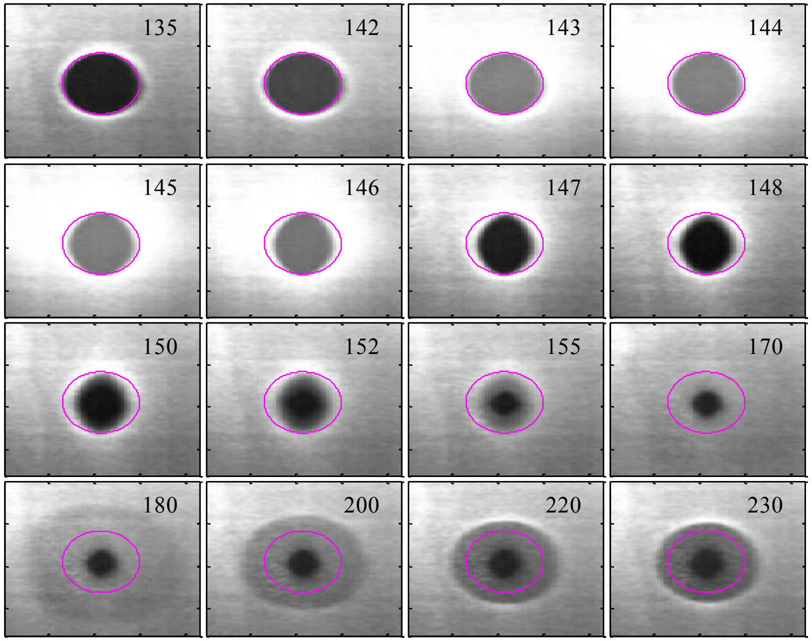

Evolution of the central column profil during one contraction-expansion sequence

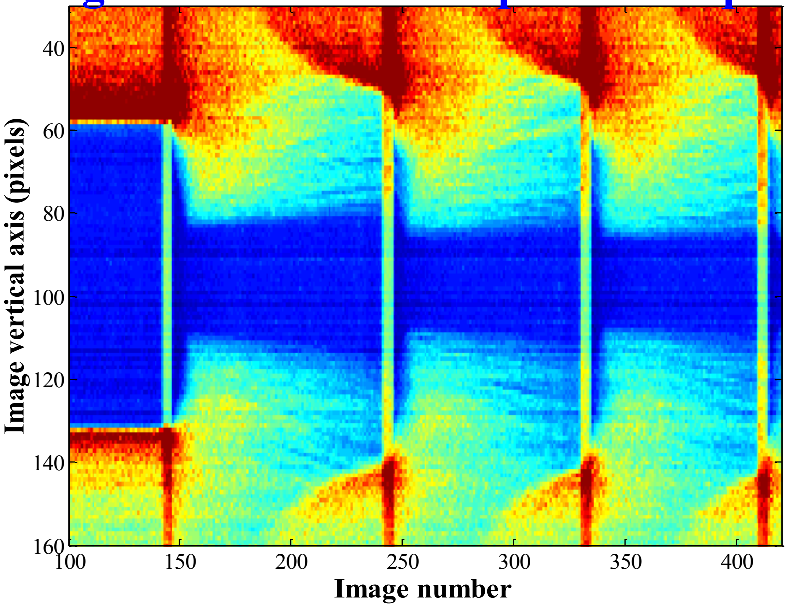

M. Mikikian, L. Couëdel, M. Cavarroc, Y. Tessier, L. Boufendi, New J. Phys. **9**, 268 (2007)

DUST PARTICLE FORMATION

DUST PARTICLE FORMATION

- The dust particle formation in a plasma can be observed in etching, PECVD and sputtering reactors.

- In all these situations, homogeneous chemical reactions are responsible of this phenomenon.

CHEMICAL REACTIONS IN PECVD REACTORS

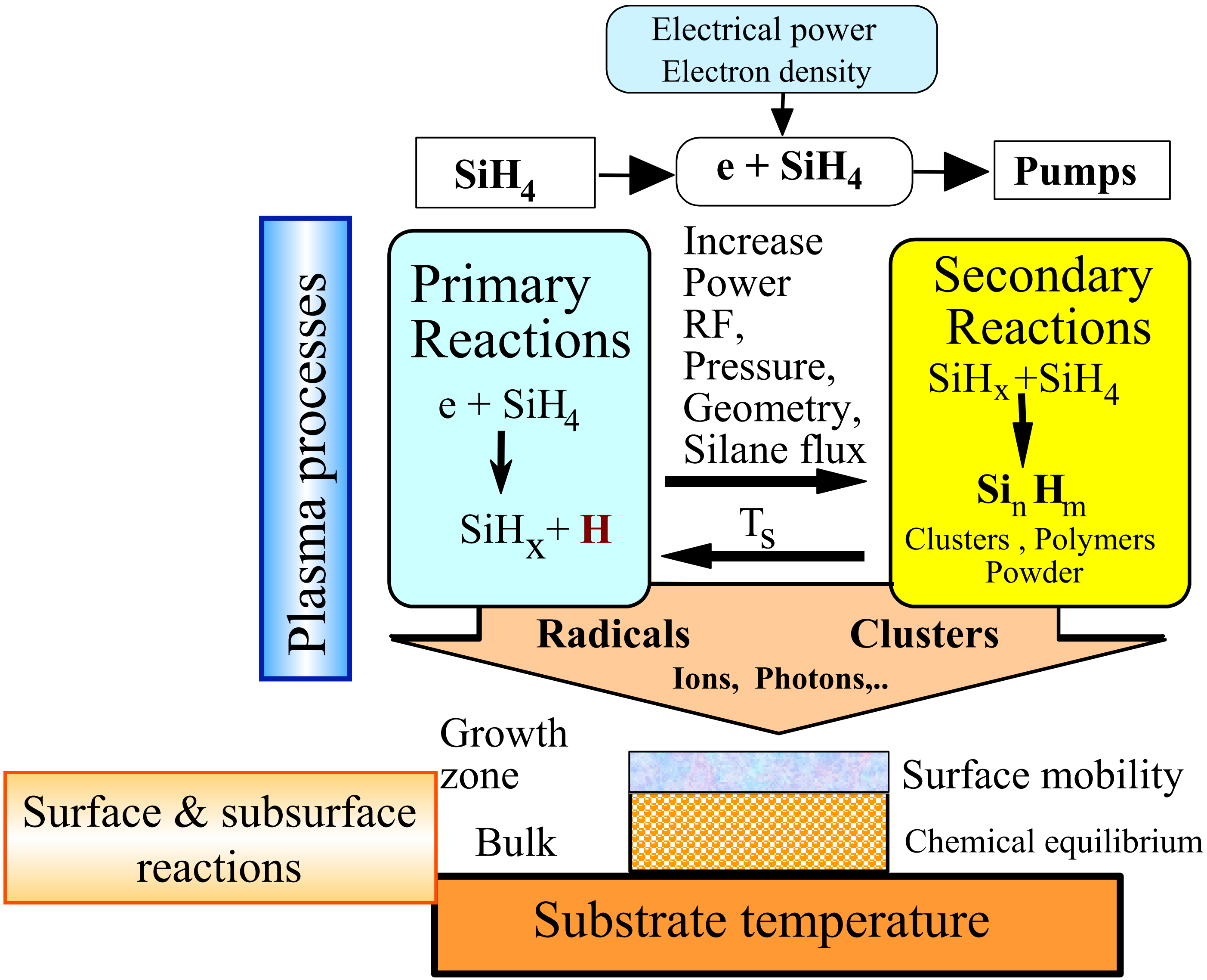

DUST PARTICLE NUCLEATION AND GROWTH

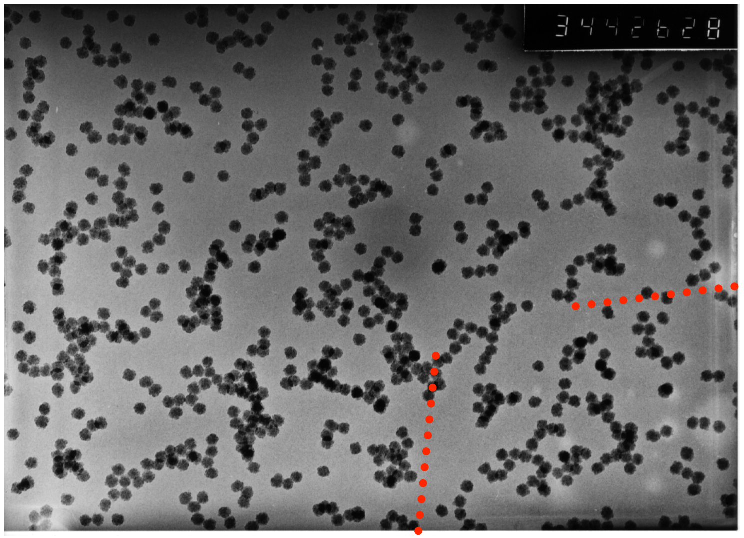

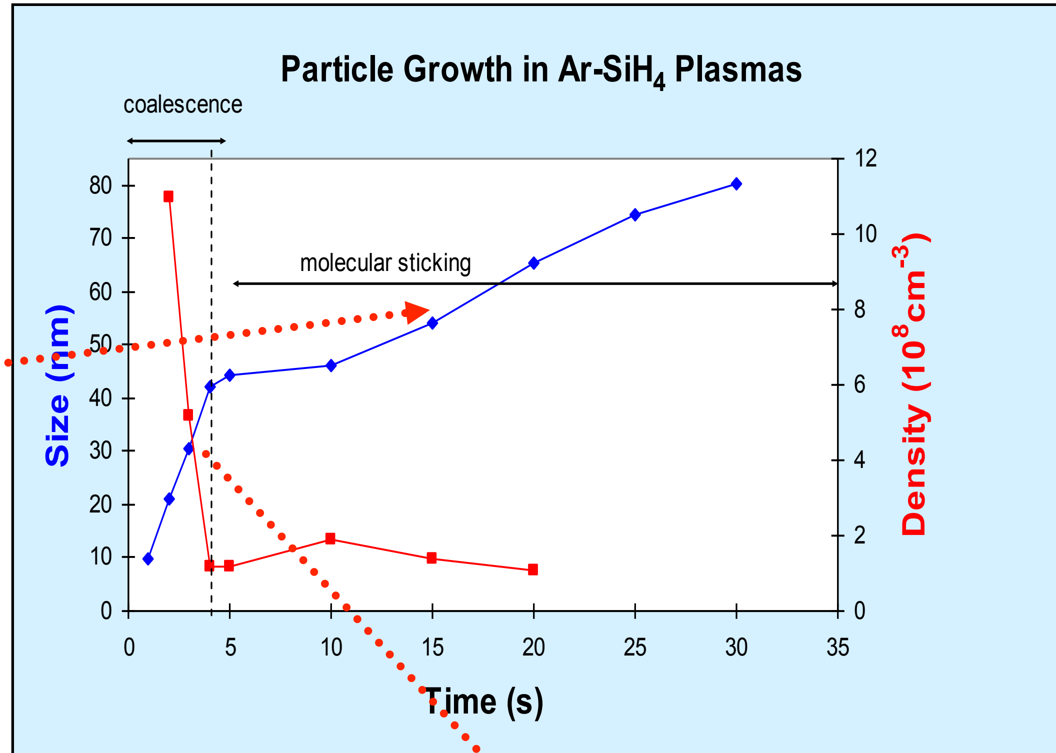

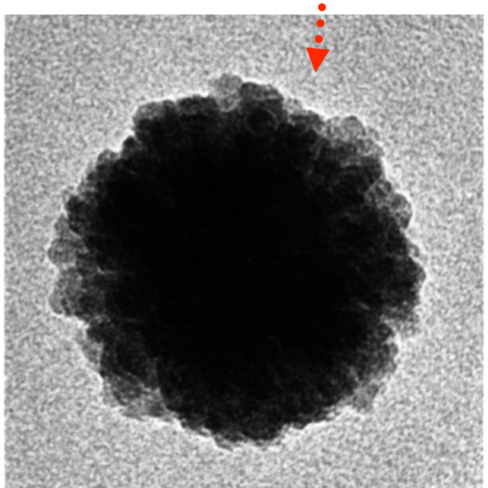

Dark field TEM micrographs evidence elementary structures as 2-3 nm diameter crystallites

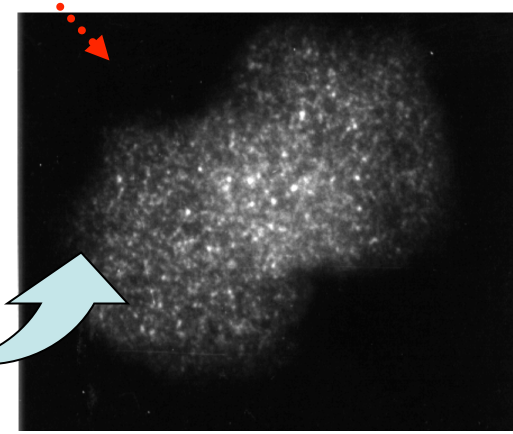

DUST PARTICLE NUCLEATION AND GROWTH

Mass spectrometry data give insights on cluster formation process (1 to few 10 Si atoms)

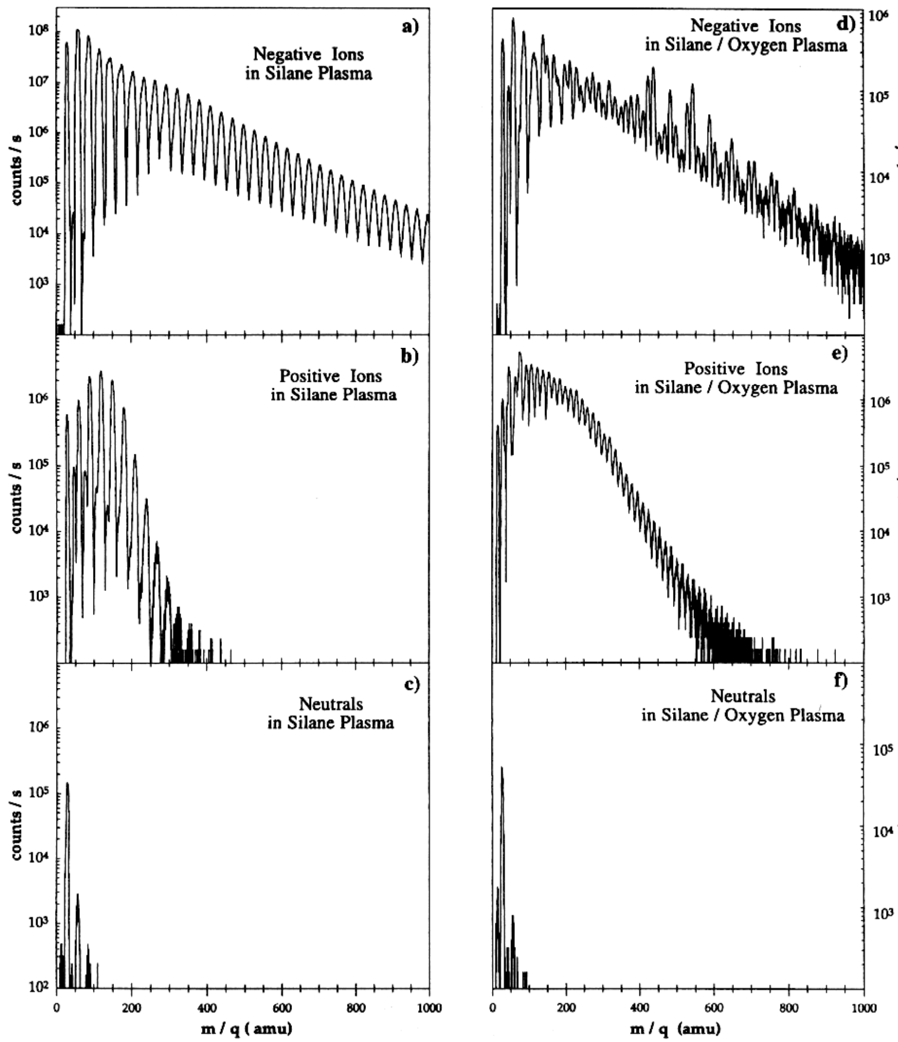

Evidence of a clustering process involving negative ions (trapped)

Clustering models: take into account neutrals, cations, anions

Main route through :

$$[Si_nH_{2n+1}]^- + S_iH_4^*$$

$$[S_{in+1+}H_{2n+3}]^- + 2H$$

$$SiH_3^-$$

Main results : from EPFL, Lausanne
Ch. Hollenstein et al. PSST 3, 278, (1994).

DUST PARTICLE NUCLEATION AND GROWTH

Particle nucleation and growth process : characteristic steps in argon - silane discharge,

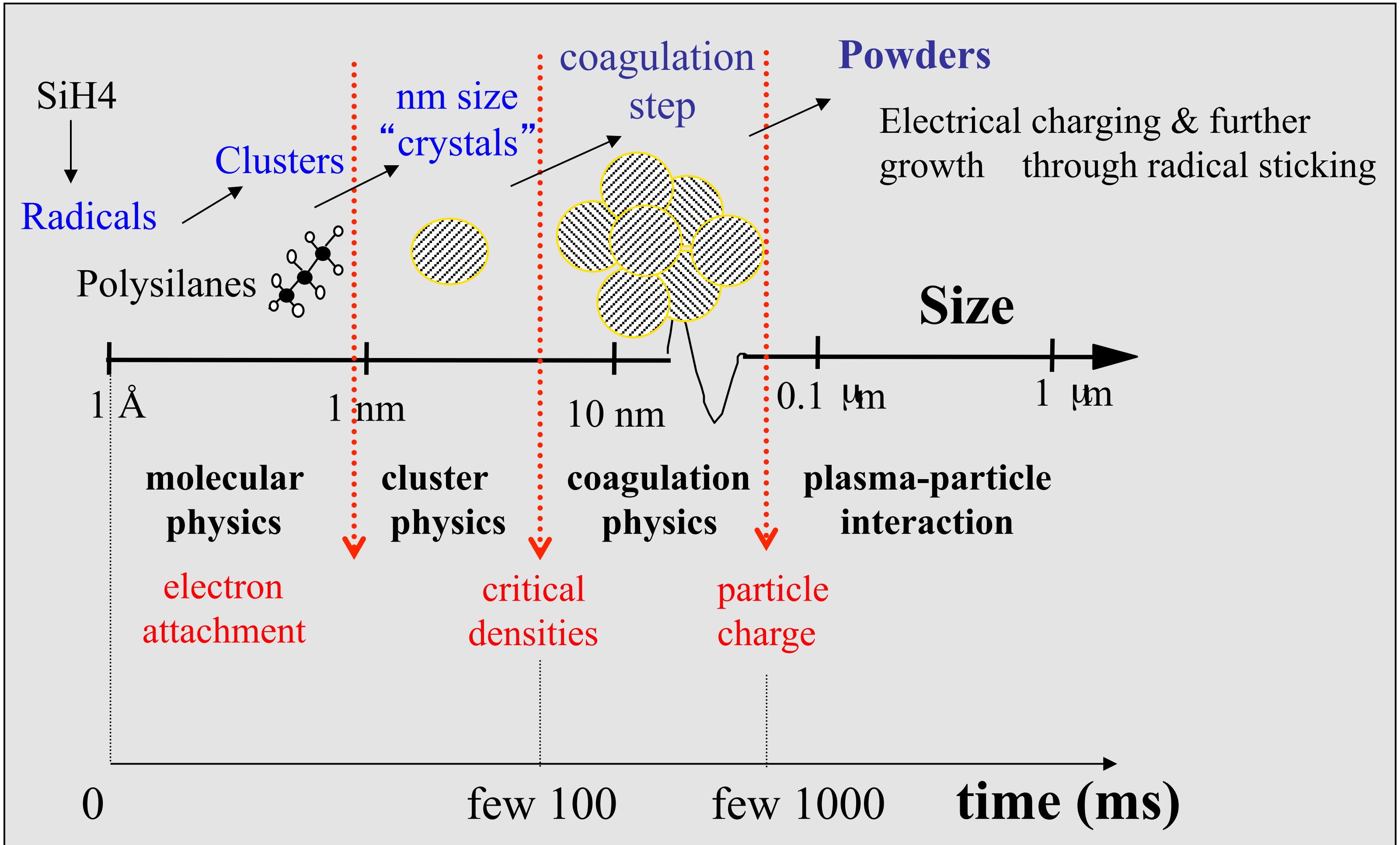

DUST PARTICLE NUCLEATION AND GROWTH

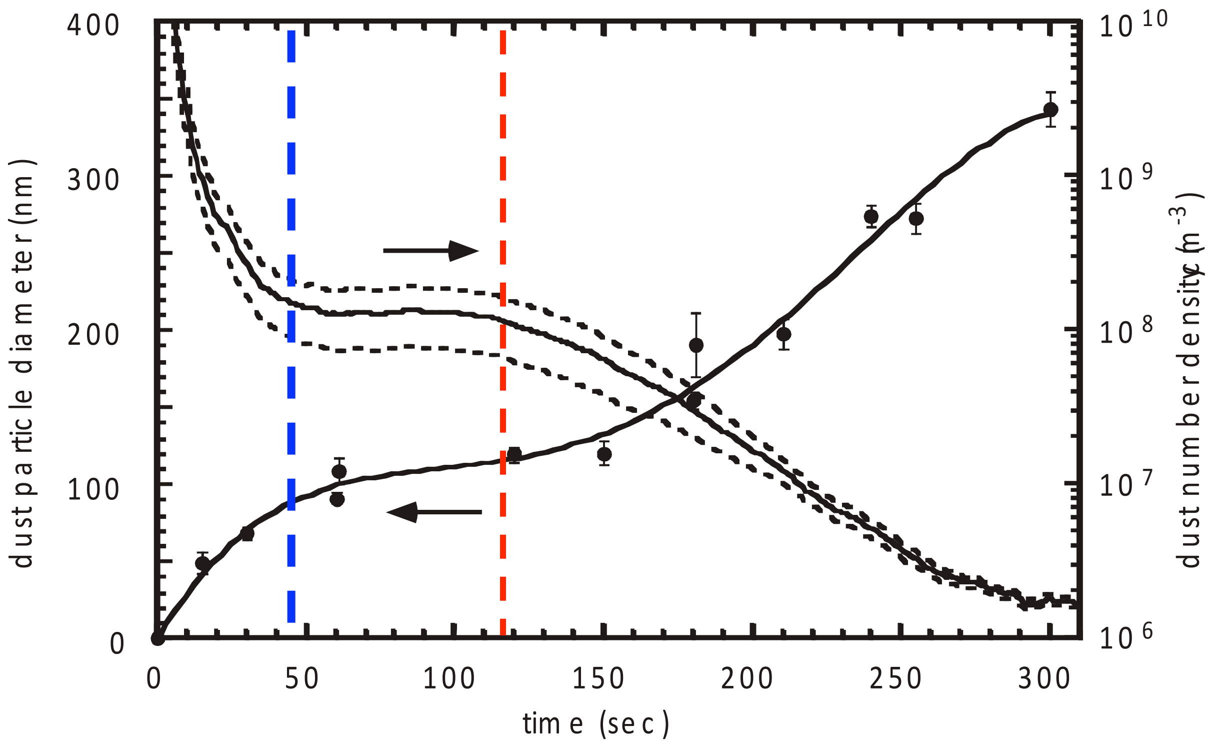

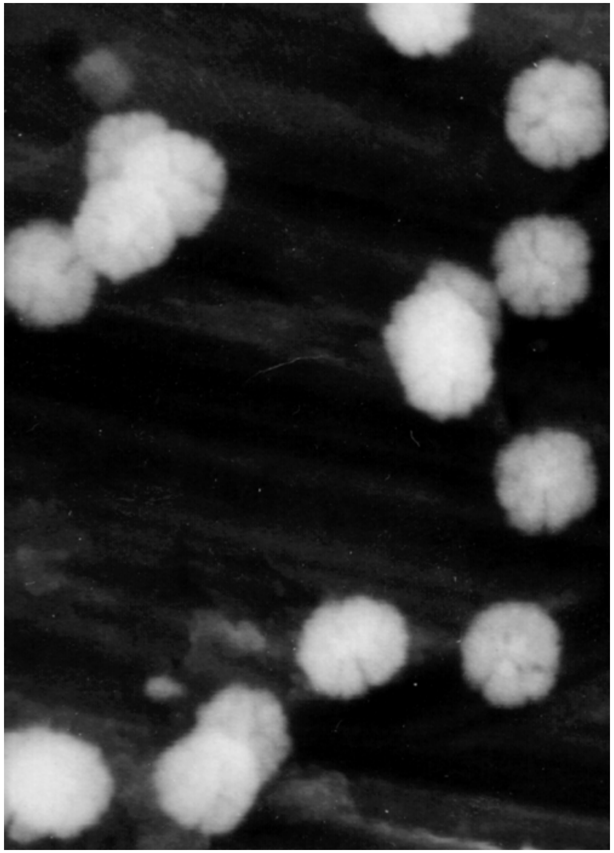

Growth of carbon particles, from sputtering graphite in an rf discharge

D. Samsonov and J. Goree
Particle growth in a sputtering discharge
J. Vac. Sci. Technol. A 1999

This kind of dust can be also obtained in PECVD plasmas in hydrocarbon chemistries. See J. Winter et al work.

DUST PARTICLE NUCLEATION AND GROWTH SIMULATION

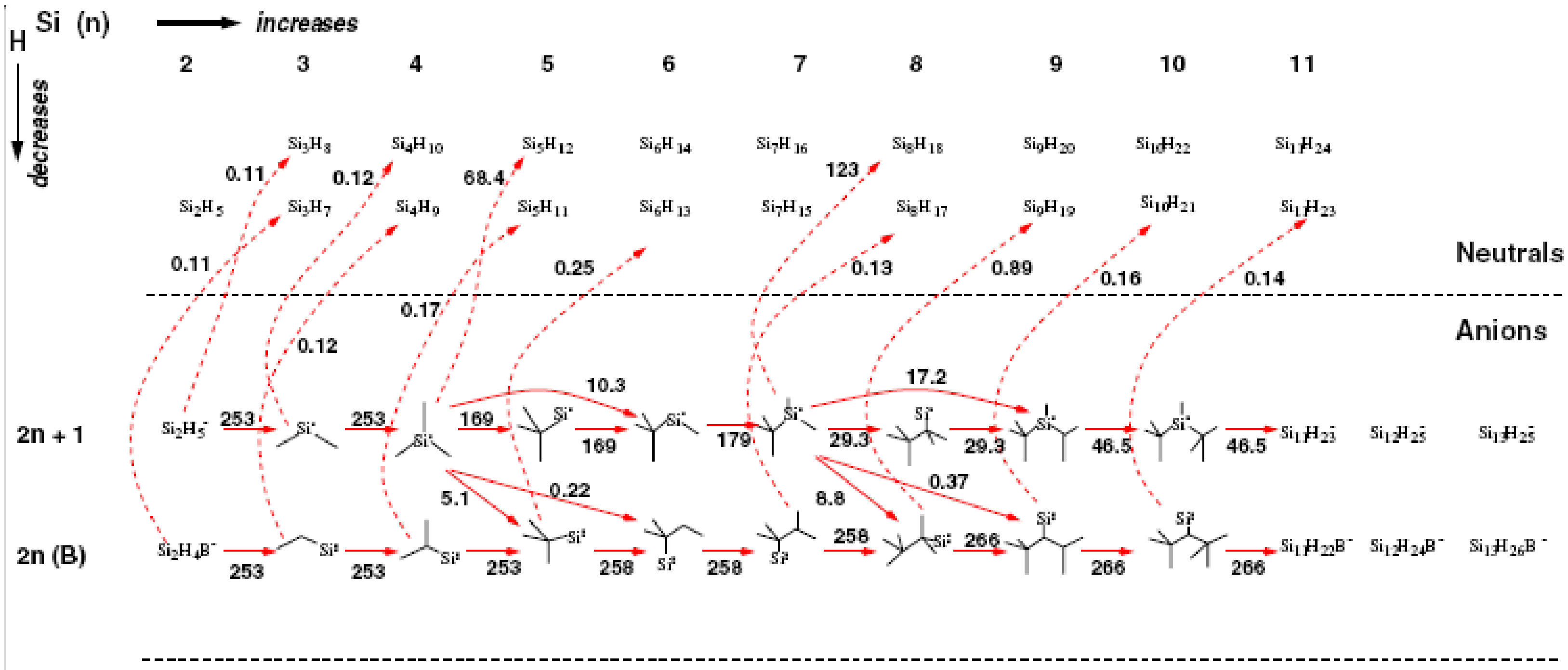

Figure 6. Dominant anionic reaction pathways at steady-state ($T_{gas} = 500$ K, $N_i = 3 \times 10^9$ cm^{-3}); the numbers indicate net reaction rates in units of 10^{-15} mol cm^{-3} s^{-1}.

A. A. Fridman, J. Appl. Phys. 79, 1303, (1996).

U. V. Bhandarkar et al, J. Phys. D 33, 2731-2746, (2000).

K. De Bleeker et al, Phys. Rev. E 69, 056409 (2004)

MOLECULAR DYNAMICS SIMULATION OF NANOCRYSTALLITES GROWTH

Role of the atomic hydrogen

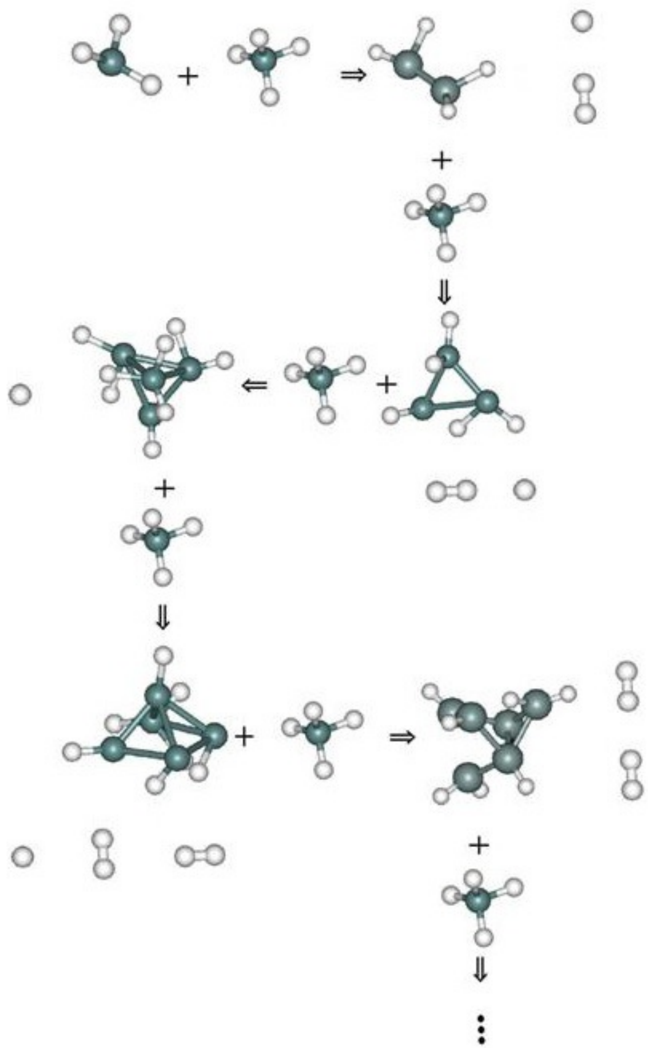

$$SiH_3^- + SiH_4 = Si_2H_5^- + H_2 \quad \Delta H = -0.07 \ \text{eV},$$

$$Si2H_5^- + SiH_4 = Si_3H_7^- + H_2 \quad \Delta H = +0.07 \ \text{eV},$$

$$Si_3H_7^- + SiH_4 = Si_4H_9^- + H_2 \quad \Delta H = +0.07 \ \text{eV},$$

$$Si_4H_9^+ + SiH_4 = Si_5H_{11}^- + H_2 \quad \Delta H = 0.00 \ \text{eV},$$

$$Si_nH_{2n+1}^- + SiH_4 = Si_{n+1}H_{2n+3}^- + H_2.$$

In order to activate these chemical reactions the silane molecules must be vibrationally excited

See Fridman et al, J. App. Phys. 79, 1303 (1996).

MOLECULAR DYNAMICS SIMULATION OF NANOCRYSTALLITES GROWTH

Typical structures of hydrogenated silicon nanoparticles formed starting from these chemical reactions

(a) Example of amorphous structure resulting from a growth mechanism in a pure silane plasma at room temperature in the absence of atomic hydrogen;

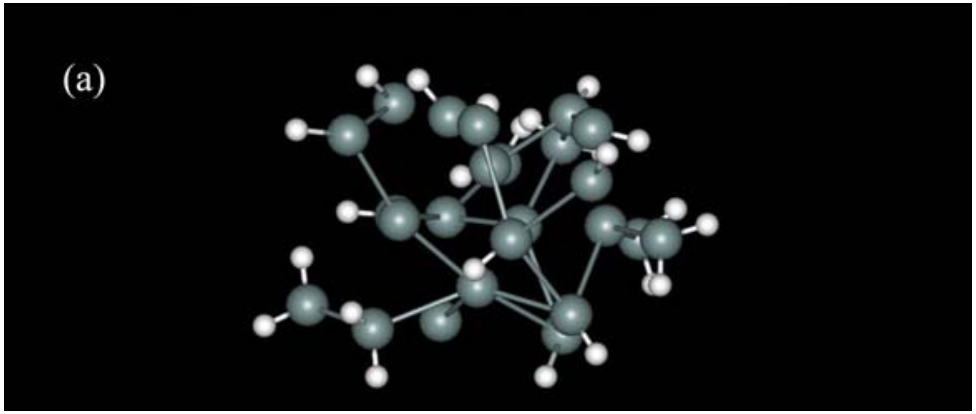

Q. Brulin, N. Ning, H Vach, J. Non-Cryst. Solids 352, 1055-1058 (2006)

MOLECULAR DYNAMICS SIMULATION OF NANOCRYSTALLITES GROWTH

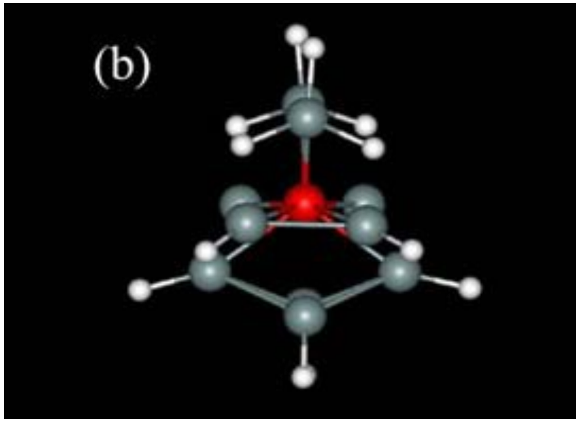

(b) **Low atomic hydrogen flux giving rise to crystalline structures that are rich in hydrogen.**

Q. Brulin, N. Ning, H Vach, J. Non-Cryst. Solids 352, 1055-1058 (2006)

MOLECULAR DYNAMICS SIMULATION OF NANOCRYSTALLITES GROWTH

(c) **High atomic hydrogen flux yielding crystalline structures relatively poor in hydrogen that are similar to those predicted for pure silicon clusters;**

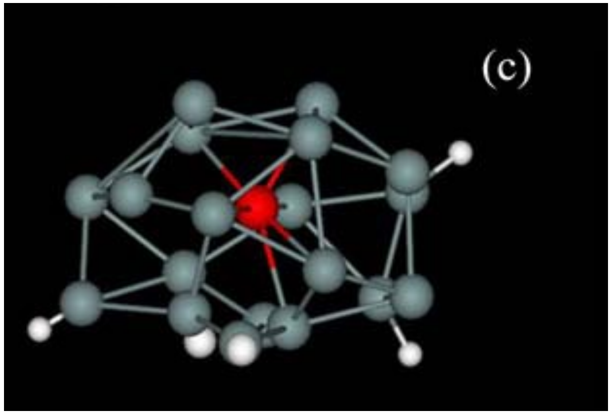

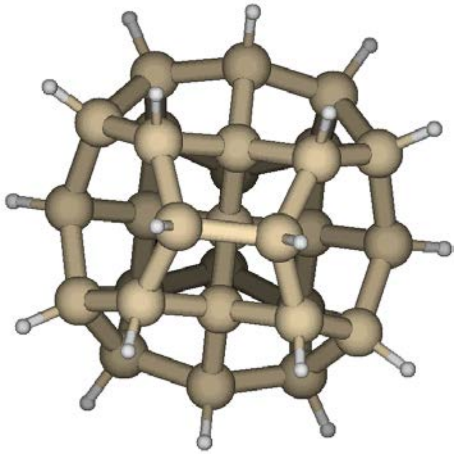

$Si_{29}H_{24}$ cluster under hydrogen bombardment

Q. Brulin, N. Ning, H Vach, J. Non-Cryst. Solids 352, 1055-1058 (2006)

NANOPARTICLE DETECTION AND METROLOGY

LASER LIGHT SCATTERING

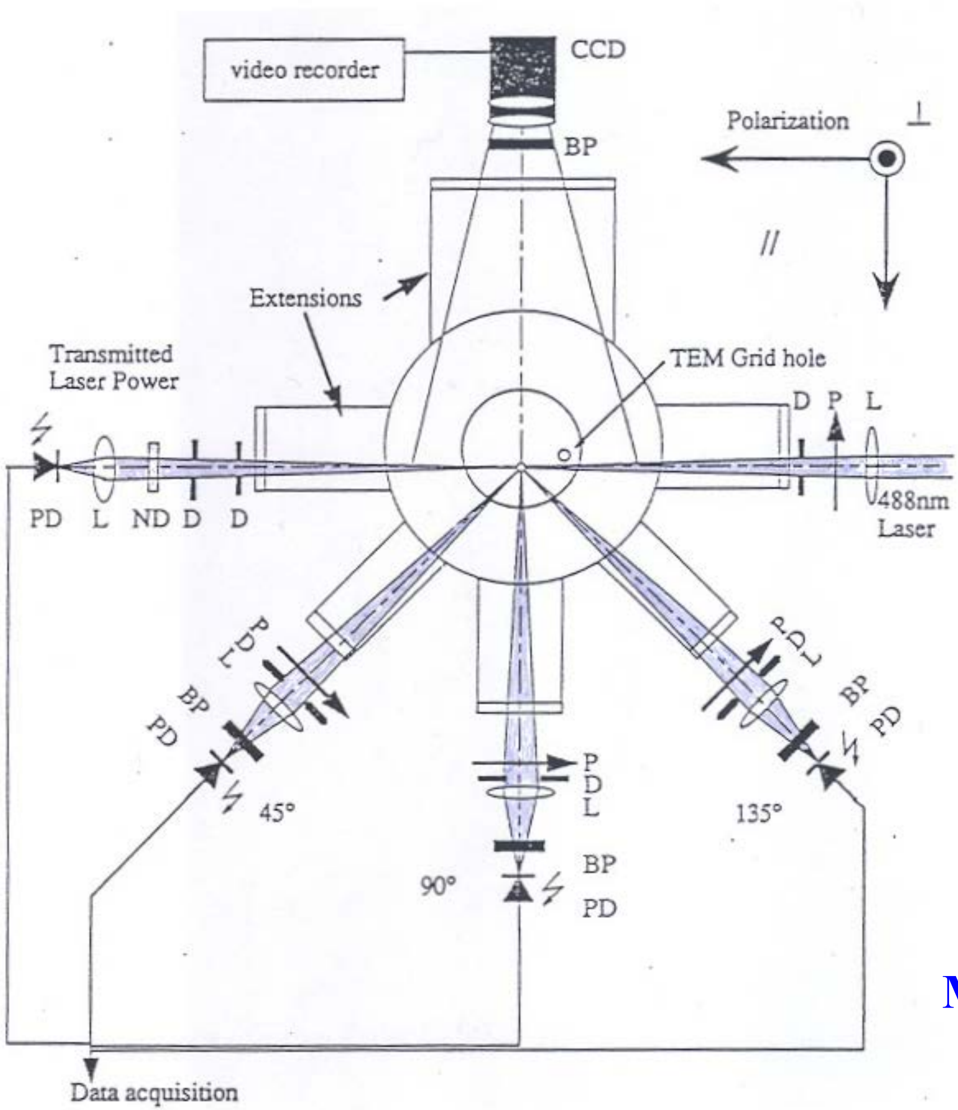

Ch. Hollenstein et al, PSST3, (1994), 278.

$$I_{\perp}=C\cdot\Delta V\cdot\Delta\Omega\cdot n_p\cdot\frac{16\pi^4}{\lambda^4}\cdot r_p^6\cdot\left|\frac{m^2-1}{m^2+2}\right|^2\cdot I_{\perp}^i$$

$$I_{//}=C\cdot\Delta V\cdot\Delta\Omega\cdot n_p\cdot\frac{16\pi^4}{\lambda^4}\cdot r_p^6\cdot\left|\frac{m^2-1}{m^2+2}\right|^2\cdot I_{//}^i\cdot\cos^2\theta$$

The scattered intensity allows the detection but contains also information about the size, concentration and refractive index.

Multi-angle laser light scattering.

NANOPARTICLE DETECTION
LASER LIGHT SCATTERING

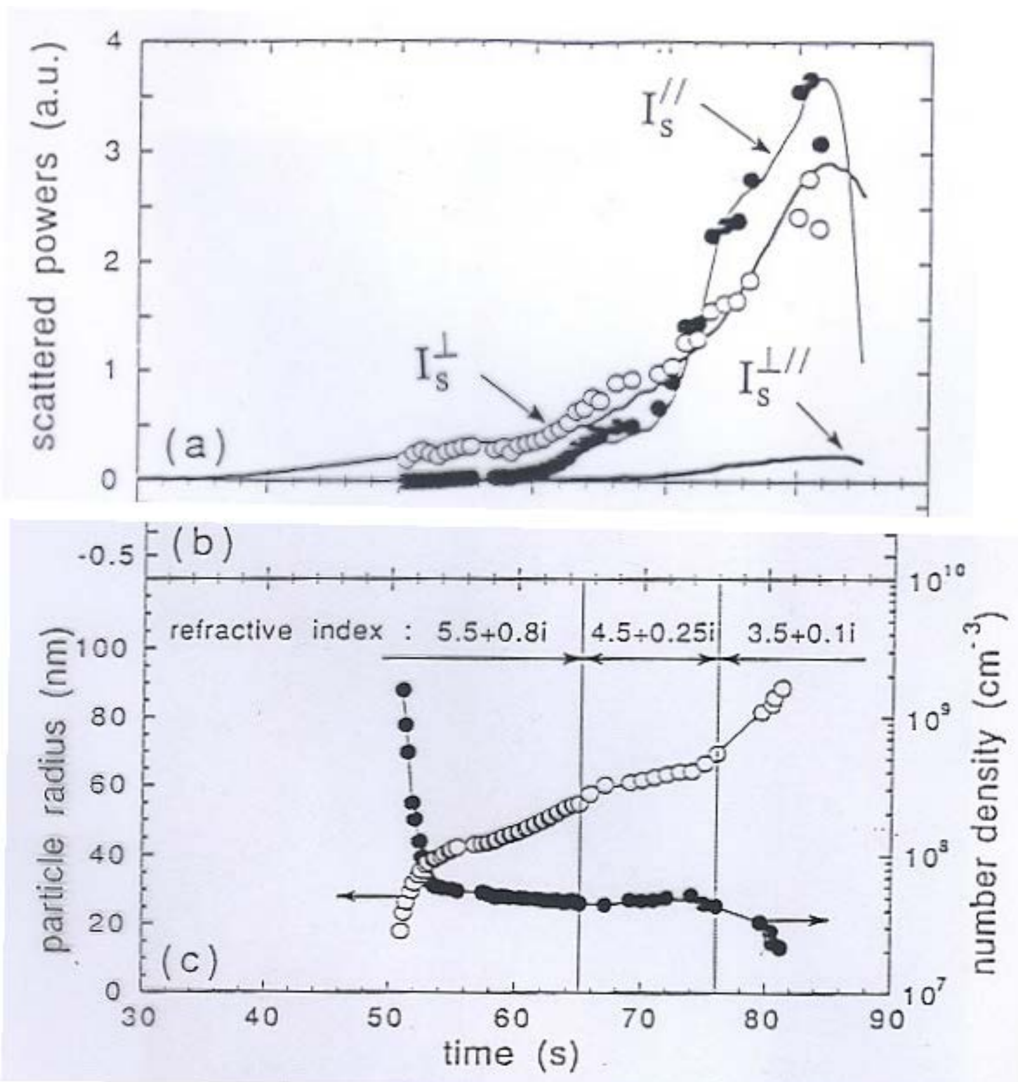

Ch. Hollenstein et al, PSST3, (1994), 278.

Time evolution of the scattered intensities for the two polarization directions.

Time evolution of the size, concentration and refractive index of the dust particles during their growth.

NANOPARTICLE DETECTION

In this size range : Rayleigh scattering $\propto r_p^6 / \lambda^4$
sophisticated techniques for signal recovery

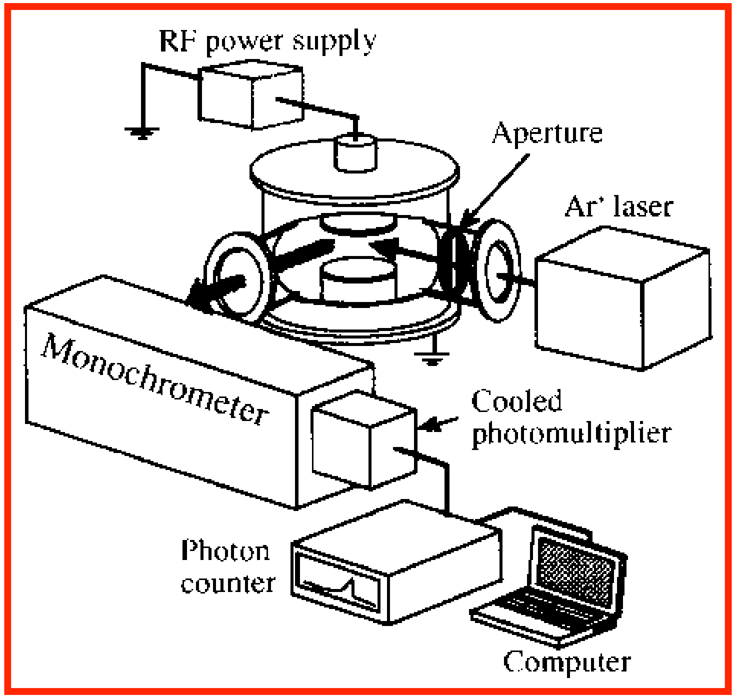

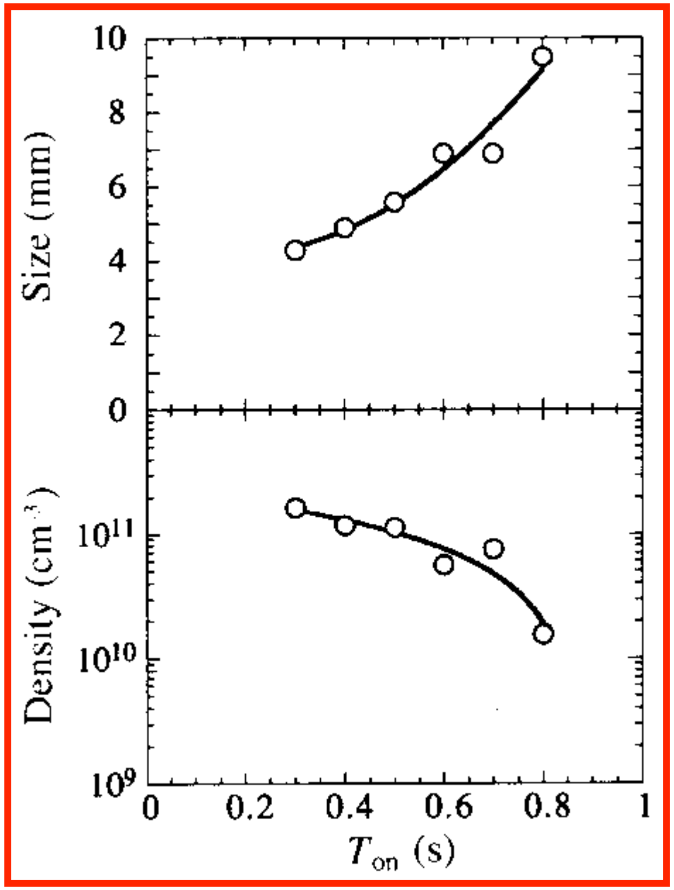

Photon counting techniques : *M. Shiratani and Y. Watanabe, The Revue of Laser Engineering 26, 449-452 (1998).*

NANOPARTICLE DETECTION
LASER INDUCED INCANDESCENCE

Mainly used for soot particles detection

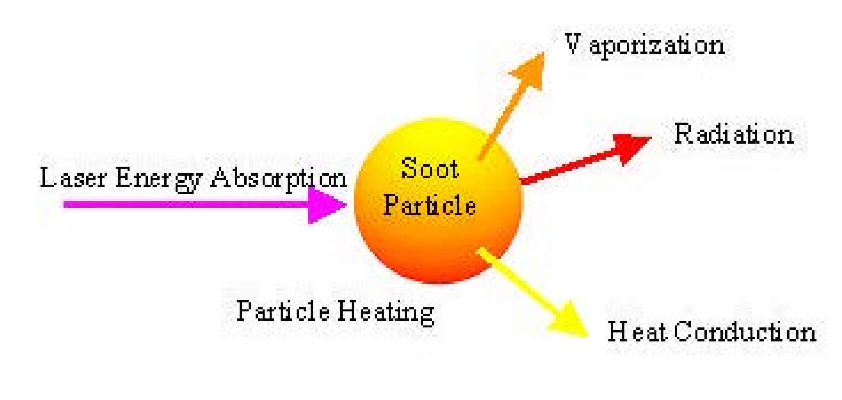

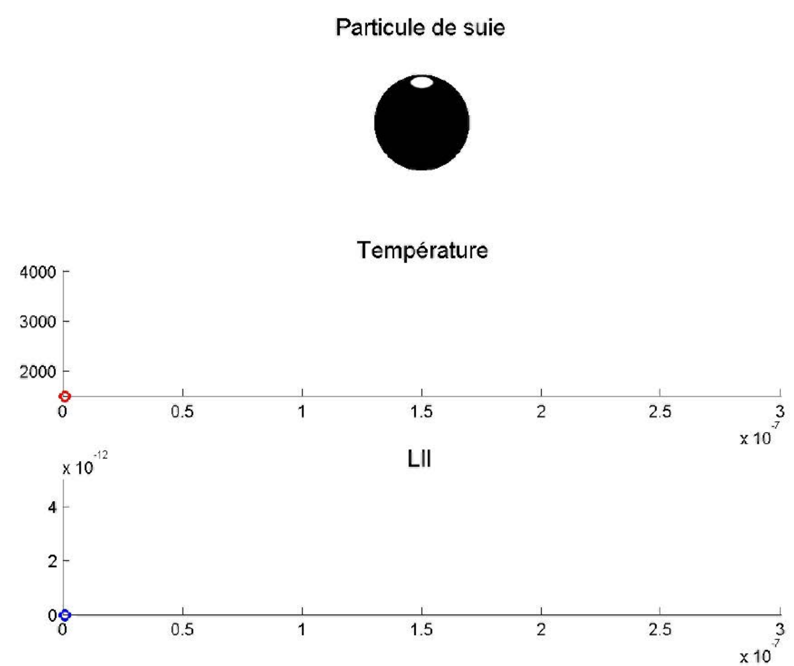

I_{LII} is proportional to the dust particles volume fraction.

Decrease characteristic time depends on the dust particle size.

A. Boiarciuc et al Applied Physics B83, (2006), 413.

NANOPARTICLE DETECTION
LASER INDUCED EVAPORATION

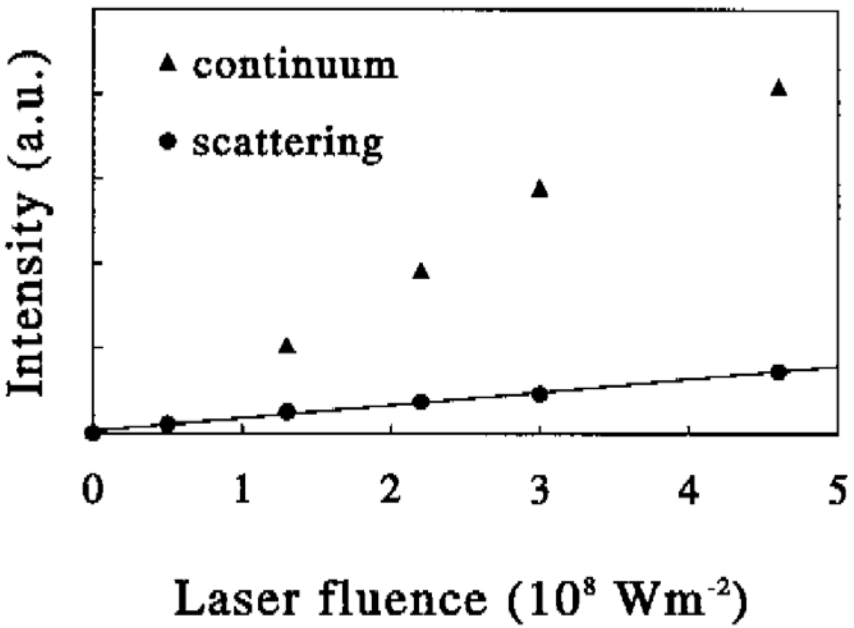

The emitted signal from the heated dust particles is much intense than the scattered one.

W. W. Stoffels et al Appl. Phys Letter 74, (1993), 259

NANOPARTICLE DETECTION
LASER INDUCED PARTICLE EXPLOSIVE EVAPORATION (LIPEE).

- Method based on the particle explosive evaporation induced by laser irradiation (LIPEE)

- Detection of particles in the nanometer scale and evidence of the 3 different growth phases.
- This experiment was performed using an XeCl laser (308 nm) with an energy density of 400 MW/cm^2.

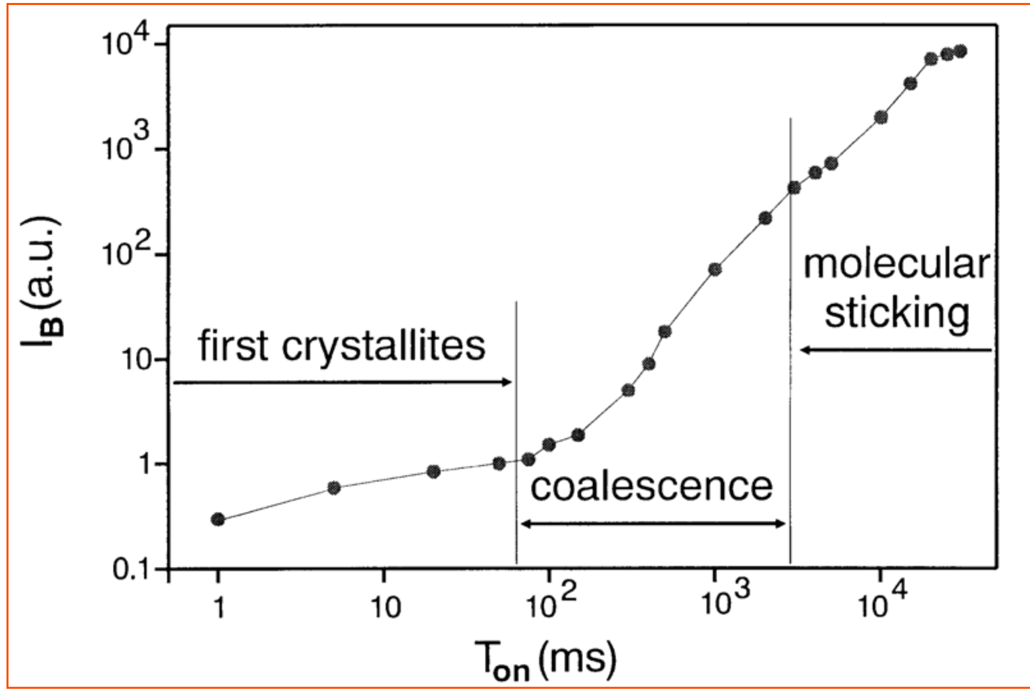

(L. Boufendi et al, J. Appl. Phys. 76, 148, 1994).

NANOPARTICLE DETECTION
LASER INDUCED PARTICLE EXPLOSIVE EVAPORATION (LIPEE).

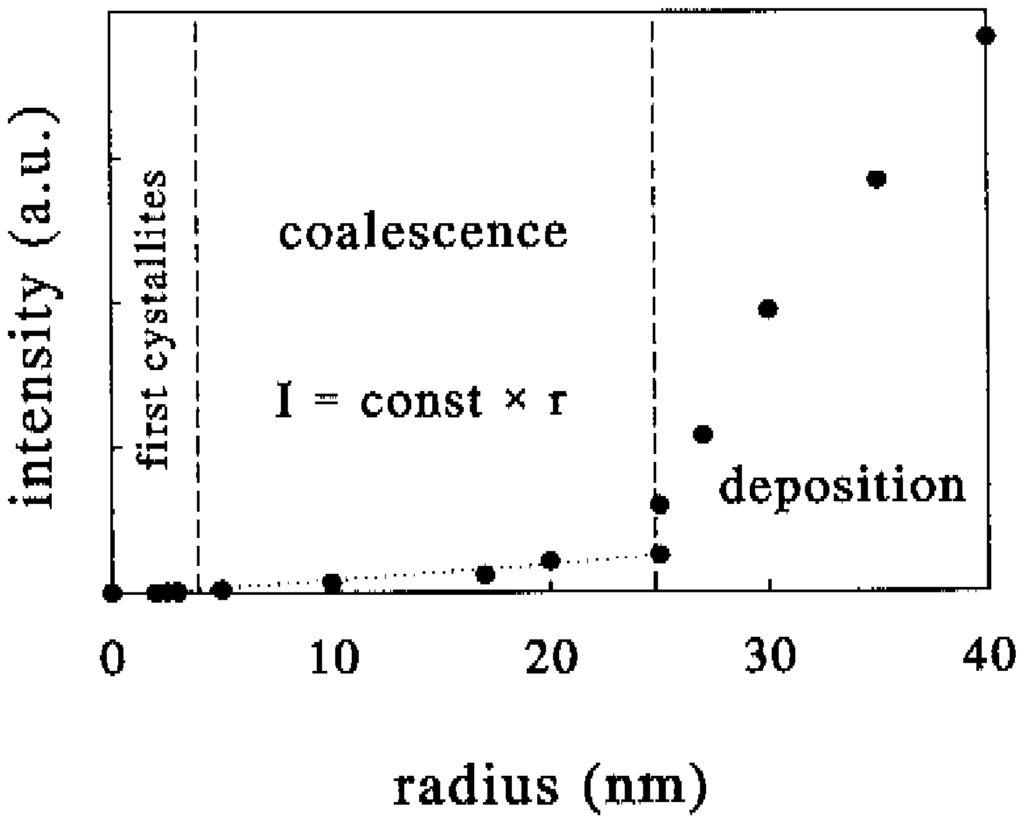

The LIPEE signal intensity is rather proportional to the dust particle size.

For the detection of particles formed in an industrial reactor these methods cannot be used. We have to look for other diagnostic tools.

We have to use the plasma and discharges properties.

NANOPARTICLE DETECTION

Using discharge properties

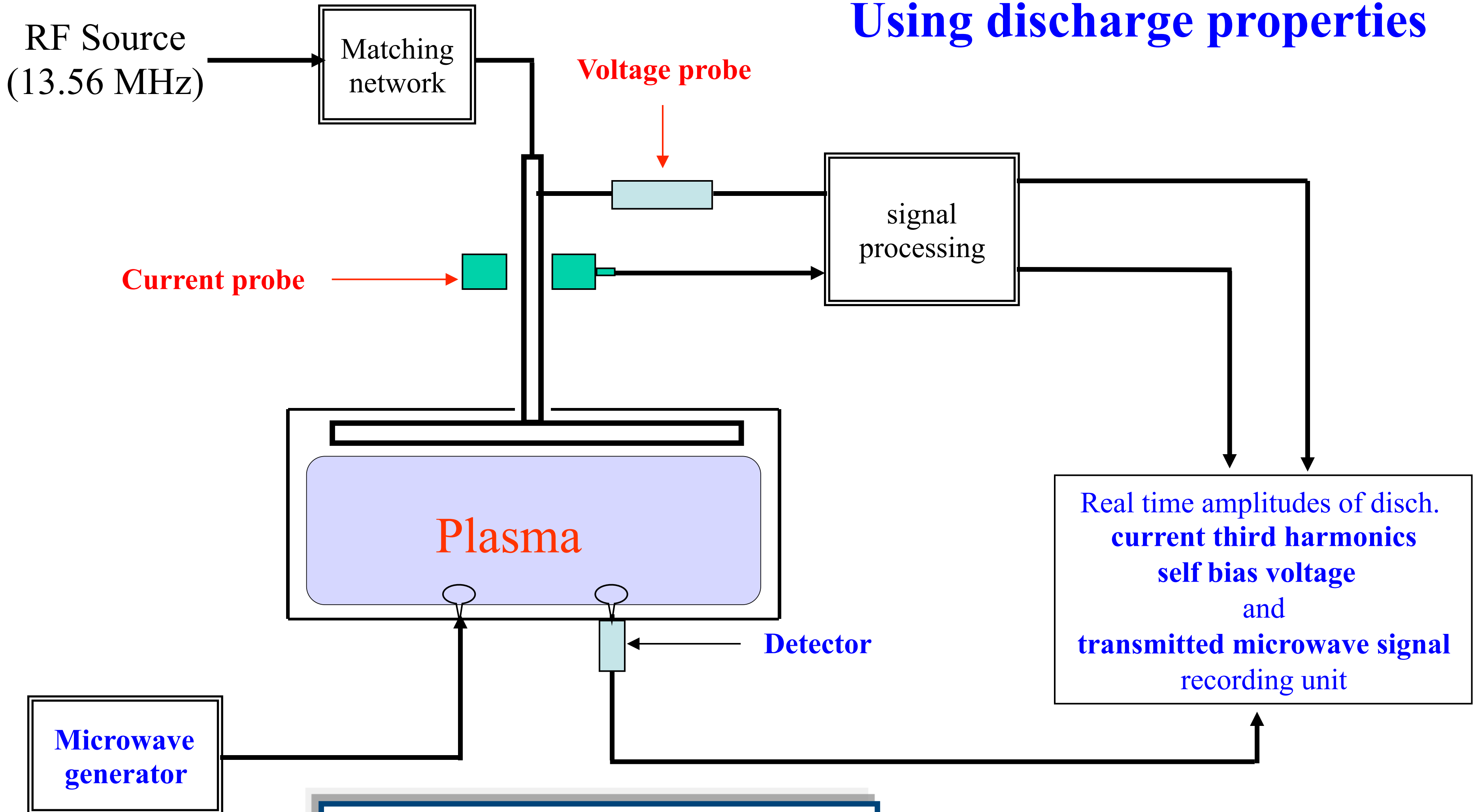

Gas Argon : 30 sccm Silane : 1.2 sccm
Pressure : 120 µbar
Gas temperature - 30°C , 150°C
RF power 10 W

NANOPARTICULES DETECTION

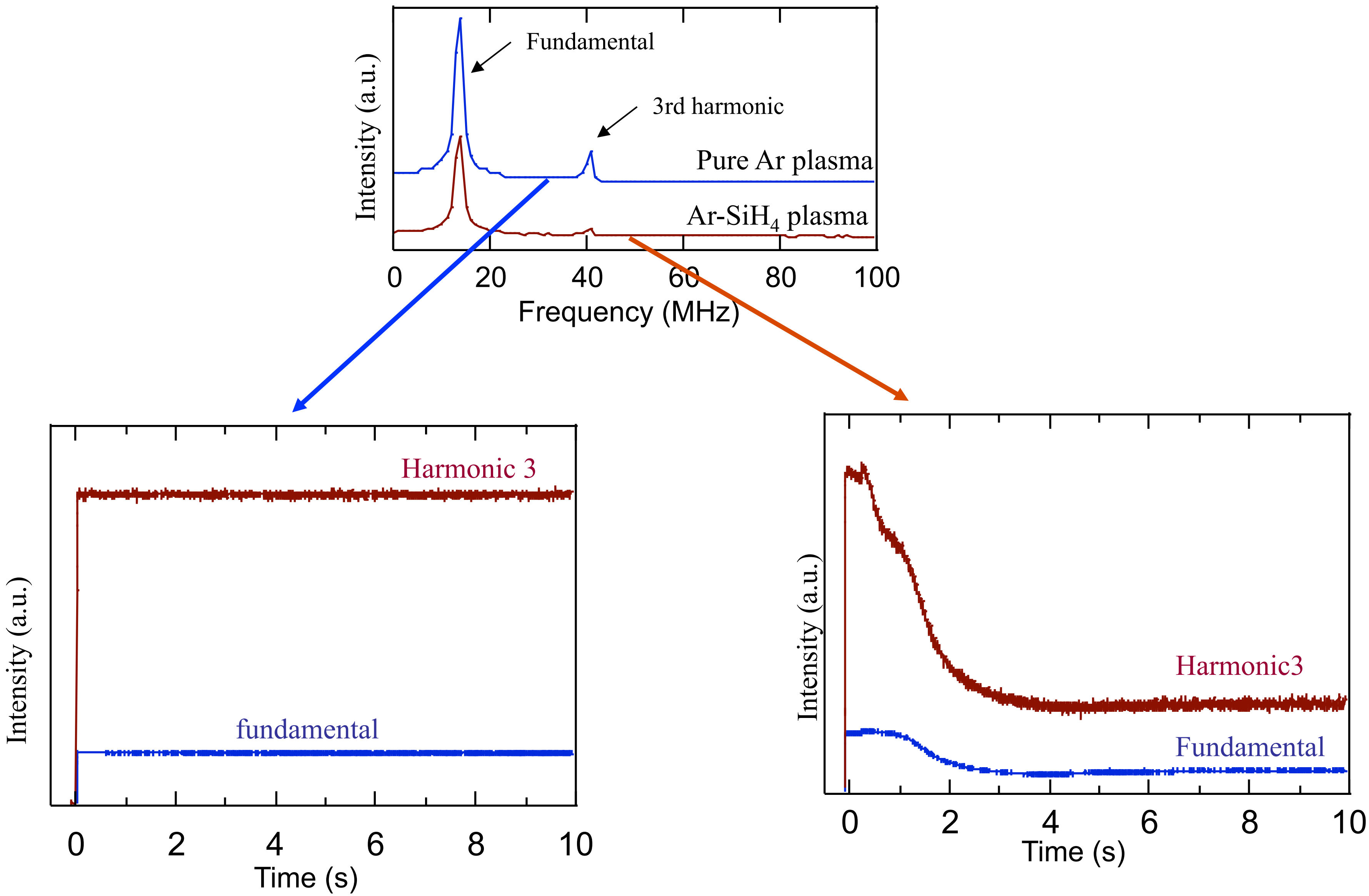

NANOPARTICLE DETECTION

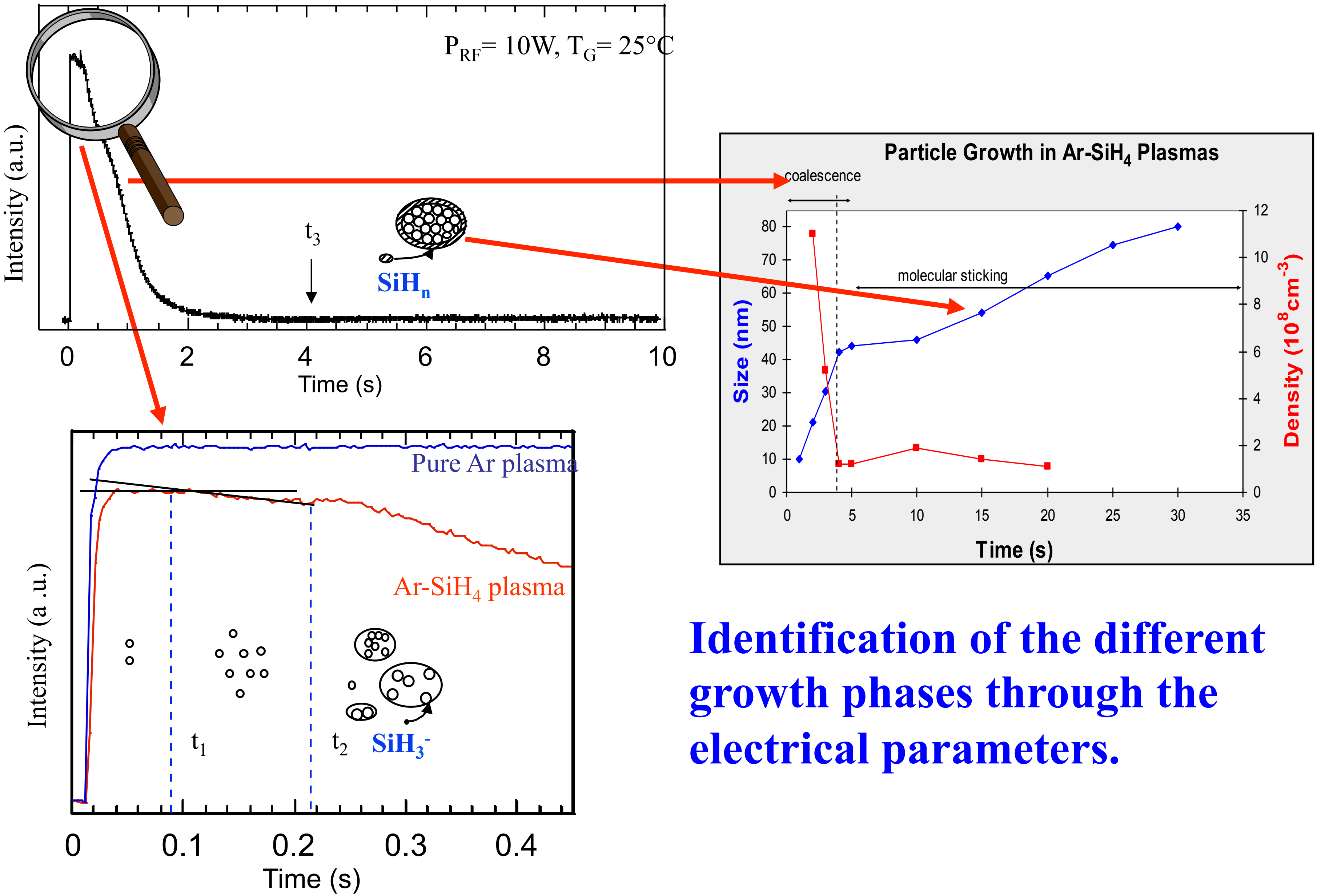

Identification of the different growth phases through the electrical parameters.

NANOPARTICLE DETECTION

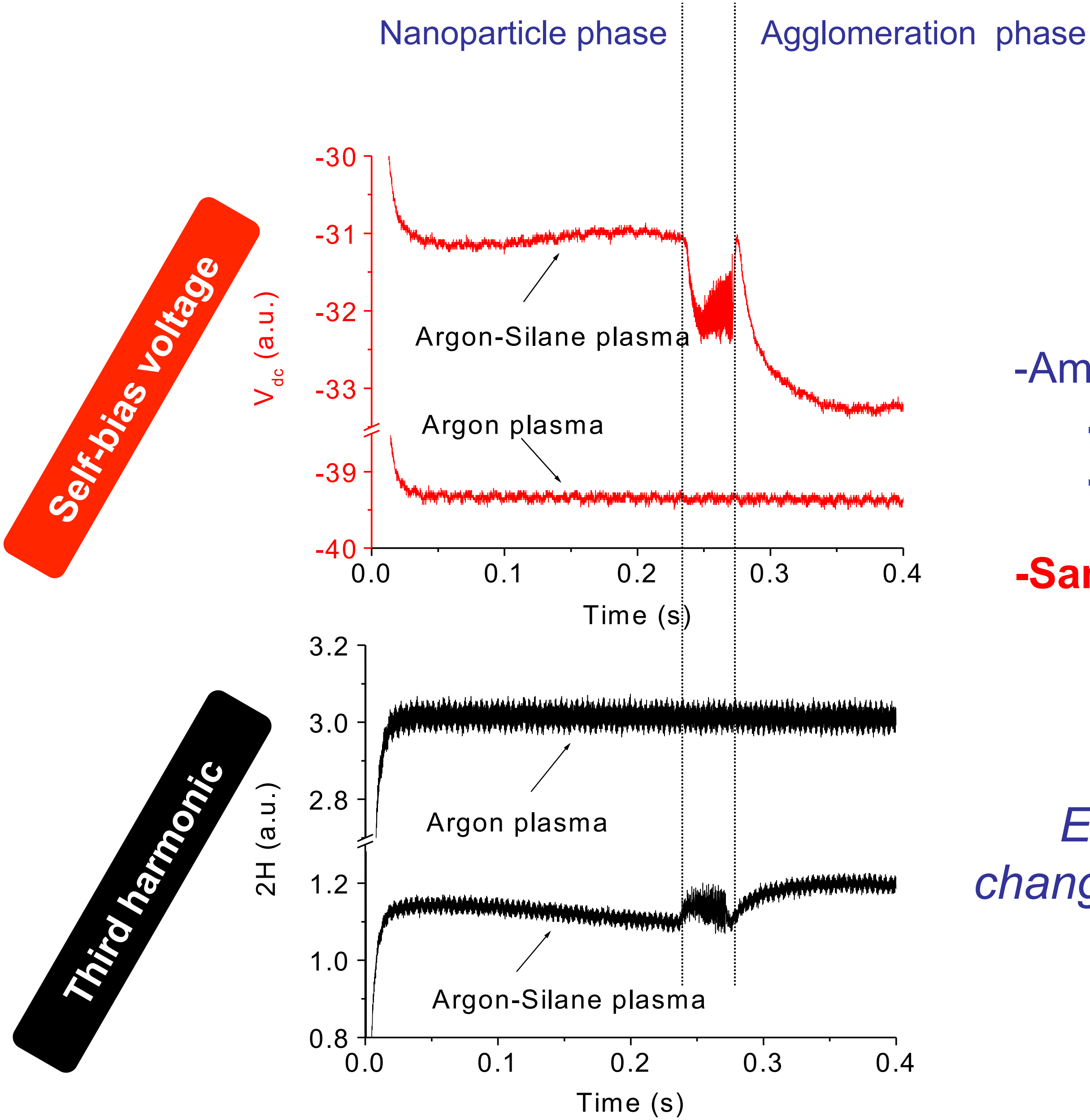

-Amplitudes of 3H and V_{dc} are :

. constant in Ar plasma

. affected in Ar-SiH4 plasma

-Same trends in 3H and V_{dc}

Evolutions are due to change in plasma impedance

NANOPARTICLE DETECTION

Electrical measurements validation

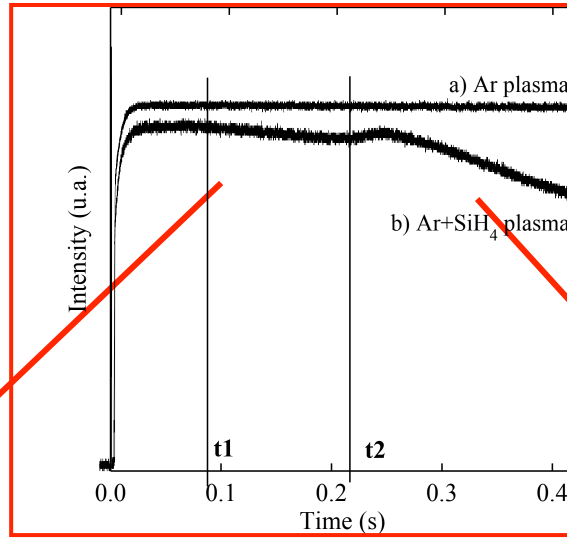

16 Run, 10 W, 100 ms

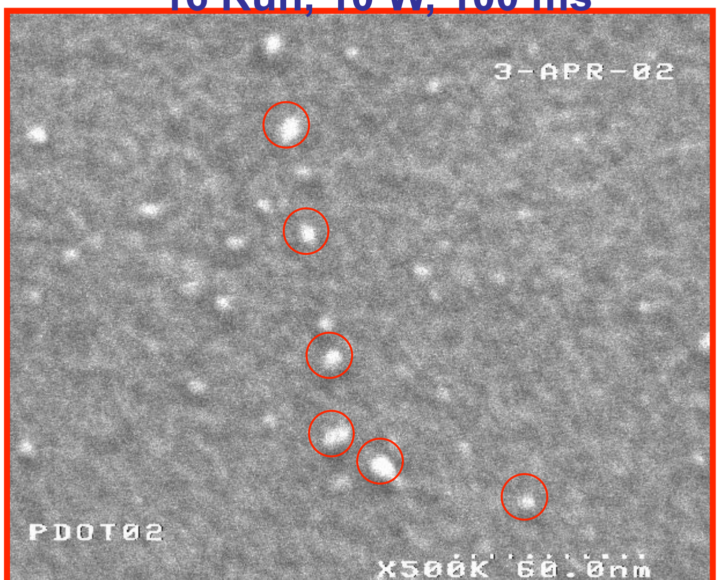

NANOPARTICLE PHASE

SEM

16 Run, 10 W, 200 ms

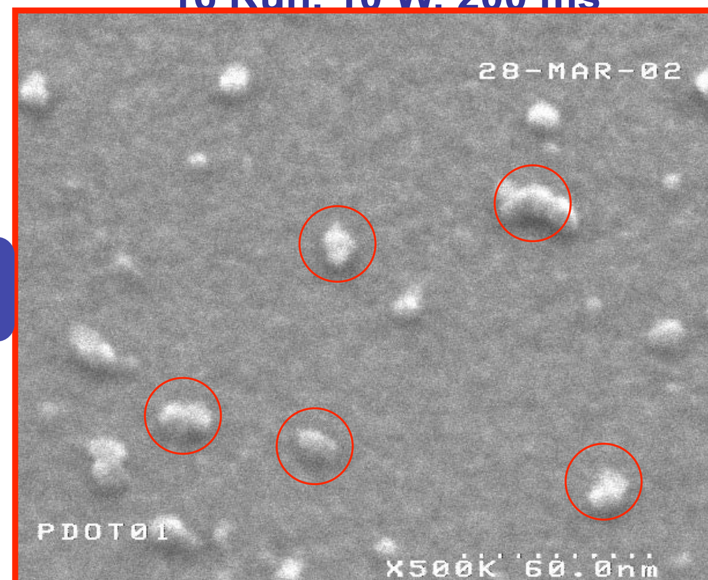

COAGULATION PHASE

NANOPARTICLE DETECTION

Detection of multigeneration systems

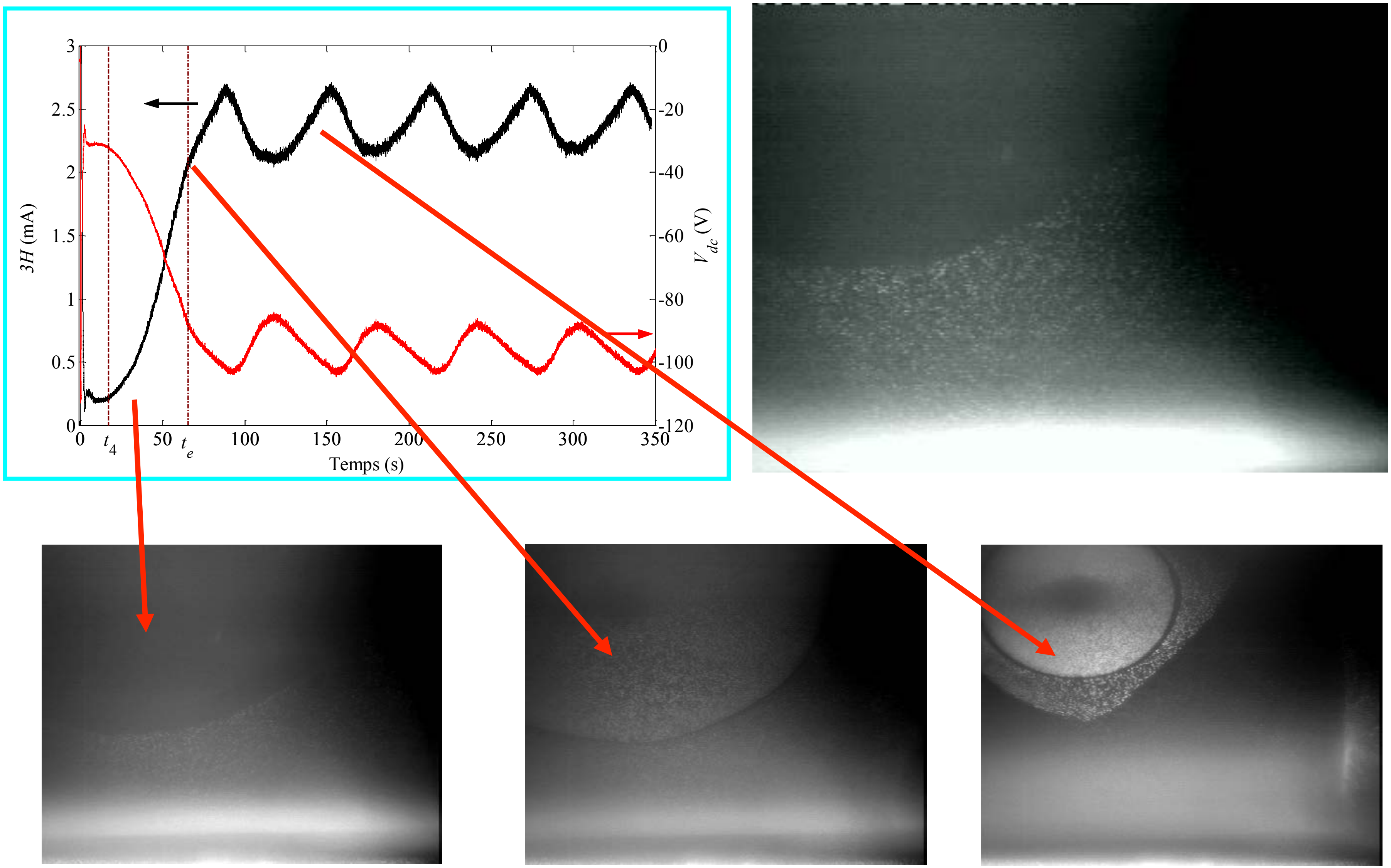

MICROWAVE RESONANT CAVITY METHOD

Basic relation used to calculate the electron density :

$$n_e = \frac{2m_e\varepsilon_0(2\pi f)^2 \Delta f}{e^2 f_0}$$

f: resonance frequency with plasma
f_0:resonance frequency without plasma
Δf: f-f_0

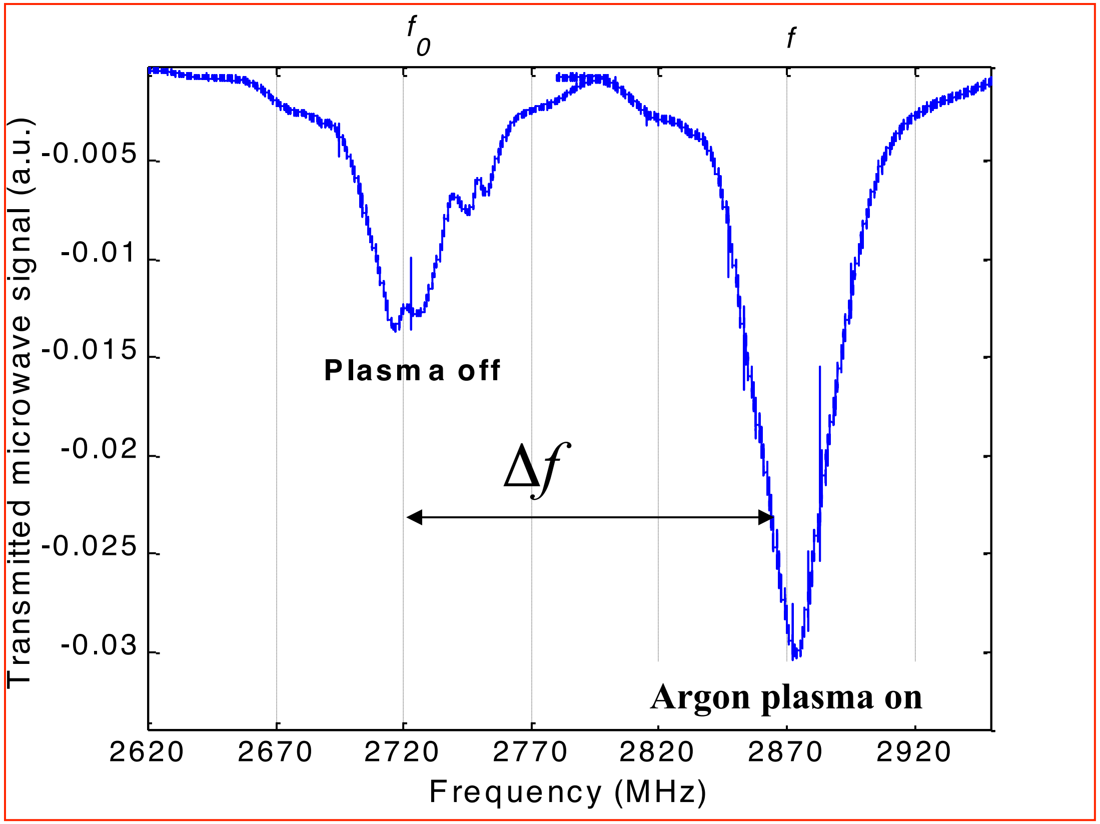

mode TM_{110} f=2.72GHz

For a pure Ar plasma (30sccm, 10W) : n_e=1.2 $10^{16}$$m^{-3}$

NANOPARTICLE DETECTION

Correlation between the electron density and electrical parameters.

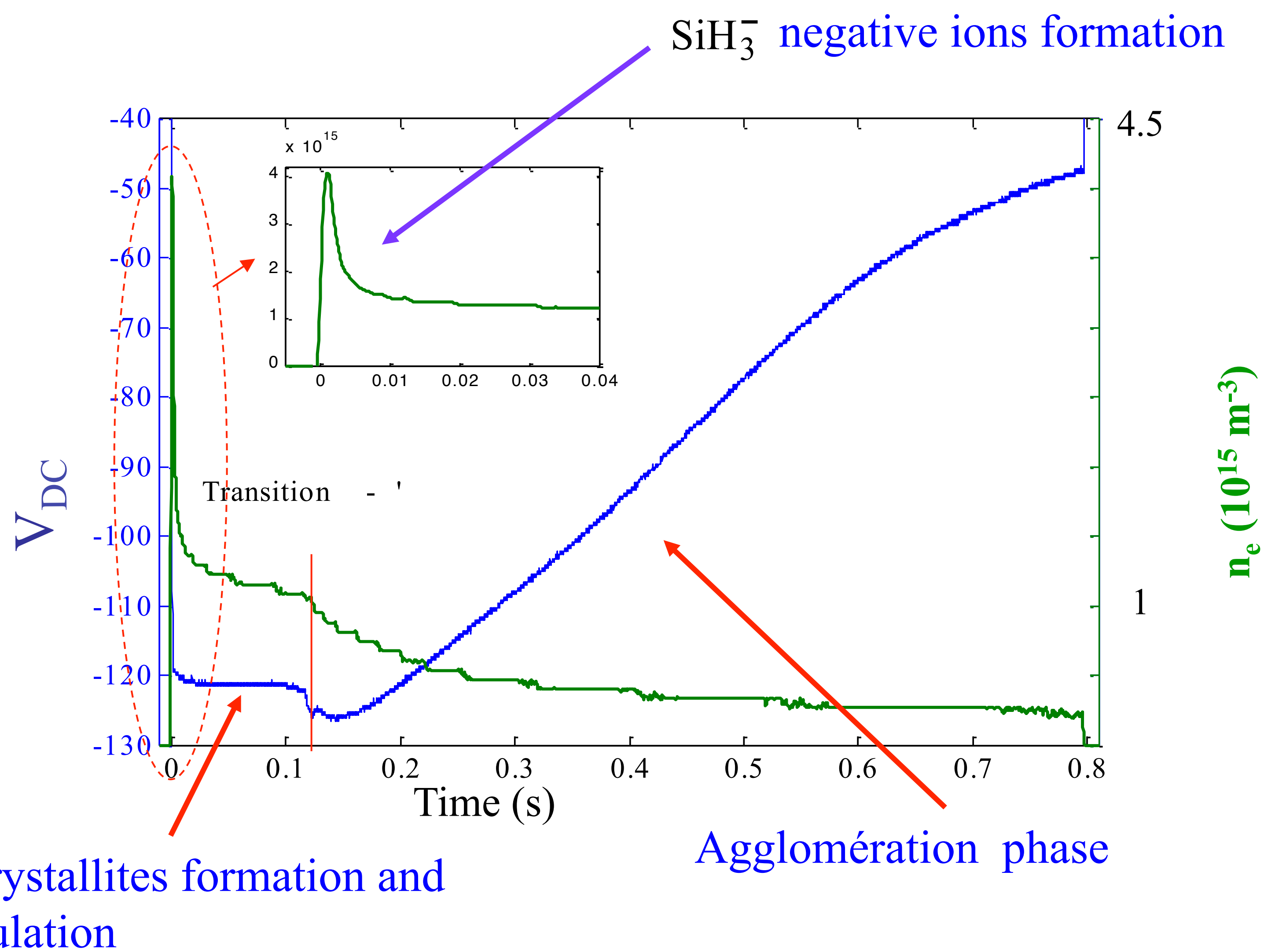

NANOPARTICLE DETECTION

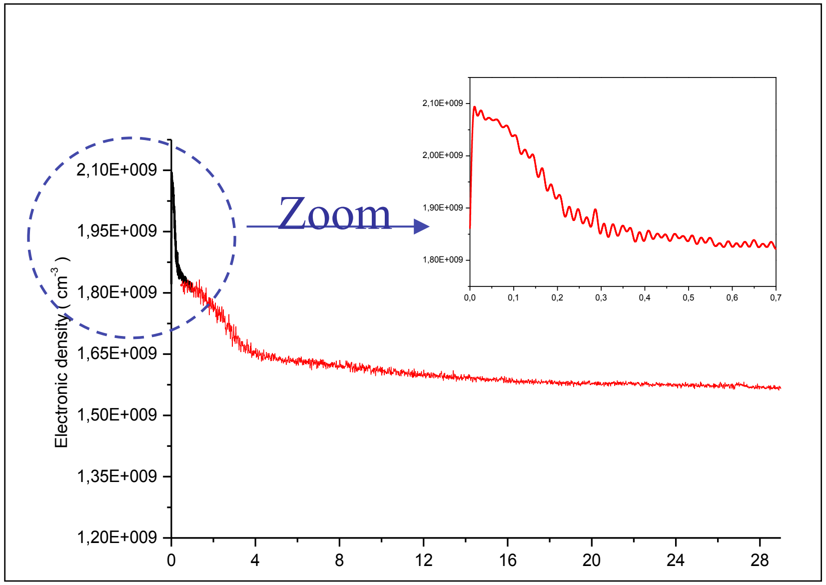

Similarity between the two chemistries

$N_2 – CH_4$ Chemistry

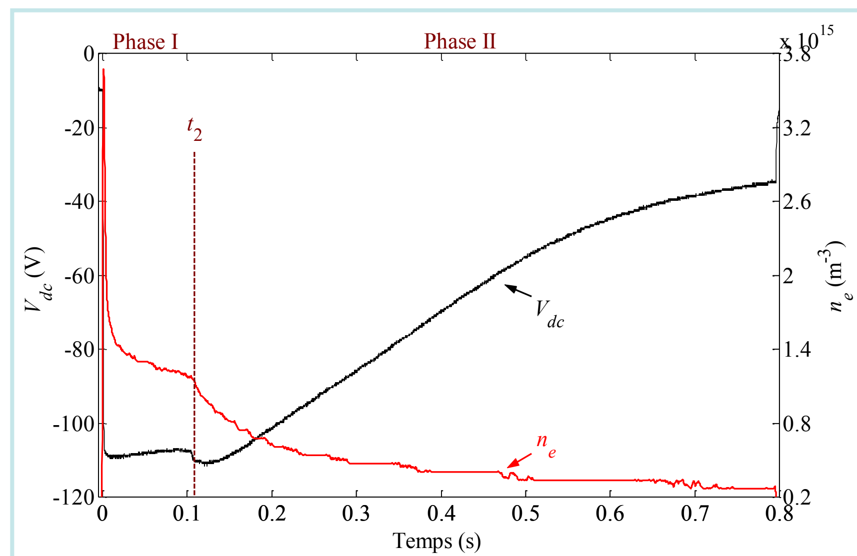

Ar-SiH_4 chemistry

The first decrease of the electron density is due to the formation of negative clusters. The time constant of this process is much longer than in the silane case.

NANOPARTICLE DETECTION

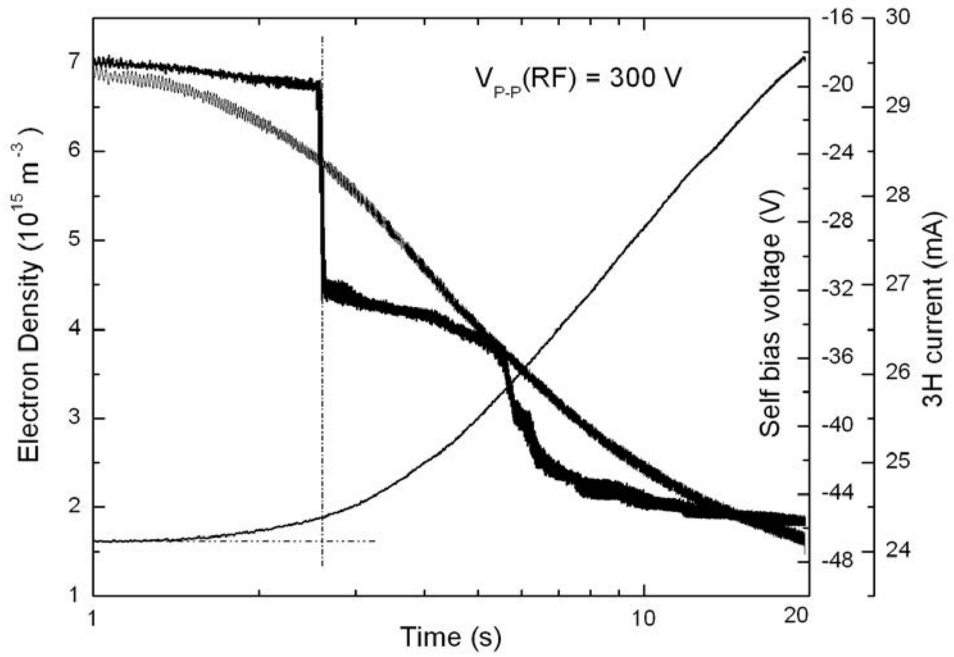

Ar-CH_4 chemistry

Three different phases:

- Nucleation, growth and accumulation of nanometer sized "clusters (nanocrystallites?),

- 1st agglomeration phase of the nanoclusters;

-2nd agglomeration phase.

All these phases are well identified from V_{DC}, 3rd harmonic of the discharge current and from the time evolution of the electron density.

GAS TEMPERATURE EFFECTS

GAS TEMPERATURE EFFECTS

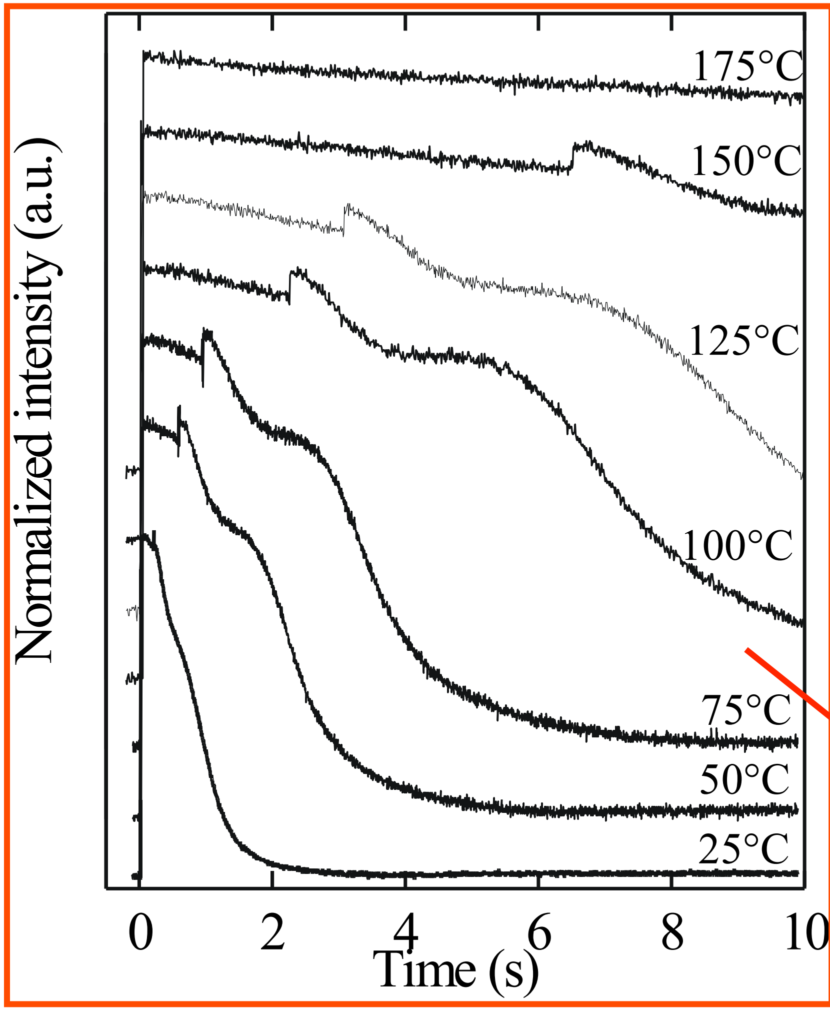

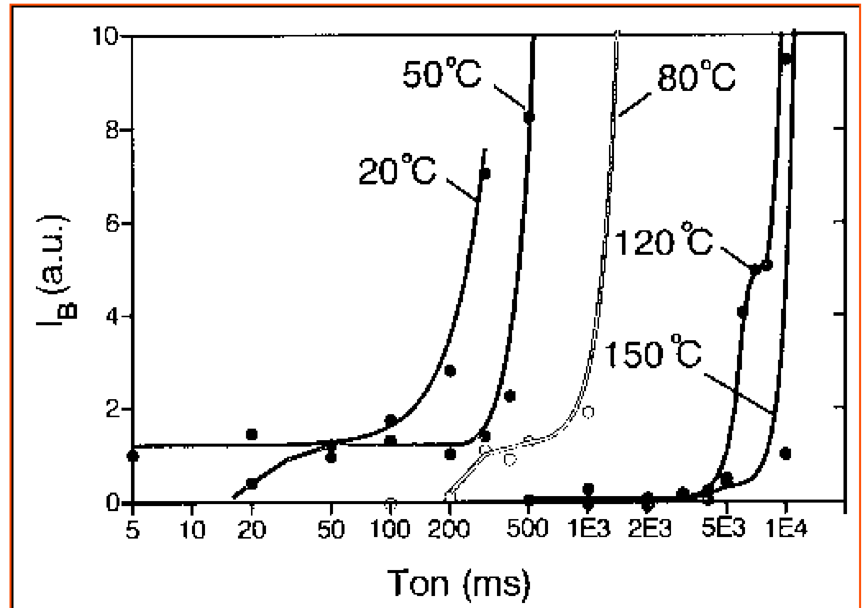

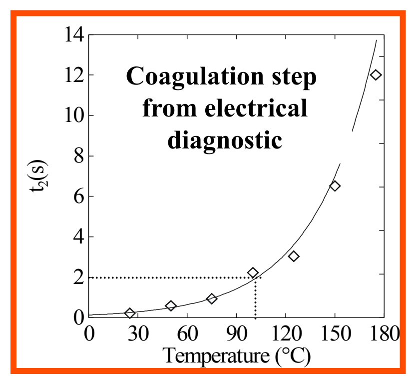

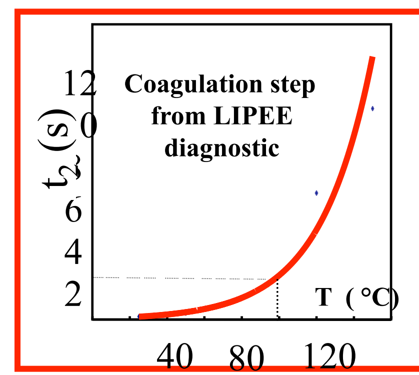

GAS TEMPERATURE EFFECTS

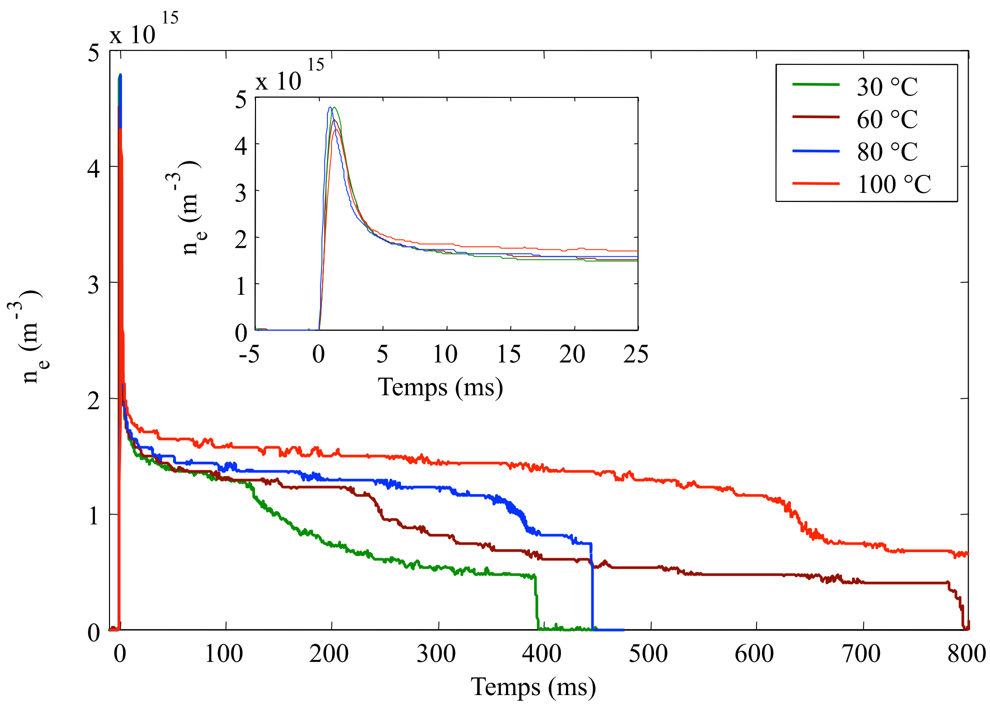

1- The gas temperature has no effect on the negative ion formation but strongly influences chemical reaction

$$Si_nH_{2n+1}^- + SiH_4^* \rightarrow Si_{n+1}H_{2(n+1)+1} + 2H$$

A. A. Fridman et al J. Appl. Phys. 79, 1303 (1996)

2- This can also be related to the temperature dependence of the Brownian diffusion coefficients when Tg increases.

U. Bhandarkar et al, J. Phys. D: Appl. Phys. 36, 1399 (2003)

The negative ions formation is not affected by the gas temperature.

GAS TEMPERATURE EFFECTS

What does it happen if we cool down the gas instead of heating?

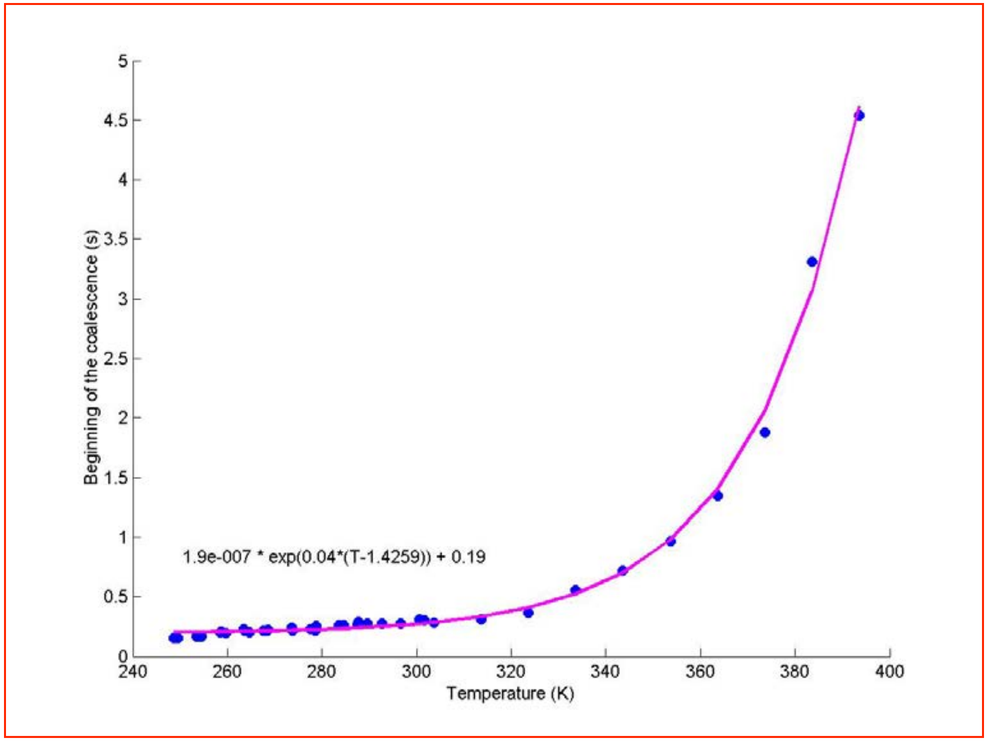

The nanocristallites critical size is also affected by the gas temperature:

Tg = 100 °C $d_{nc} \approx 2$ nm

Tg = 25 °C $d_{nc} \approx 3$ nm

Tg = 0 °C $d_{nc} \approx 6$ nm

DISCUSSION

The observed temperature effect on the dust particle formation can show that this phenomenon is close to the homogeneous nucleation and growth of nanocrystallites in a supersaturated medium (gas or liquide).

See for example:

1- J. B. Anderson et al, J. Atm. Sci., 33, 822, 1976.

2- S. Auer and D. Frenkel, Nature Vol. 409, 1020, 2001.

3- P. Peeters et al, J. Chem. Phys., 12, 5647, 2002.

4- J. W. P. Schmelzer, Mater. Phys. Mech., 6, 21, 2003.

In our experiments, we are operating at very low silane dilution in argon. However, the induction of nucleation seeds SiH_3^- could change the conditions.

DISCUSSION

In this case the nucleation rate is given by

$$J = J_0 \exp\left[-\frac{\Delta G}{k_B T}\right]$$

ΔG is the free energy variation during the phase transition or the required energy to form a nanocrystallite and the kinetics prefactor J_0 is related to

- the number of nucleation centers (seeds) which are for us the number of negative ions SiH_3^-, and

-the number of formed nanocristallites

DISCUSSION

The free energy variation ΔG between the two phases can be expressed as follow:

$$\Delta G = -n_a \Delta\mu + \sigma A$$

with:

n_a the number of atoms in the nanocristallites,

$\Delta\mu$ is the difference of the chemical potentials per mole or particles in both phases,

σ is the surface tension on the nanocrystallites and

A their area.

DISCUSSION

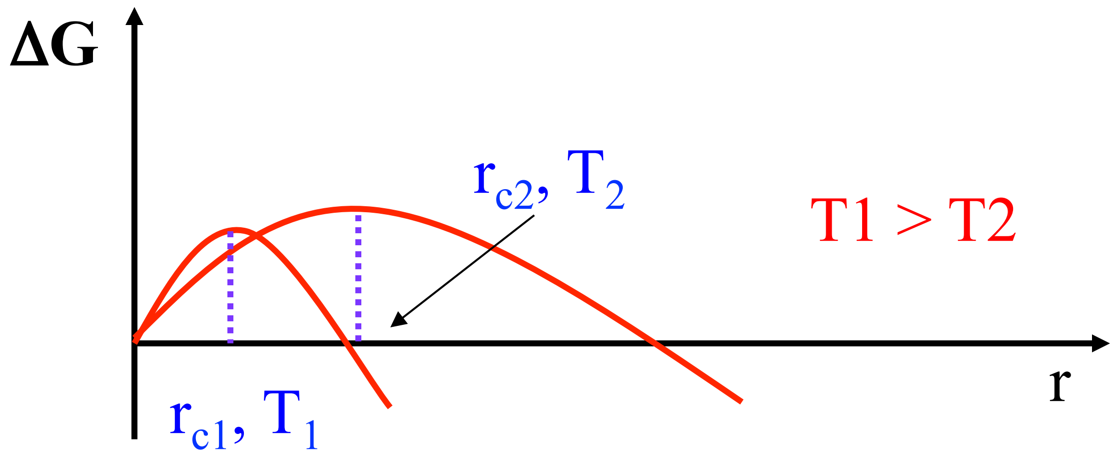

The critical radius of the nanocrystallites corresponds to the maximum of ΔG and is given by

$$r_c = \frac{2\sigma}{n_c \Delta\mu}$$

r_c increases when T decreases.

Therefore if we decrease the gas temperature we can grow up bigger nanocrystallites.

Results

$$r_{nc} = \frac{A}{T - T_0}$$

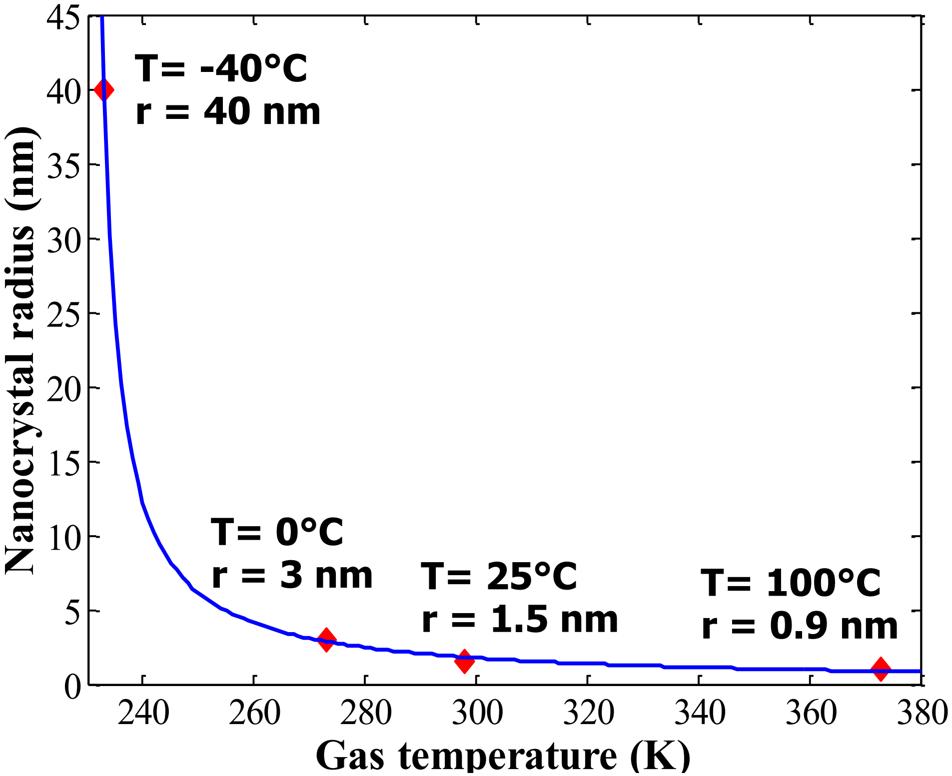

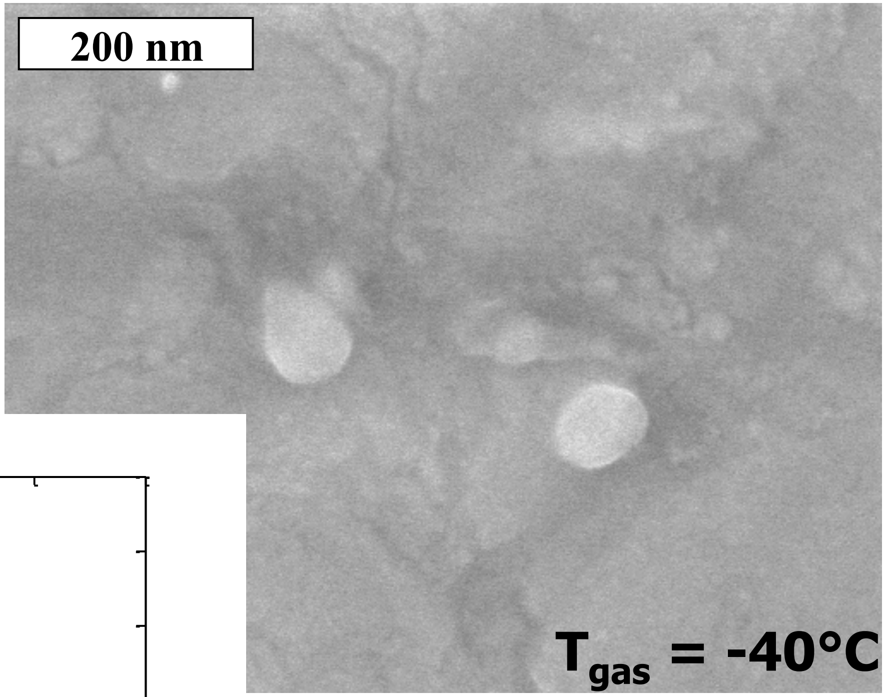

Aknowlegement : Annie Richard

Nanocrystal radius reaches 40 nm for T_{gas} = -40°C

APPLICATIONS

NANOTECHNOLOGIES CAN BRING SOLUTIONS IN MANY DOMAINES SUCH AS:

- Energy production and storage
- Reduction of the size and energy consumption of nanoelectronique components
- Production and storage of Hydrogen
- Water cleaning
- Solution for the actual diseases (cancer etc…)
- Biomedical applications
- …..

NANOSTRUCTURED THIN LAYERS

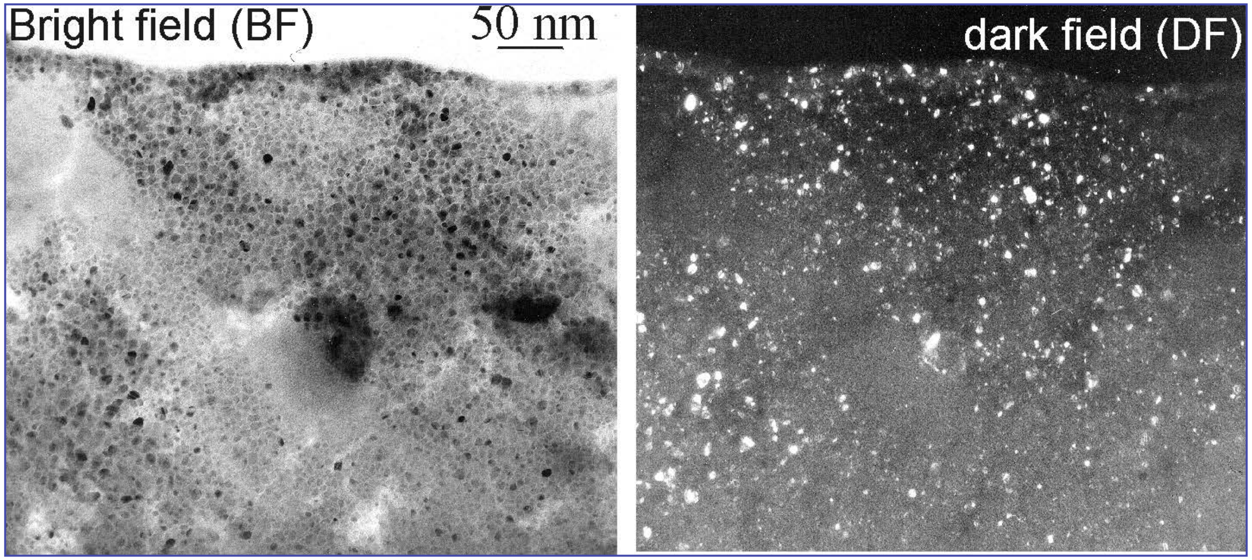

WIDE RANGE OF APPLICATIONS

Chemistry : nanocatalysts synthesis, specific area 100 m^2/g for 100 nm size particles.

Mechanics : super-hard coatings (ceramic or metallic particles or CNT's included in amorphous or polymer matrixes).

Photoluminescente devices : the wavelength is size dependent.

Optoelectronics: silicon nanocrystallites based sensors for UV radiations detection for example.

Solar cells : Polymorphous silicon based cells (higher and stable efficiency vs a-Si:H

New lasers : Silicon based lasers. Relatively important optical gain has been obtained in nanostructured SiO_2. A challenge for silicon

POLYMORPHOUS SILICON THIN LAYERS

Strategy for film deposition :

optimizing nanoparticles contribution and avoiding powder formation

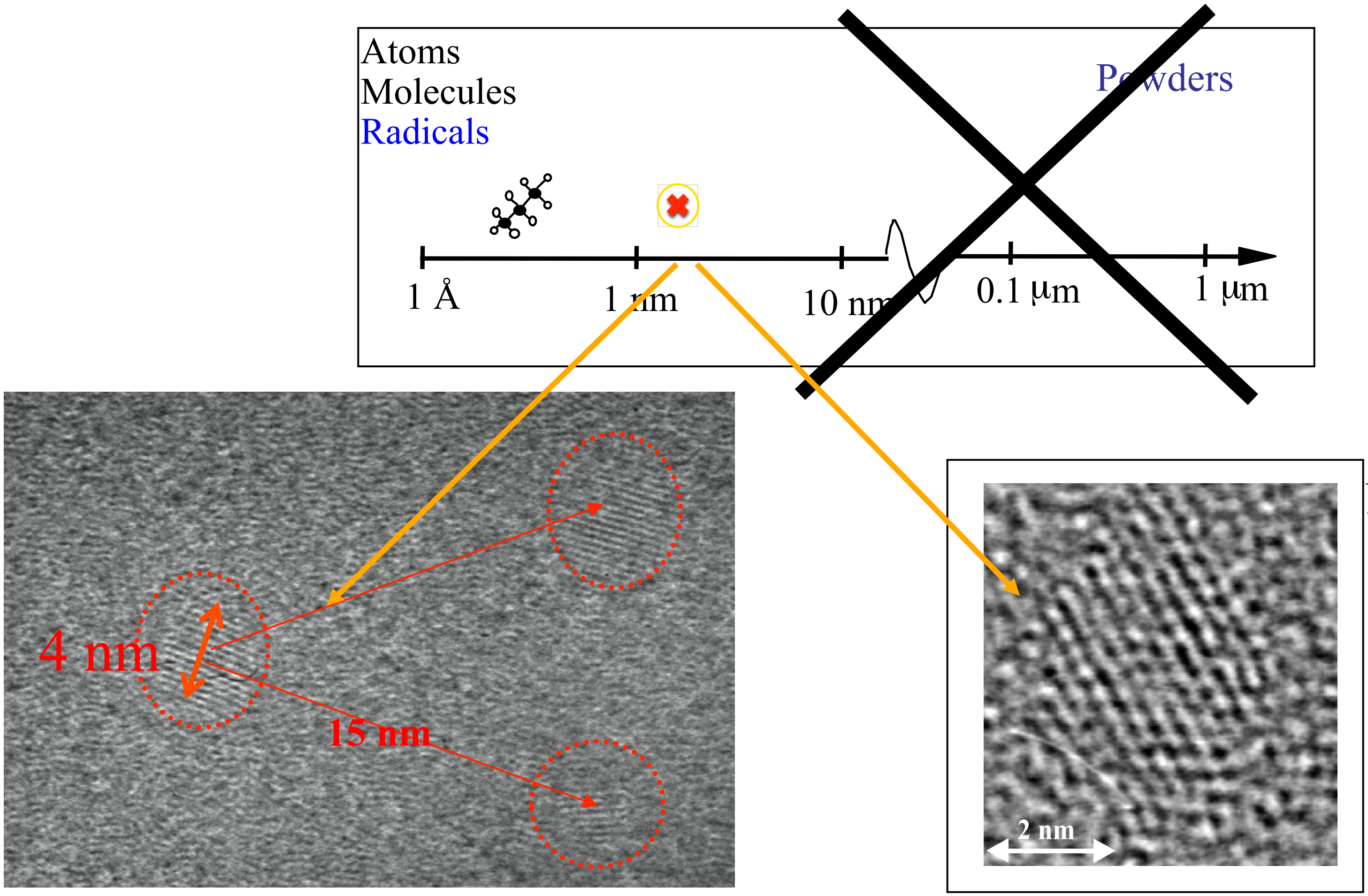

Nanocrystalline silicon particle

(HRTEM)

Higher efficiency and stability compared to a-Si:H

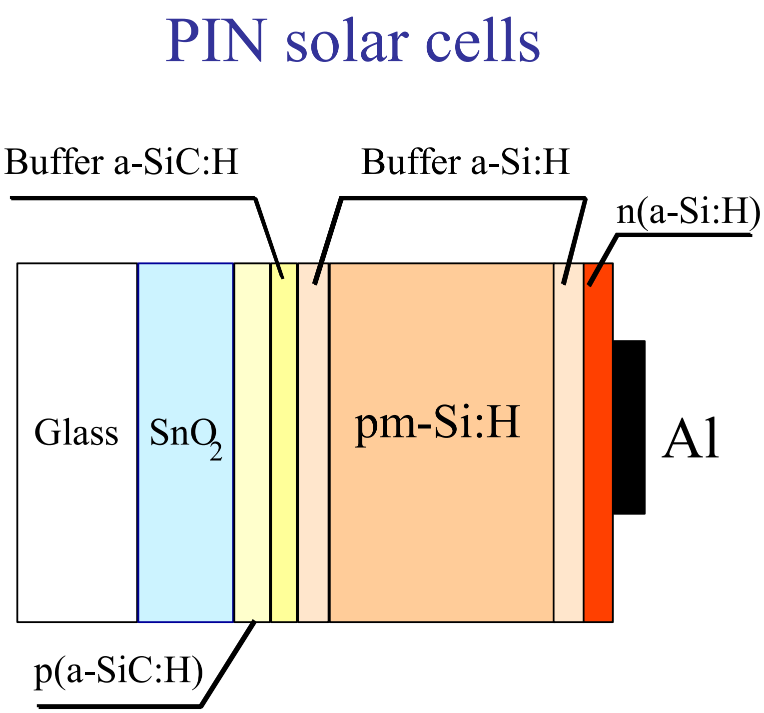

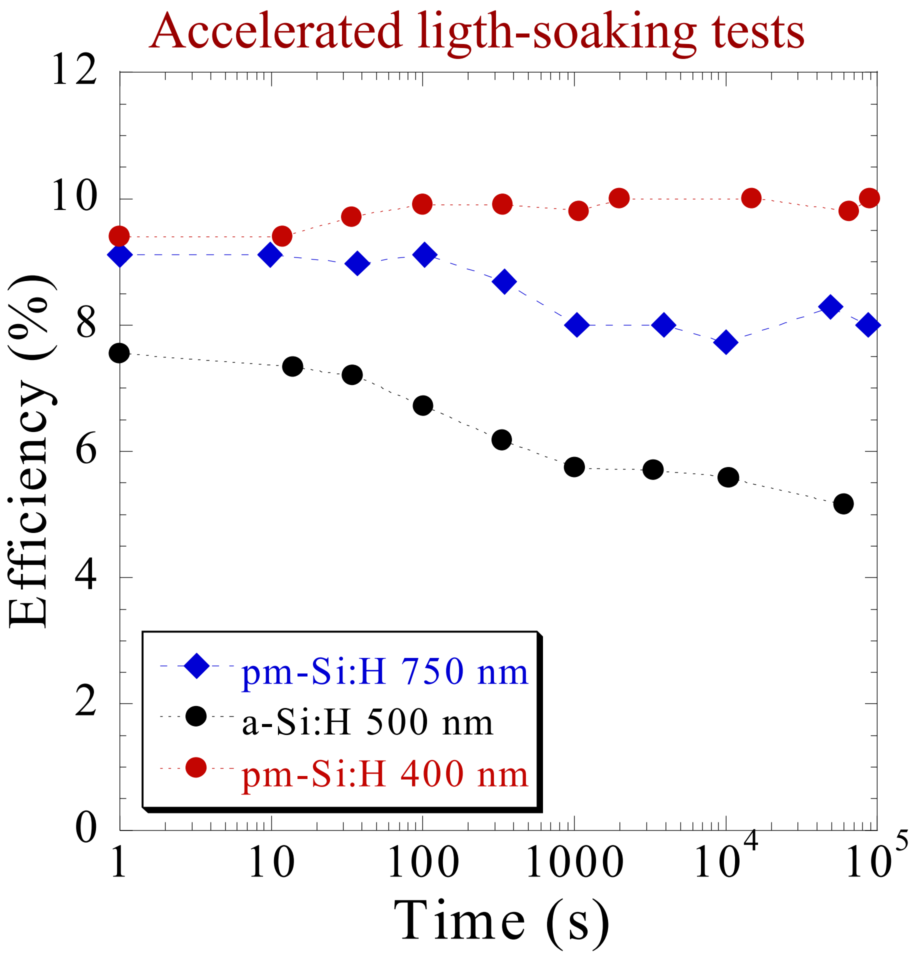

SAED analysis. ns-Si:H; T_{on}=5s, 100°C

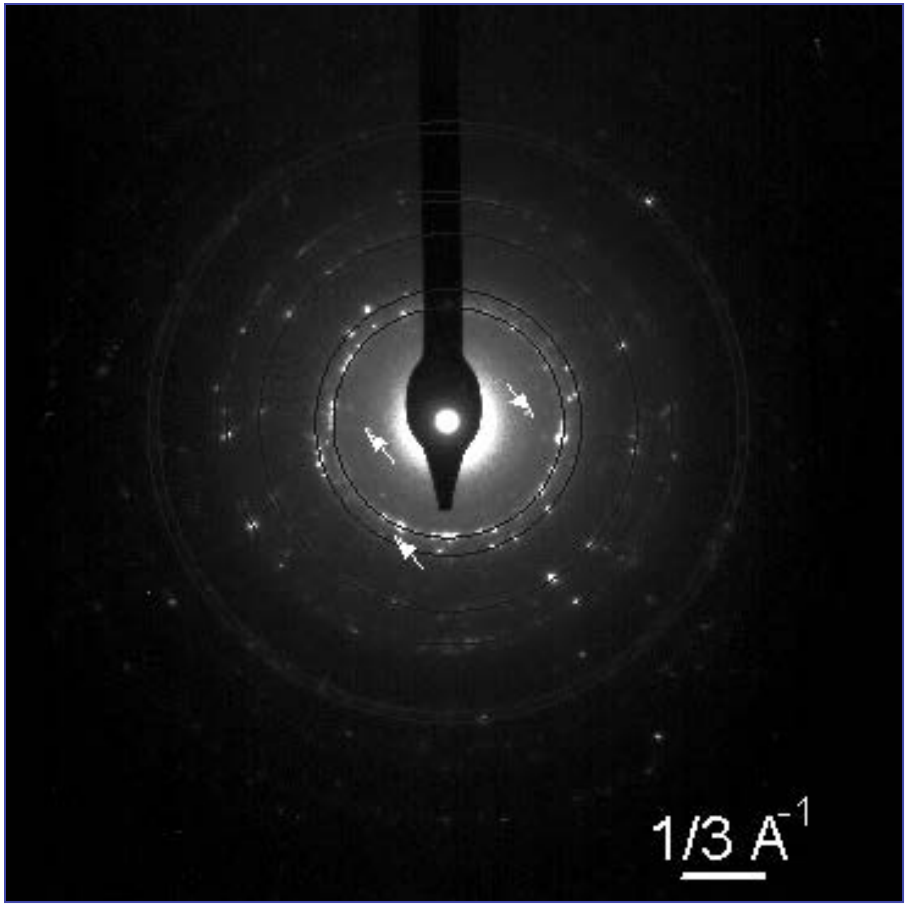

Sample	ring	d_{hkl}	hkl	a (Å)	Space group
ns-Si:H	1	2,11	111	3.659	FCC
	2	1,83	200	3.654	Fm3m (225)
	3	1,29	220	3.649	
	4	1,10	311	3.640	
	5	1,05	222	3.625	
	6	0,84	331	3.647	
	7	0,81	420	3.616	

FCC structure, a= 0.365 nm.

The arrows point out also Diamond like diffraction spots

Micro-Raman analysis

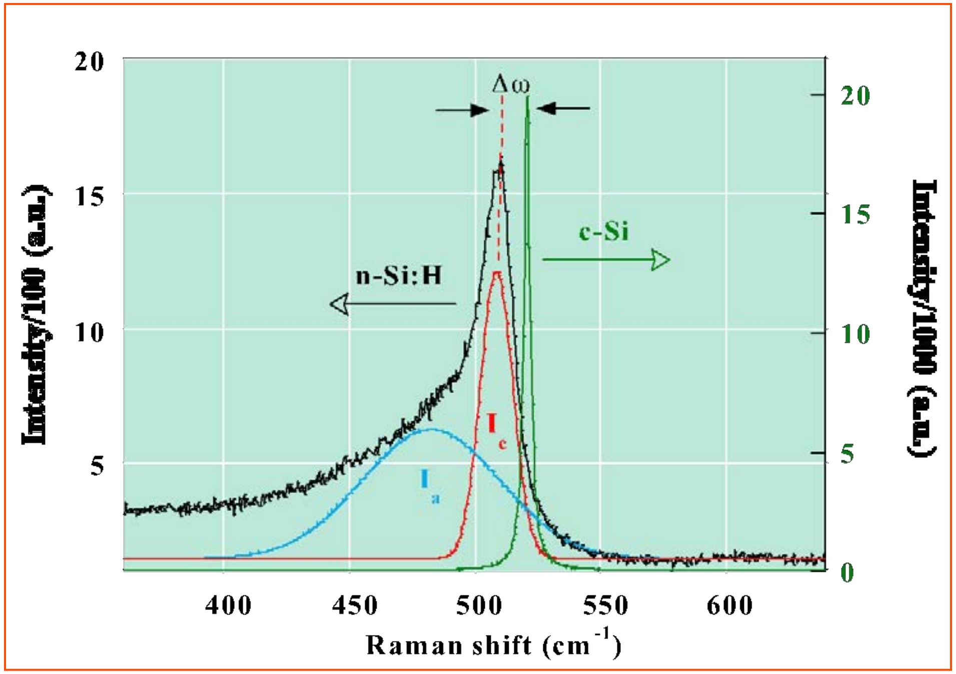

Δω is the Raman peak shift related to the crystallite size;

W is the peak width.

Sample	P_{LASER} (kW/cm^2)	Parameters		Size and volume fraction	
		Δω *(cm^{-1})*	*W* *(cm^{-1})*	*X_C* *(%)*	*D_Z* *(nm)*
ns-Si:H	0.34	8.1	17.8	20.1	**2.85**

SINGLE-ELECTRON DEVICES

Requirements : devices operating at room temperature.

-nanocrystallites (quantum dots) of 2-5 nm

-concentration of 10^{11} to 10^{12} cm^{-2}

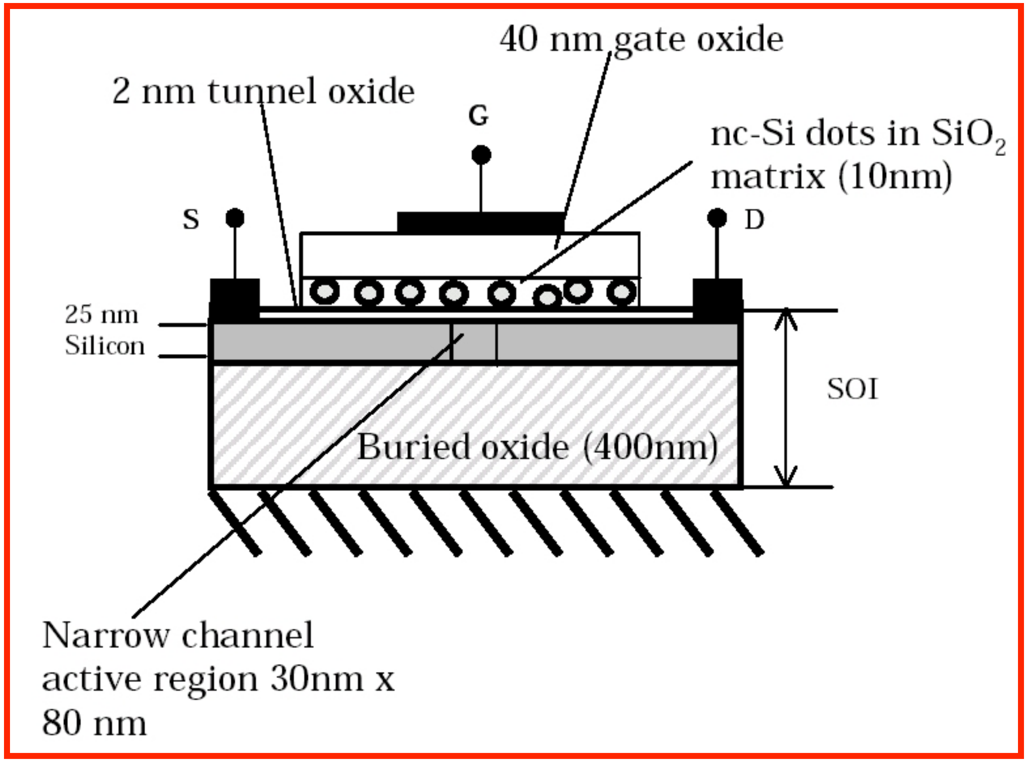

In general the crystallites are deposited using LPCVD. They have a dome like shape.

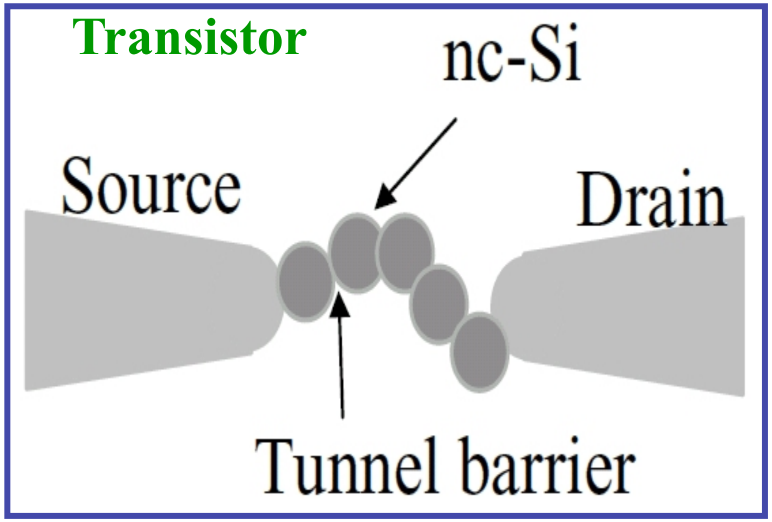

T. Baron et al, Applied Surface Science 164, 29-34 (2000)

A. Dutta et al, Jpn. J. Appl. Phys. 39, 264-267 (2000).

S. Oda, Tokyo Insitute of Technology, Japan

OTHER CHALLENGES

Size of "killer particles" is rapidly shrinking into the nano-regime

YEAR **2000** **2003** **2006** **2009** **2012**

Memory 1G 4G 16G 64G

256G **Feature size, nm** 180 130 100 70

50

D$_{\textbf{killer particle}}$**, nm** 60 43 33 23 17

Source: ***National Technology Roadmap for Semiconductors Workshop*, 2004**

http://www.itrs.net

FUSION PLASMA CONTAMINATION

Wall erosion
Impurities in the plasma
Radio-toxicity of dust particles

DIII-D
NATIONAL FUSION FACILITY
SAN DIEGO

J. Winter, Phys. Plasmas 7, 3862 (2000)

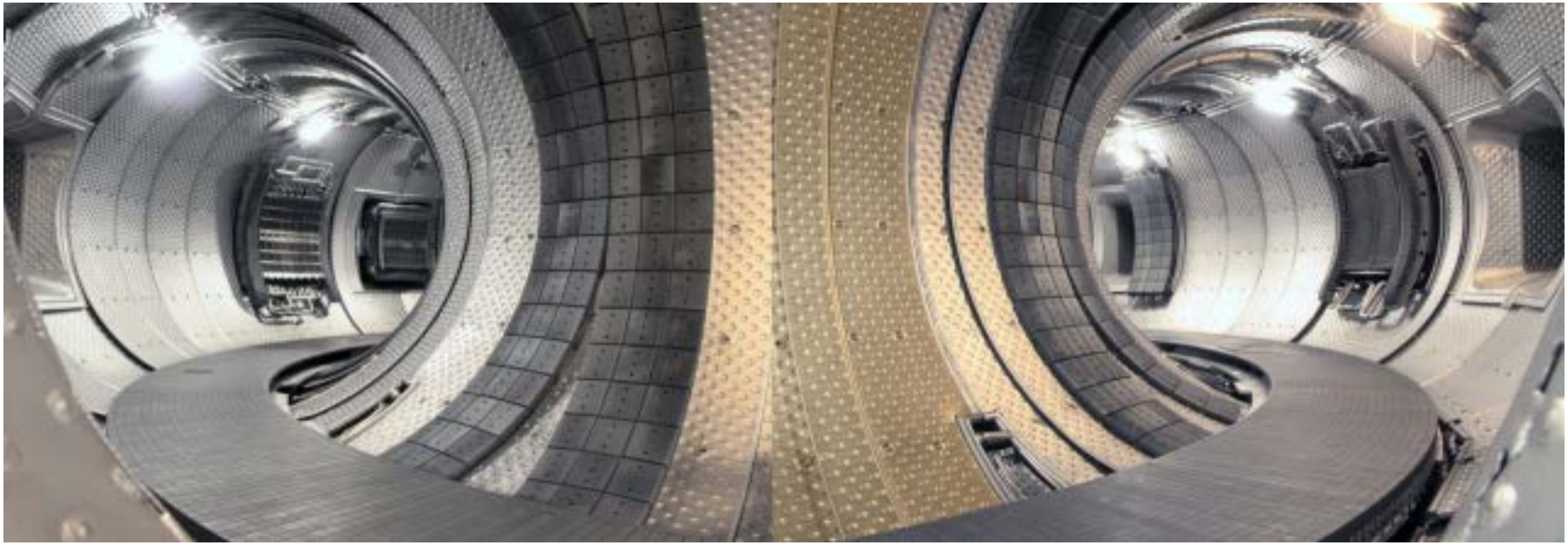

TOKAMAKS CONTAMINATION

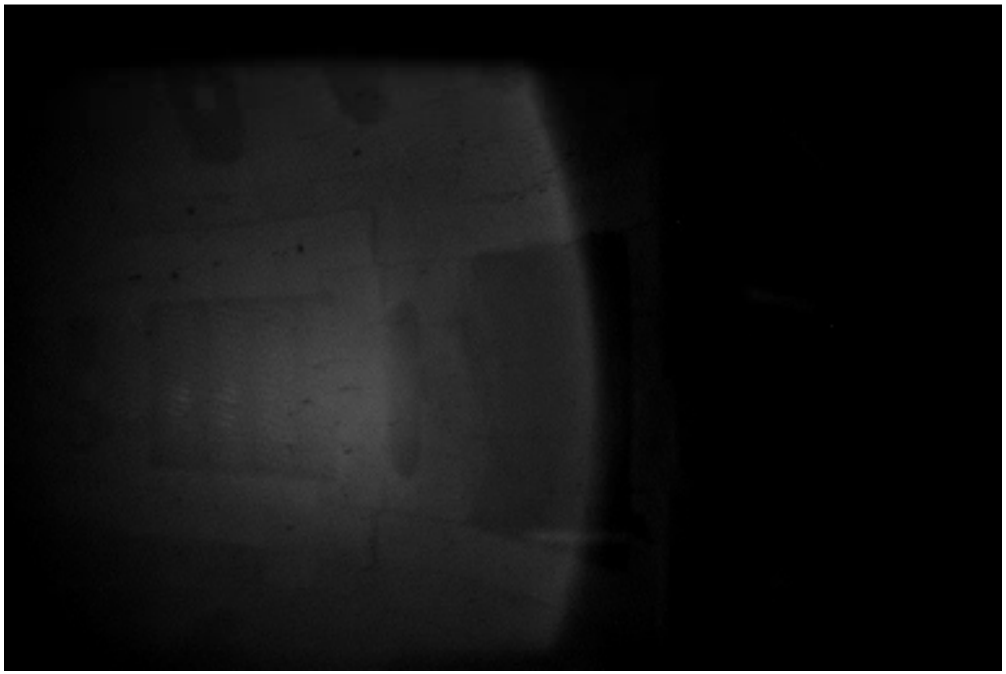

- Difficulty
  - Powder formation;
  - Flaking of the deposited layers on the walls during the plasma phases.

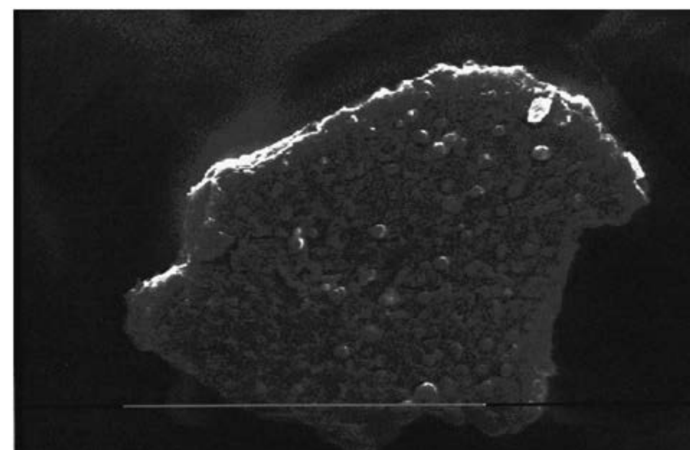

FIG. 2. Large flake of redeposited material from a TEXTOR limiter. The length of the white bar corresponds to 0.1 mm.

SAFETY AND HEALTH CARE ISSUES

There is a lack of regulation codes in the area of nanoparticles manipulation and working conditions

Also due to their size nanoparticles can remain hours in levitation in air at atmospheric pressure.

They can also penetrate and accumulate deeply in human tissues.

This require the development of robust tools for the detection, metrology and chemical and morphological properties characterization of the nanoparticles.

SAFETY AND HEALTH CARE ISSUES

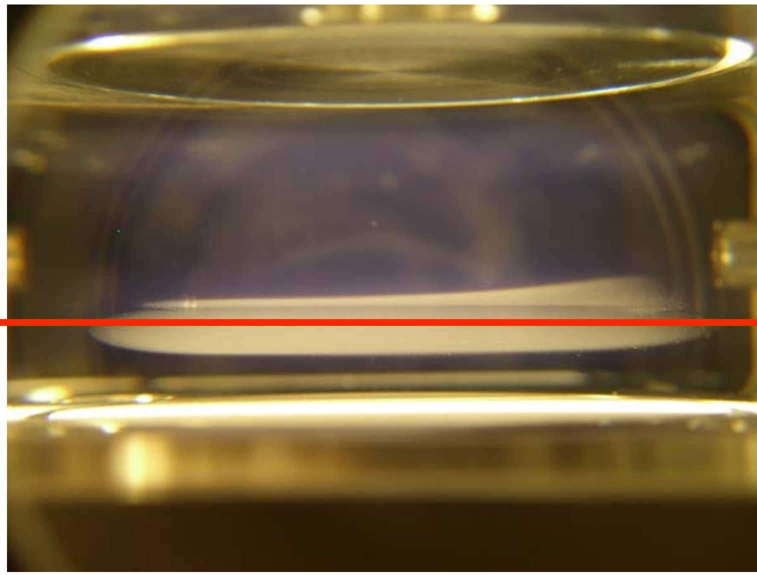

The particle size and concentration cannot be measured using light scattering due to the very small scattering cross section.

Development of method based on the analysis of the modification of the plasma and discharge properties induced by the presence of the nanoparticles.

Chemical composition can be analyzed using LIBS

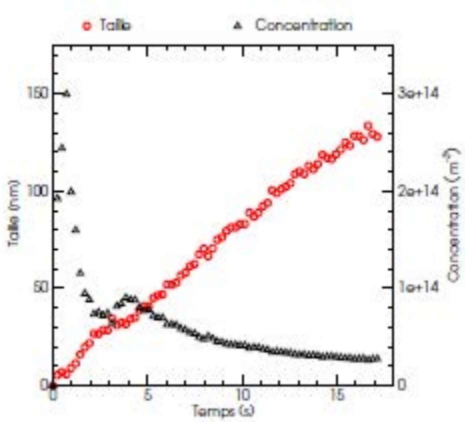

$$r_D = -\frac{\epsilon_0 V_s (A_B + A_M)}{q V_0 X} \times \frac{\Delta V_{DC}}{V_{DC}\Delta n_{e_{max}}}$$

$$r_D N_D = \frac{q V_0}{4\pi\epsilon_0 V_s}\Delta n_{e_{max}}$$

SAFETY AND HEALTH CARE ISSUES

MORPHOLOGY ANALYSIS

DUST PARTICLE MORPHOLOGY CHARACTERIZATION USING SAXS AND WAXS

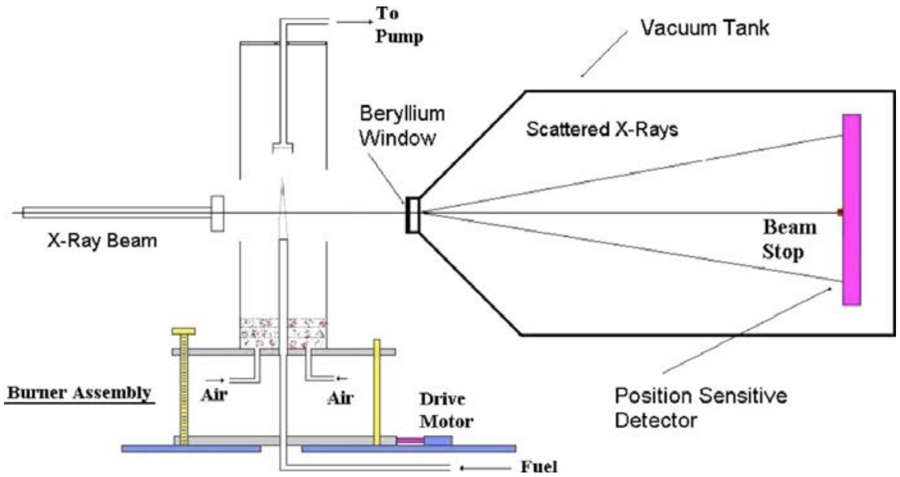

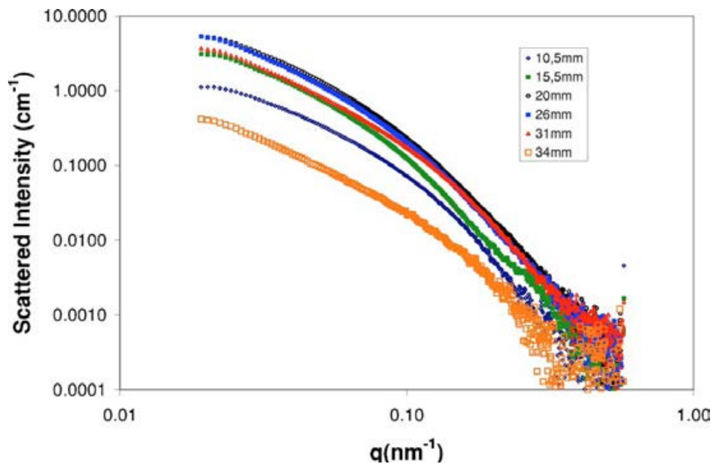

J. B. A. Mitchell et al J. Appl. Phys. 100, 124918 2006

From this kind of measurements we can deduce the size distribution functions and also the form and the surface properties of the dust particles.

Asbestos for example has no chemical reactivity but has fibber morphology.

CONCLUSIONS

- Dusty or complex plasmas are a rather new research field in physics with new aspects. It is still in development.
- Step-wise dust particle formation mechanisms; new theoretical models for carbon and silicon chemistries.
- Many new applications have been developed, others are underway.
- Connection between different communities.
- Many challenges


Nébuleuse du crabe (objet Messier 1)
Image OPIO , mont Mégantic,2000
Évolution après explosion (1054)
d'une étoile géante

Thank you

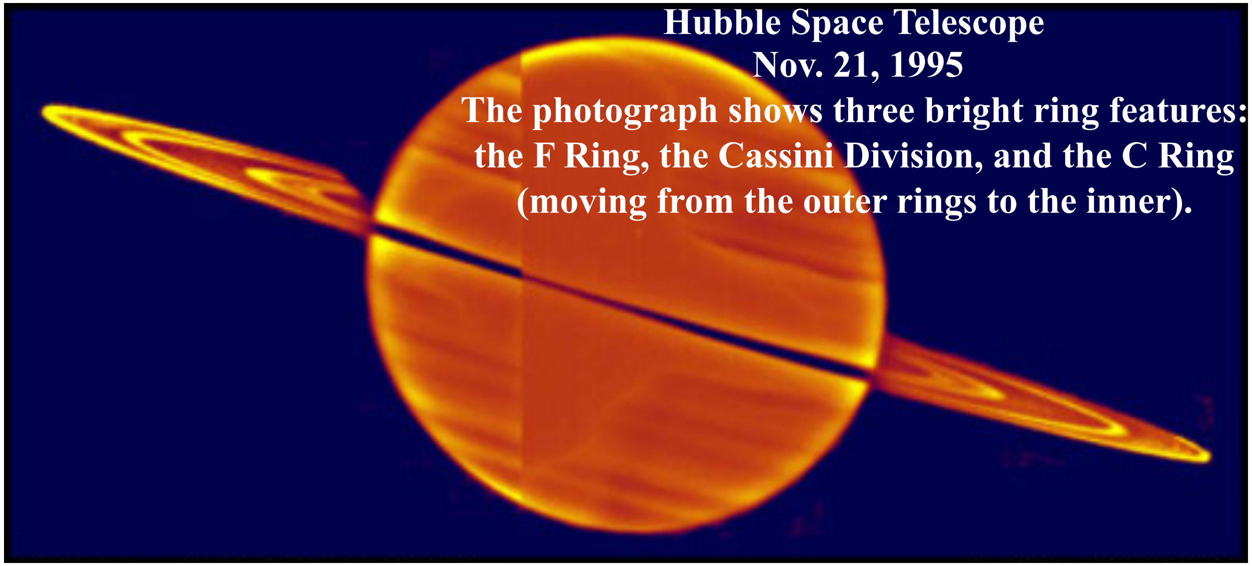
Hubble Space Telescope
Nov. 21, 1995
The photograph shows three bright ring features:
the F Ring, the Cassini Division, and the C Ring
(moving from the outer rings to the inner).